

หน่วยแรงเนื่องจากการบิดในสะพานคานเหล็กรูปไอเชิงประกอบ

นายชิตติก ฮิตายัต โมชัยหมัด

วิทยานิพนธ์นี้เป็นส่วนหนึ่งของการศึกษาตามหลักสูตรปริญญาวิศวกรรมศาสตรมหาบัณฑิต

สาขาวิชาวิศวกรรมโยธา ภาควิชาวิศวกรรมโยธา

คณะวิศวกรรมศาสตร์ จุฬาลงกรณ์มหาวิทยาลัย

ปีการศึกษา 2551

ลิขสิทธิ์ของจุฬาลงกรณ์มหาวิทยาลัย

DISTORTION-INDUCED STRESSES IN COMPOSITE STEEL I-GIRDER BRIDGES

Mr. Mochammad Syidik Hidayat

A Thesis Submitted in Partial Fulfillment of the Requirements
for the Degree of Master of Engineering Program in Civil Engineering

Department of Civil Engineering

Faculty of Engineering

Chulalongkorn University

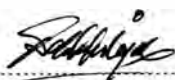
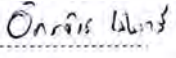
Academic Year 2008

Copyright of Chulalongkorn University

นาย ชีตติง อิตายัต โมซั่มหมัด : หน่วยแรงเนื่องจากการบิดในสะพานคานเหล็กรูปตัวไอ
เชิงประกอบ. (Distortion-induced Stresses in Composite Steel I-Girder Bridges)
อ.ที่ปรึกษาวิทยานิพนธ์หลัก : [อาจารย์ ดร. อัครวัชร เล่นวารี] จำนวนหน้า 125 หน้า.

น้ำหนักรบรรทุกกระทำซ้ำบนสะพานสามารถนำไปสู่การเกิดรอยร้าวในเอวคานในสะพานคานเหล็ก
ที่ตำแหน่งรอยต่อระหว่างคานหลักกับชิ้นส่วนนอกระนาบ เช่น โดอะแฟรม หรือ โครงเฟรมขวาง เป็นต้น ได้ โดย
รอยร้าวมักเกิดในเอวบริเวณปลายของแผ่นเหล็กเสริมกำลัง เนื่องจากเกิดหน่วยแรงสูงในบริเวณดังกล่าว ภายใต้
ได้การบิดตัวของสะพานอันมีสาเหตุหลักจากการโก่งตัวสัมพัทธ์ระหว่างคานข้างเคียง งานวิจัยนี้ศึกษา
ผลกระทบของตัวแปรต่างๆ ของสะพานต่อการโก่งตัวสัมพัทธ์ของคาน, หน่วยแรงในคานที่ตำแหน่งรอยต่อ
ระหว่างคานหลักกับชิ้นส่วนนอกระนาบ และ ตัวคูณการกระจายน้ำหนักทางขวางของสะพานคานเหล็กรูปตัวไอ
เชิงประกอบ ตัวแปรสะพานเหล่านี้ประกอบด้วย ระยะห่างระหว่างคานข้างเคียง, ความหนาของพื้น, โมเมนต์
อินเนอร์เซียของคาน และ ความยาวช่วงของสะพาน ในงานวิจัยได้ใช้ระเบียบวิธีไฟไนต์เอลิเมนต์ โดยทำการ
สร้างแบบจำลองใน 2 รูปแบบ เรียกว่า global model และ submodel โดยแบบจำลองแรกใช้ในการศึกษาการ
โก่งตัวสัมพัทธ์ระหว่างคานและค่าตัวคูณการกระจายน้ำหนักทางขวาง ในขณะที่แบบจำลองหลังใช้ศึกษาหน่วย
แรงในคานที่ตำแหน่งรอยต่อระหว่างคานหลักกับชิ้นส่วนนอกระนาบ จากผลการศึกษาทำให้สามารถเรียงลำดับ
ความสำคัญของตัวแปรสะพานที่มีผลกระทบต่อค่าตัวคูณการกระจายน้ำหนักทางขวาง, หน่วยแรงในคานที่ตำแหน่งรอยต่อ
ระหว่างคานหลักกับชิ้นส่วนนอกระนาบ และ ค่าตัวคูณการกระจายน้ำหนักทางขวางในสะพานคานเหล็กรูปตัว
ไอเชิงประกอบได้ โดยพบว่า ตัวแปรที่มีผลกระทบต่อหน่วยแรงเนื่องจากการบิดในเอวคานมากที่สุด คือ ความ
ยาวช่วงของสะพาน และคุณสมบัติของเอวคาน

ภาควิชา วิศวกรรมโยธา
สาขาวิชา วิศวกรรมโยธา
ปีการศึกษา 2551

ลายมือชื่อนิสิต 
ลายมือชื่ออ.ที่ปรึกษาวิทยานิพนธ์หลัก 
ลายมือชื่ออ.ที่ปรึกษาวิทยานิพนธ์ร่วม _____

507 06537 : MAJOR CIVIL ENGINEERING

KEYWORDS : FINITE ELEMENT / DISTORTION-INDUCED STRESS / PARAMETRIC STUDY / COMPOSITE STEEL I-GIRDER BRIDGE

MOCHAMMAD SYIDIK HIDAYAT : DISTORTION-INDUCED STRESS IN COMPOSITE STEEL I-GIRDER BRIDGES. ADVISOR : Dr. AKHRAWAT LENWARI, MASTER, 125 pp.

Repeated traffic loading assists distortion-induced fatigue cracks in the web gaps at connections between the steel girders and out-of-plane elements such as diaphragms and cross frames in the steel bridges. Unstiffened girder web gaps at the ends of transverse stiffeners, which also serve as diaphragm connection plates, are subjected to high local stresses during cyclic out-of-plane distortion. The out-of-plane distortion was mainly caused by relative girder deflection. This research investigates the effects of bridge parameters on the relative displacement between adjacent girders, vertical web gap stresses, and lateral load distribution factor. The parameters include the girder spacing, slab thickness, girder stiffness, and span length. By using finite element method, dual-level analyses using the global model and submodel were performed. The global model was used to study the relative displacement between adjacent girders and lateral load distribution factor, while the submodel was used for the critical web gap stress. From a parametric study, the rankings of bridge parameters that influence the relative displacement between adjacent girders, web gap stress and lateral load distribution factor are reported. For the web gap stress, the results showed that it is primarily dependent on bridge span length and web gap properties.

Department : ..Civil Engineering.....

Student's Signature 

Field of Study : ..Structural Engineering.....

Advisor's Signature 

Academic Year : 2008.....

Contents

	page
Abstract (Thai)	iv
Abstract (English)	v
Acknowledgments	vi
Table of Contents	vii
List of Tables	x
List of Figures	xi
CHAPTER I	
INTRODUCTION	
1.1 Introduction	1
1.2 Motivation / Research Significance	4
1.3 Objectives	4
1.4 Scopes of Work	5
1.4 Methodology	5
CHAPTER II	
LITERATURE REVIEW	
2.1 Lateral Load Distribution	6
2.2 Out-of-plane Bending Mechanism	9
2.3 Previous Finite Element Model	12
CHAPTER III	
THEORETICAL BACKGROUND	
3.1 Introduction to Fatigue	20
3.1.1 Load-Induced Fatigue	20
3.1.2 Distortion-Induced Fatigue	21
3.2 Finite Element Types	21
3.2.1 3D Beam Element	21
3.2.2 Shell Element	22
3.3 Multiple Linear Regression in Matrix Form	23
CHAPTER IV	
FINITE ELEMENT STUDY	
4.1 Overview	26
4.2 Model Verification	27
4.2.1 Field Test Data	27

4.2.1.1 Bridge Dimension	27
4.2.1.2 Truck Loadings	29
4.2.1.3 Field Test Data	31
4.2.2 Finite Element Model	32
4.2.2.1 Global Model	32
4.2.2.2 Submodel	43
4.2.3 Verification to The Finite Element Model	47
4.2.3.1 Global Model	47
4.2.3.2 Submodel	54
4.2.3.3 Web Gap Stress	55

CHAPTER V

PARAMETRIC STUDY	60
5.1 Overview	60
5.2 Description of Finite Element Model	60
5.3 Bridge Parameters	61
5.4 Truck Loading	62
5.5 Discussion on Finite Element Model Result	63
5.5.1 Critical Longitudinal and Transverse Position of Truck Loading ..	63
5.5.2 Maximum Relative Displacement Between Adjacent Girders	64
5.5.2.1 Effect of Girder Spacing	64
5.5.2.2 Effect of Slab Thickness	65
5.5.2.3 Effect of Girder Stiffness.....	65
5.5.2.4 Effect of Bridge Length	66
5.5.3 Maximum Web Gap Stress	67
5.5.3.1 Effect of Girder Spacing	69
5.5.3.2 Effect of Slab Thickness	71
5.5.3.3 Effect of Girder Stiffness.....	71
5.5.3.4 Effect of Bridge Length	72
5.5.4 Lateral Load Distribution Factor	73
5.5.4.1 SAP2000 Result	73
5.5.4.2 Effective Width	74
5.5.4.3 Moment in The Girder Section	75
5.5.4.4 Moment from Beam Analysis	77
5.5.4.5 LDF Calculation	77
5.6 Comparison AASHTO and Thai truck	80
5.6.1 Lateral load distribution factor	80
5.6.2 Web gap stress	82

CHAPTER VI	
DEVELOPMENT FORMULA FOR RELATIVE DISPLACEMENT BETWEEN ADJACENT GIRDERS AND WEB GAP STRESS	84
6.1 The Ranking of Influencing Bridge Parameter	84
6.1.1 Relative Displacement Between Adjacent Girders	84
6.1.2 Web Gap Stress	86
6.1.3 Lateral Load Distribution Factor	88
6.2 Development of Formula	90
CHAPTER VII	
SUMMARY AND CONCLUSIONS	95
7.1 Summary and conclusion	95
7.2 Suggestion of future work	97
Appendix A Construction of Global Model	98
Appendix B Construction of Submodel	115
REFERENCES	122
Biography	125

List of Tables

	page
4.1 Truck properties (Wongsawang in-bound)	29
4.2 Field test data	31
4.3 Comparison stress in the bottom flanges in the midspan between global model, submodel, and field test data	55
5.1 Bridge's finite element model parameter	62
7.1 Ranking influencing bridge parameters	96

List of Figures

	page
1.1 Composite I-girder bridges at intersections in Thailand	1
1.2 Typical cross section of Wongsawang composite I-Girder bridges	2
1.3 Differential deflection of adjacent girder	2
1.4 Web-gap on web girder of Wongsawan bridge	3
1.5 Schematic of web gap stress in the end of stiffener (Fisher, 1978)	3
2.1 Fatigue crack in the web gap near bottom flange of a girder (Zhou, 2005)	10
2.2 Schematic representation of web gap rotation (Jajich and Schultz, 2003)	11
2.3 Diaphragm rotation and the web gap deflection according to Fisher et al.(1990)	11
2.4 First finite element model (Mabsout el al.1997)	13
2.5 Third finite element model (Mabsout el al.1997)	13
2.6 Finite element model (Roddis and Zhao, 2000)	14
2.7 Finite element model (Roddis and Zhao, 2003)	14
2.8 Finite element model (Jajich et al. 2000)	15
2.9 Deformed shape of web gap and stiffener (Jajich et al. 2000)	15
2.10 Macro model (Li and Schultz, 2005)	16
2.11 Micro model (Li and Schultz, 2005)	17
2.12 Finite element model (Phuvoravan, 2006)	17
2.13 Finite element model (Chung et al, 2006)	18
2.14 Finite element model (Sotelino et al, 2004)	18
2.15 Girder's model techniques (Chung and Sotelino, 2006)	19
2.16 Partial cross section through FE model (Berglund and Schultz 2006)	19
3.1 Beam element on the x axis of a rectangular coordinate system (Computer and Structure, 2000)	21
3.2 Degree of freedom (Computer and Structure, 2000)	22
4.1 Global model	26
4.2 Submodel	27
4.3 Wongsawang bridge section	28
4.4 Truck loading cases in the field test	30
4.5 Strain gage position in web gap area	31
4.6 Two types of cross frame	32
4.7 Model of truss cross frame	33
4.8 Beam element	34
4.9 Global model of Wongsawang bridge	34

4.10	Partial bridge section	35
4.11	Modeling of truck 1	36
4.12	Modeling of truck 2	36
4.13	Modeling of truck 3	37
4.14	Truck loading lane of one truck on left lane case (case a)	37
4.15	Truck loading lane of one truck on left lane case (case b)	37
4.16	Truck loading lane of two truck on both lanes (case c)	38
4.17	Global model for sensitivity study Type A (293 elements)	39
4.18	Global model for sensitivity study Type B (817 elements)	39
4.19	Global model for sensitivity study Type C (2773 elements)	40
4.20	Global model for sensitivity study Type D (5772 elements)	40
4.21	Longitudinal stress in G1 from sensitivity study result	41
4.22	Longitudinal stress in G2 from sensitivity study result	41
4.23	Longitudinal stress in G3 from sensitivity study result	42
4.24	Global model modification	42
4.25	Modified longitudinal stress comparison	43
4.26	Finite element model	44
4.27	Mesh of Submodel for sensitivity study	45
4.28	Convergence of submodel	46
4.29	Stress distribution in vertical direction of web gap	46
4.30	Comparison of longitudinal stresses in the bottom flange of all three girders at quarter span from unmodified global model	48
4.31	Comparison of longitudinal stresses in the bottom flange of all three girders at midspan from unmodified global model	49
4.32	Comparison of longitudinal stresses in the bottom flange of all three girders at three quarter span from unmodified global model	50
4.33	Comparison of longitudinal stresses in the bottom flange of all three girders at quarter span from modified global model	51
4.34	Comparison of longitudinal stresses in the bottom flange of all three girders at midspan from modified global model	52
4.35	Comparison of longitudinal stresses in the bottom flange of all three girders at three quarter span from modified global model	53
4.36	Web gap area mesh	54
4.37	Distribution of web gap stress along the girder length	56
4.38	Strain gage placement	56
4.39	Comparison between measured web gap stress and prediction from results	57
4.40	Web gap deformed shape	58
4.41	Displacement of web gap	58
5.1	Typical FEM with base bridge parameter	61
5.2	AASHTO truck configuration (HS20-44)	62
5.3	Transverse loading combination	63

5.4	Girder spacing effect	64
5.5	Slab thickness effect	65
5.5	Girder stiffness effect	66
5.7	Bridge length effect	66
5.8	Web gap sides	67
5.9	Midspan transverse section deformation shape in case of one truck.....	67
5.10	Midspan transverse section deformation shape in case of two truck	67
5.11	Stress distributions in web gap area of girder G1.....	68
5.12	Stress distributions in web gap area of girder G2	68
5.13	Critical vertical web gap stress position	69
5.14	End of stiffener stress	69
5.15	Near bottom flange stress	69
5.16	Girder spacing effect	70
5.17	Slab thickness effect	71
5.18	Girder stiffness effect	71
5.19	Bridge length effect	72
5.20	Notation of beam element result	74
5.21	Notation of <i>section cut</i> result	74
5.22	Effective width	74
5.23	Notation of <i>section cut</i> result	75
5.24	<i>Section cut</i> form in SAP2000	76
5.25	One lane wheel load in SAP2000	77
5.26	Girder spacing effect	78
5.27	Slab thickness effect	78
5.28	Girder stiffness effect	79
5.29	Bridge length effect	79
5.30	Characteristic of truck	80
5.31	Characteristic of truck loading in SAP2000	81
5.32	End of stiffener vertical web gap stress in each girder	83
6.1	Girder spacing effect	84
6.2	Slab thickness effect	85
6.3	Girder stiffness effect	85
6.4	Bridge length effect	85
6.5	Girder spacing effect	87
6.6	Slab thickness effect	87
6.7	Girder stiffness effect	87
6.8	Bridge length effect	88
6.9	Girder spacing effect	89
6.10	Slab thickness effect	89
6.11	Girder stiffness effect	89

6.12	Bridge length effect	90
------	----------------------------	----

CHAPTER I

INTRODUCTION

1.1 Introduction

Composite I-girder steel bridges, as shown in figure 1.1, are commonly used in many countries. These bridges face the problems such as corrosion and fatigue that reduce a bridge's service life (Nishikawa et al. 1997; Jajich and Schultz, 2003).



Figure 1.1 Composite I-girder bridges at intersections in Thailand

There are two types of elements in composite I-girder bridges. The first type includes the primary elements such as girders, concrete slab (concrete deck), and supports, while the secondary elements consist of the cross bracings, diaphragms, and parapets. The concrete deck and steel girders form the composite structural system. They are typically connected by shear studs embedded in the concrete and tied together by diaphragms or other horizontal bracings, as shown in figure 1.2. Diaphragms or horizontal bracing are intended to resist lateral load and to help distribute traffic loading. Additionally, the diaphragms stabilize the girders against lateral buckling during construction before the concrete deck is poured and hardened.



(a)



(b)

Figure 1.2 Typical cross section of Wongsawang composite I-Girder bridges

(a) Diaphragm (b) Cross frame

Figure 1.3 shows rigid body rotations of diaphragms that connect adjacent girders due to the differential deflection between adjacent girders (Δ). This causes a torsional moment in the girders and a flexural moment in the diaphragm.

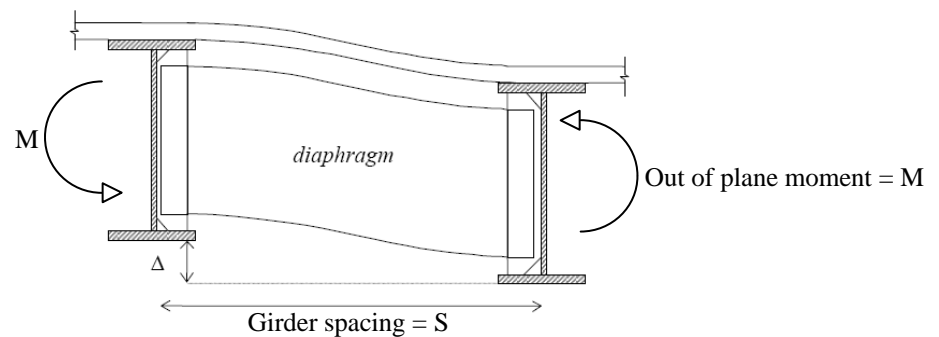


Figure 1.3 Differential deflection of adjacent girder

The transverse stiffeners connecting the diaphragm and girder are rigidly welded to the girder web. It causes the latter to take up the majority of the out-of-plane displacement and rotation which is more critical when the transverse stiffeners terminate a few inches from girder flange. The space between the transverse stiffeners and the girder flanges is called the “web gap” (see figure 1.4). The unstiffened web gap region attracts the majority of this out-of-plane distortion because of its relative flexibility. When the out-of-plane stress is higher than the stress capacity of girder web, crack can be occur in the end of stiffener as shown in figure 1.5 or above the bottom flanges.

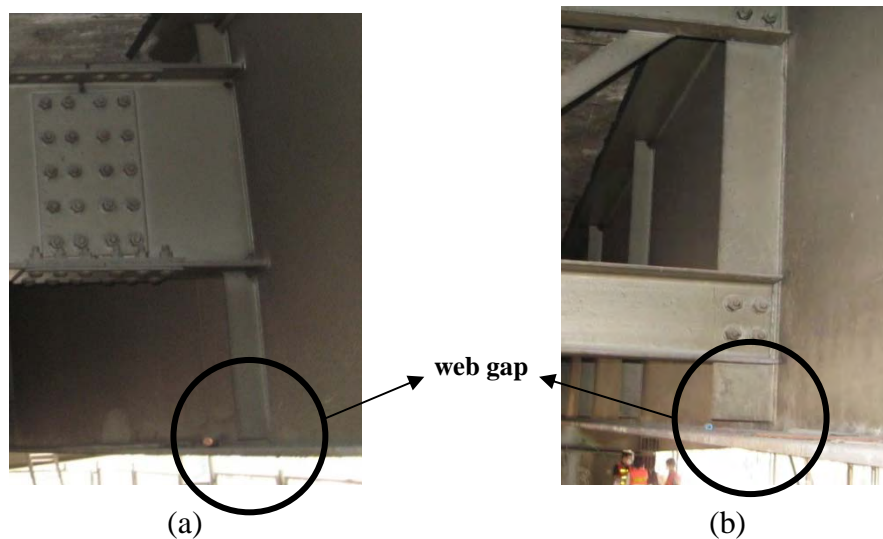


Figure 1.4 Web-gap on web girder of Wongsawan bridge (a) at diaphragm
(b) at cross frame

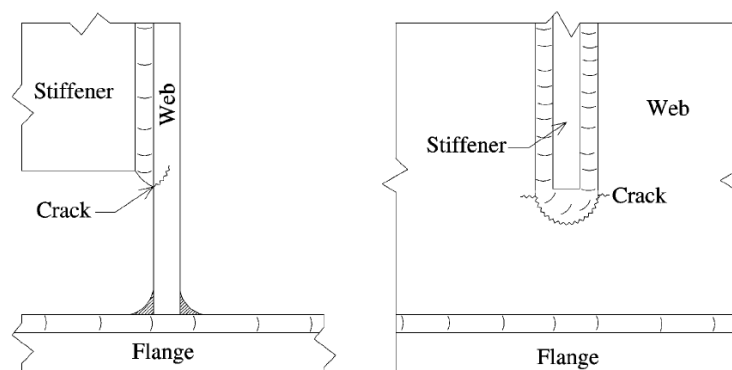


Figure 1.5 Schematic of web gap stress in the end of stiffener (Fisher, 1978)

Due to the presence of concrete slab in the superstructure of composite I-girder bridge, the live loads are not applied directly to the beam. In view of this, the concept of distribution factor is needed to determine the maximum shear and moments of girders under the live load. Then the maximum shear and moments in beams caused by the given live load will be multiplying with the appropriate load distribution factor to obtain the critical live load shear and moment in girders.

Load transfer from concrete slab to steel girder is a three dimensional problem and involves complex behavior. The AASHTO bridge specifications suggest several methods for analysis such as finite element analysis, grillage analysis, and lateral load distribution factor equation. Currently, the lateral load distribution factor of the live load moment in highway bridge design is commonly determined using the method from AASHTO LRFD standard specification (1996, 1998). Bridge parameters that influence the lateral load distribution factors include girder spacing, span length, slab thickness, modular ratio between steel and concrete, girder stiffness, girder area, and eccentricity between centroids of girder and slab.

1.2 Motivation / Research Significance

The motivations of this research are:

1. To understand the mechanism of distortion induced stress in the web gap area of composite steel I girder bridges.
2. To review the bridge parameters that influence the lateral load distribution of composite steel I-girder bridges.
3. To find the bridge parameter that influence the distortion-induced stress
4. To study the relationship between distortion-induced stresses and lateral load distribution.

1.3 Objectives

The objectives of this research are:

1. To investigate the effects of bridge parameters on distortion induced stresses
2. To investigate the effects of bridge parameters on lateral load distribution factor.

1.4 Scope of Works

The scopes of this research are:

1. The number of girders in composite I-girder bridges is three.
2. Truck types include AASHTO HS20-44 and Thai truck.

1.5 Methodology

Methodologies of the research are:

1. Perform the literature review on the bridge parameters that influence the lateral load distribution and the distortion-induced fatigue.
2. Using SAP2000, implement the finite element analysis of composite I-girder steel bridges to determine LDF and distortion-induced stress in the web gap area. The global finite element model will be validated with field test data.
3. Perform a parametric study on the relative girder deflections and distortion-induced stress.
4. Derive the formula for the relative displacement and out-of-plane stresses as a function of bridge parameters and truck loadings.
5. Prepare a research report and technical paper for publication.

CHAPTER II

LITERATURE REVIEW

The technical literature documented past problems associated with damage from distortion-induced fatigue in steel bridges. There are two main categories of this technical literature documentation. The first category is the most previous research, includes field observation of the causes of distortional stresses, extent of fatigue damage and characteristics common to affected bridges. The second category explores the sources of distortional stresses used laboratory experiments. Both research categories has prompted design code changes and proposed design guidelines for future structures. The understanding of the nature and severity of the distortional fatigue problem was improved from the research documented in the literature, and the observations have provided guidance on the maintenance and design of composite I-steel girder bridges. Computer finite element model analysis was also used to observe the susceptible details and to provide information about repair investigations and field tests.

2.1 Lateral Load Distribution

An important issue of bridge design is lateral load distribution factor. It shows the maximum moment and shear of each girder due to live load in the concrete slab. The effect of bridge parameters on lateral load distribution factor is critical in order to know the maximum moment distribution in the bridge structure. The maximum moment in a girder is obtained by multiplying the moment from a one-dimensional bridge analysis by the value obtained from the LDF equation.

Since the 1930s, the AASHTO simple S/D formula has been used for live load distribution factors in most common case, where S = girder spacing and D = a constant that depends on the type of the bridge superstructure and the number of lane loaded. It can be found in AASHTO's Standard Specification (AASHTO, 1996). LDF for concrete slab on steel girder with two or more design lanes loaded is:

$$LDF = \frac{S}{5.5} \quad (\text{US customary unit})$$

$$LDF = \frac{S}{1676} \quad (\text{SI unit})$$
(2.1)

where S = girder spacing.

The above formula shows the valid results only for typical geometry but loses its accuracy when the bridge parameters are varied. In addition, the formulas do not include the effects of bridge skewness (Zokaie 1991). To improve the S/D formula, The National Cooperative Highway Research Program (NHRCP) 12-26 project develops the AASHTO-LRFD (AASHTO 1994) live load distribution. Additional parameters that were included in this new formula are the bridge span (L), slab thickness (t_s), girder spacing (S), and longitudinal stiffness parameter (K_g). But it should be realized that the formulas were developed based on the models with uniform girder spacing, beam inertia, and skew angle. The continuous models with equal spans and the diaphragm effects are not included in this study.

Mabsout el al (1997) obtained the lateral load distribution factor by dividing the maximum moment from finite element analysis model by the maximum moment found in simply supported beam. Using the same methods, Zokaie (2000) presented the formula for moment distribution to interior girders in bridges with two or more lanes:

$$LDF = 0.15 + \left(\frac{S}{2895} \right)^{0.6} \left(\frac{S}{L} \right)^{0.2} \left(\frac{K_g}{L t_s^2} \right)^{0.1}$$
(2.2)

Where S = girder spacing (mm); L = span length (mm); $K_g = n(I + Ae^2)$ = longitudinal stiffness (mm⁴); t_s = slab thickness (mm); n = modular ratio between steel and concrete; I = girder stiffness (mm⁴); A = girder area (mm²); and e = eccentricity between *centroids* of girder and slab (mm).

AASHTO LRFD specification (1998) introduced lateral load distribution factor for all type of the bridge. This equation based on finite element and statistical analysis of the large number of bridges. The LDF for interior girder with two or more lanes for beam and slab bridges is given by

$$LDF = 0.075 + \left(\frac{S}{2900}\right)^{0.6} \left(\frac{S}{L}\right)^{0.2} \left(\frac{K_g}{Lt_s^2}\right)^{0.1} \quad (2.3)$$

Where S = girder spacing (mm); L = span length (mm); $K_g = n(I + Ae^2)$ = longitudinal stiffness (mm^4); t_s = slab thickness (mm); n = modular ratio between steel and concrete; I = girder stiffness (mm^4); A = girder area (mm^2); and e = eccentricity between *centroids* of girder and slab (mm).

Lateral distribution factor above only can be used for type of bridge with concrete deck, filled grid or partially filled grid on steel or concrete beams, concrete, concrete T-beams, T- and double T- section.

The equation above is applicable for the bridge with width between 1100 mm and 4900 mm, length of the bridge is between 6 m and 73 m, and the slab thickness between 110 mm and 300 mm.

Sotelino et al (2004) proposed a new simplified LDF equation, based on the AASHTO LRFD LDF equation, and the longitudinal stiffness parameter included through its relationship to the span length:

$$LDF = 0.15 + 0.042 \frac{S^{0.8}}{L^{0.3}} \exp\left(\frac{L}{180,000}\right) \quad (2.4)$$

where S = girder spacing (mm) and L = span length (mm).

Another simplified method was developed for the calculation of the distribution factors of live load moment by a former engineer of the Structure Division of the Tennessee Department of Transportation (TDOT), namely Henry Derthick. This method was used in Tennessee since 1963 where it requires only the information on the width of the roadway, number of traffic lanes, number of beam lines, and the multiple-presence factor of the bridge. The LDF from this method is very close to the AASHTO LRFD LDF equation in the variation of span length, beam spacing, slab thickness, and beam stiffness (Zhu et al. 2004)

Another attempt to further develop these formulas was done by Phuvoravan (2006) when he studied the sensitivity of the LDF parameter. The purpose was to eliminate parameters for which the LDF is not as sensitive as others and also those that require iterative design procedure. From the results of this study, girder spacing and span length was found to influence the LDF value, while the slab thickness and the longitudinal stiffness parameter could be eliminated. The new simplified formula:

$$\sigma_{wg} = 0.15 + \frac{S^{0.8}}{85L^{0.16}} \quad (2.5)$$

where S = girder spacing (mm) and L = span length (mm).

The parameters used in the study include those given in the lateral load distribution factor (LDF) equation (AASHTO, 1998). The LDF equation for beam and slab bridges with two or more lanes is:

$$LDF = 0.075 + \left(\frac{S}{2900} \right)^{0.6} \left(\frac{S}{L} \right)^{0.2} \left(\frac{K_g}{Lt_s^3} \right)^{0.1} \quad (2.6)$$

where S = girder spacing (mm); L = span length (mm); $K_g = n(I + Ae^2)$ = longitudinal stiffness (mm^4); t_s = slab thickness (mm); n = modular ratio between steel and concrete; I = girder stiffness (mm^4); A = girder area (mm^2); and e = eccentricity between centroids of girder and slab (mm). The above equation is applicable for the bridge having the width between 1100 mm and 4900 mm, the length between 6 m and 73 m, and the slab thickness between 110 mm and 300 mm.

2.2 Out-of-Plane Bending Mechanism

Since live loads in the bridges do not distribute uniformly to the entire slab, there is a difference in displacement between adjacent girders. The differential vertical displacement between adjacent girders can cause the torsional moment on the girder and rotation of the diaphragm. Assuming that the connection between girder and concrete slab are rigid, the flexural moment in the connection between girder and diaphragm can be calculate when the relative displacement of the girder is known. Repetitive live loads especially heavy vehicles causes fatigue crack damage in welded areas subjected to secondary or distortion-induced fatigue (Nishikawa et al. 1998). Figure 2.1 shows a fatigue crack in the web gap area.

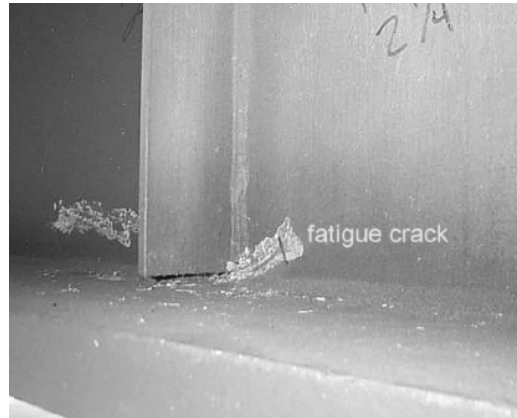


Figure 2.1 Fatigue crack in the web gap near bottom flange of a girder (Zhou, 2005)

The field measurement data from Cousin et al. (1998) shows that the stress occurring in the connection plate to the web welds and flange radius on the original welded connections are large enough to cause fatigue cracking. The fatigue cracking was caused by out-of-plane distortion usually occurring at locations where transverse structural components such as floor-beams, diaphragms and cross-frames are connected by connection plates to the longitudinal girders (Roddiss and Zhao, 2001). In Japan, the most common cracks occur at the top end of vertical stiffener welded to the top flange. Some web cracks also exist at the fillet-weld toe connecting the web and the top flange of the main girder. These cracks were caused mainly by secondary stresses due to both the relative deflection of the main girders and the deflection of the RC deck by the wheel load of heavy traffic (Nishikawa et al, 1998).

Jajich and Schultz (2003) give a simple technique for predicting web-gap stress using the basic concepts for linear, elastic systems, as shown in figure 2.2. Treating the web gap as a beam that is fixed at both ends and undergoing rotation at one end, the maximum moment at the base of web gap $M_{wg} = 4EI_{wg} \frac{\theta}{g}$ is obtained, where E = modulus of elasticity; I_{wg} = moment of inertia of web gap section resisting out-of-plane bending; and g = web-gap length. Hence, the maximum stress at the stiffener end of the web gap is $\sigma_{wg} = 0.5M_{wg} t_w / I_{wg}$ where t_w = web thickness. Combining these expressions and substituting the diaphragm rotation $\theta = \Delta/L$ where L = length of diaphragm and Δ = displacement adjacent girder, gives the maximum web gap stress as a function of girder differential deflections $\sigma_{wg} = (2Et_w/g)/(\Delta/L)$.

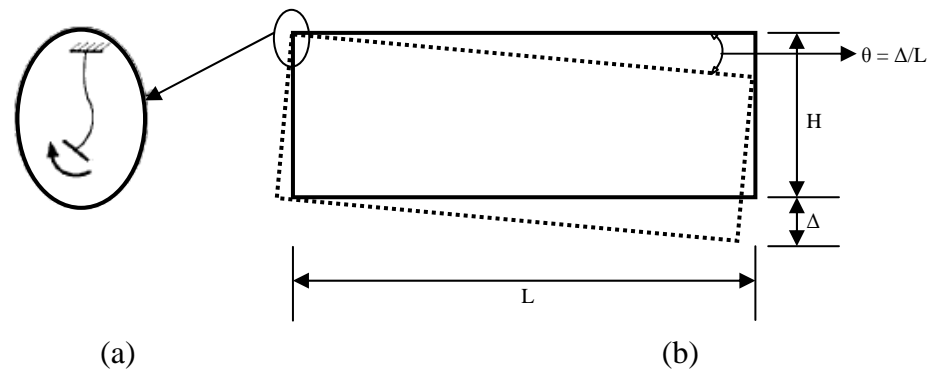


Figure 2.2 Schematic representation of web gap rotation (a).web-gap rotation
(b).diaphragm rotation (Jajich and Schultz, 2003)

Figure 2.3 shows the diaphragm rotation and the web gap deflection according to Fisher et al (Li and Schultz, 2005), web gaps are postulated to behave much like short, fixed-fixed beams undergoing lateral deflection, δ , without end rotations. Neglecting the component of stress due to rotation at one end of the web gap under this assumption, the maximum out-of-plane web gap stress, σ_{wg} , is

$$\sigma_{wg} = \left(\frac{3Et_w}{g^2} \right) \left(\frac{h\Delta}{S} \right) \quad (2.7)$$

where E is Young's Modulus, t_w is the thickness of the web, h is the depth of the diaphragm, S is the girder spacing, g is the length of the web gap and Δ is the differential deflection between adjacent girders, as shown in figure below.

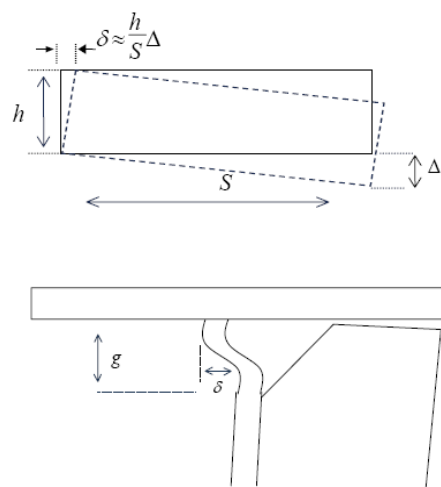


Figure 2.3 Diaphragm rotation and the web gap deflection according to Fisher et al.(1990)

The amount of differential deflection between two adjacent girders, Δ , cannot be easily predicted because the transverse interaction of concrete decks, reinforcement, girders, and diaphragms are difficult to predict without detailed finite element analysis. Berglund and Schultz (2006) investigated the parameter which significantly causes girder differential deflection. Generally, differential deflection decreases as the bridge span length increases but increases as the angle of skew increases, and increases with larger girder spacing.

2.3 Previous Finite Element Models

Mabsout et al. (1997) used four finite-element models to evaluate the wheel load distribution factors of steel bridges with different span length and girder spacing. They obtained the lateral load distribution factor by dividing the maximum moment from finite element analysis model by the maximum moment found in simply supported beam. In the first finite element model, concrete slabs were idealized as quadrilateral shell elements and the steel girder was idealized as space frame member, as shown in figure 2.4. The second model was similar to the first model, but the rigid links were imposed to accommodate the eccentricity of the girders with respect to the slab. Figure 2.5 shows the third finite element model with idealizes the concrete slab and the girder web as quadrilateral shell elements. Girder flanges were modeled as a space frame elements, while flange to deck eccentricity was modeled by imposing a rigid links. The first, second, and third were generated by program SAP90. The fourth finite element model was developed and analyzed using the general computer program ICES-STRUDL II. The concrete was idealized using isotropic eight node brick element and the steel girder flanges and webs were modeled using quadrilateral shell element. The load distribution factor for steel girder bridges correlates well with the first and fourth finite element model.

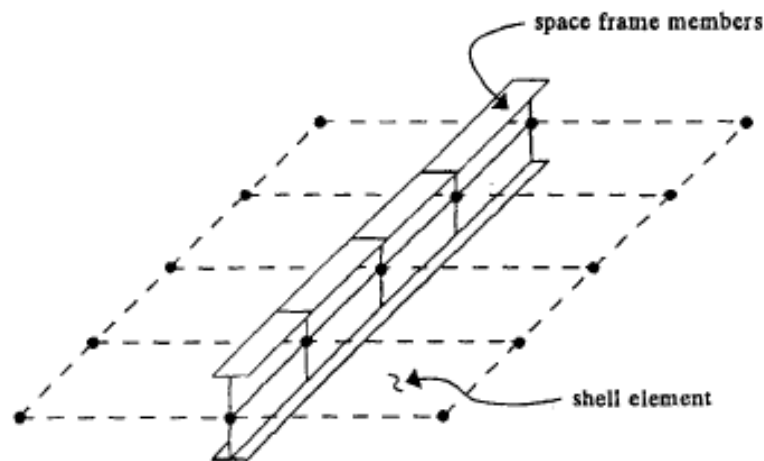


Figure 2.4 First finite element model (Mabsout et al.1997)

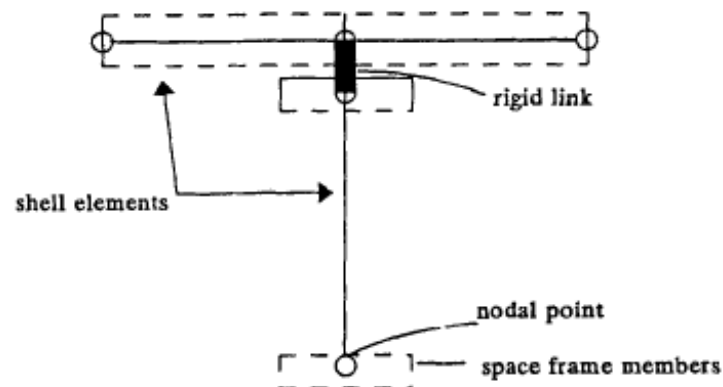
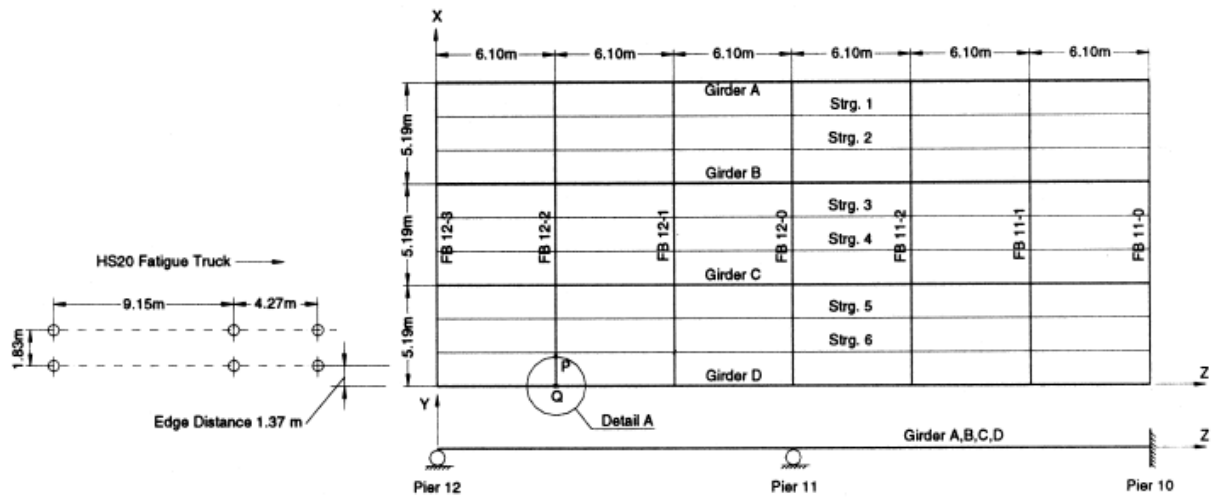


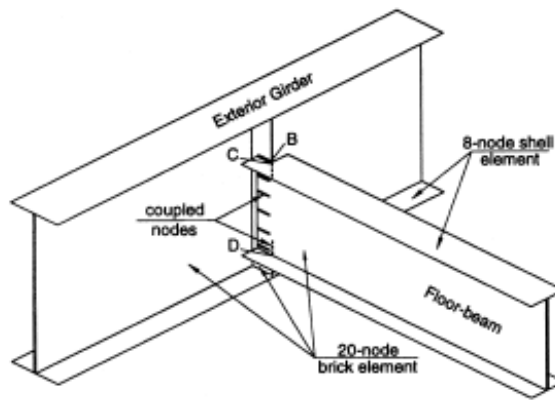
Figure 2.5 Third finite element model (Mabsout et al.1997)

Chaisomphob and Lertsima (2000) study generated bridge model using the finite element package called MARC. The quadrilateral four-node plate element was used to idealize orthotropic steel deck, concrete slab, and the steel girder including all stiffeners. The rigid link element was used to take into account the eccentricity between middle plane of concrete slab and steel flange plate of the girder.

Roddis and Zhao (2000 and 2003) presented the stick frame analysis and finite element method for modeling a bridge. The stick frame analysis was used to obtain the girder displacement. It was generated by using STAAD/Pro 3.1. The 'cut out' floor beam or truss frame to girder web was modeled using finite element program ANSYS 5.6 with the displacement from stick frame analysis as a loading. The finite element model is shown in figure 2.6 and figure 2.7.

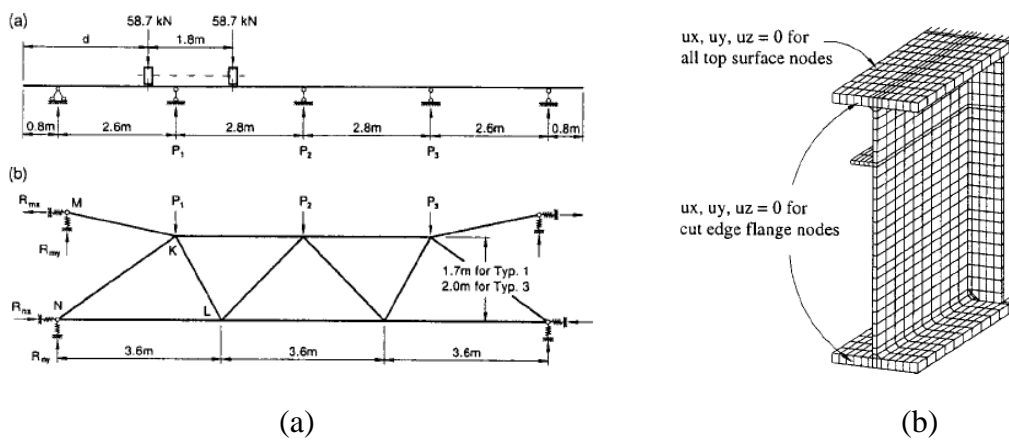


(a)



(b)

Figure 2.6 Finite element model (a) Stick frame model (b) 'cut out' truss frame to girder web model (Roddis and Zhao, 2000)



(a)

(b)

Figure 2.7 Finite element model (a) Stick frame model (b) 'cut out' truss frame to girder web model (Roddis and Zhao, 2003)

Jajich et al. (2000) and Jajich and Schultz (2003) performed a linear finite element study of a diaphragm-stiffener-web connection. A three dimension finite element model was created using SAP2000. All portions of steel (web, flanges, diaphragm, and stiffeners) were represented by shell element as shown in figure 2.8. The model consists of two adjacent girders connected by diaphragm. All dimensions were taken either directly from the bridge or from the design plan. The concrete deck was excluded in the model, but the rotational fixity of girder top flanges due to the presence of the deck was assumed. The vertical displacement from truck test data was applied to obtain the web gap strain. The mesh in the web gap area was refined to get better result, as shown in the deformed shape in figure 2.9.

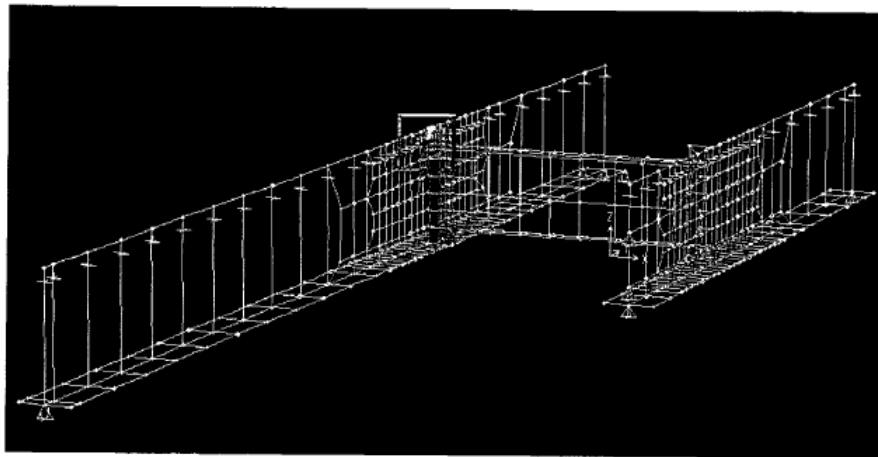


Figure 2.8 Finite element model (Jajich et al. 2000)

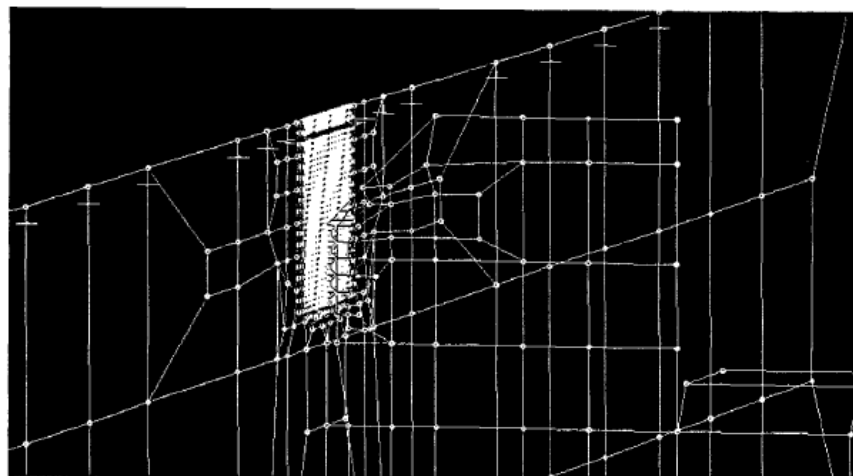


Figure 2.9 Deformed shape of web gap and stiffener (Jajich et al. 2000)

Huo et al (2004) used the finite element program ANSYS 5.7 to model the steel I-beam bridges. The deck slab was modeled by the four-node shell element with six degrees of freedom per node. The shell elements accounted both membrane and bending stiffness, including in- and out-of-plane bending. The longitudinal beams were modeled by three-dimensional two node beam element with six degree of freedom per node. The slab shell element was directly above the beam which is integrated to account for the composite action. The finite element model was used to obtain the LDF defined as the ratio of moment from finite element model and moment from single beam loaded by truck axle load.

Schultz and Li. (2005) use the truck loads reported in Jajich and Schultz (2003) field tests were simulated and applied to a so-called macro model, as shown in figure 2.10. The model included the entire bridge and a portion of the bridge surrounding the diaphragm to determine the deformations to be imposed on the bridge micro-model. Deck rotation and diaphragm deflections from macro-model finite element analyses were applied as boundary conditions for the micro-model finite element analyses at the locations where these members were disconnected from the rest of the bridge. Figure 2.11 shows the girder top flanges and the portion of the concrete deck connecting the two girder segments in the micro model as shell elements and connected by rigid elements at closely spaced intervals. The deck boundary was fixed against translation along the edges parallel to the girders. Girder differential and deck rotations from macro-model were applied to the micro-model to determine the web-gap movement and stress field.

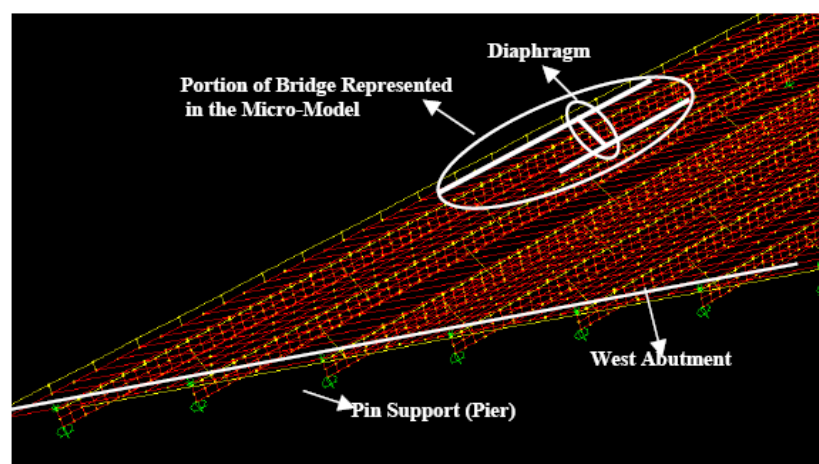


Figure 2.10 Macro model (Li and Schultz, 2005)

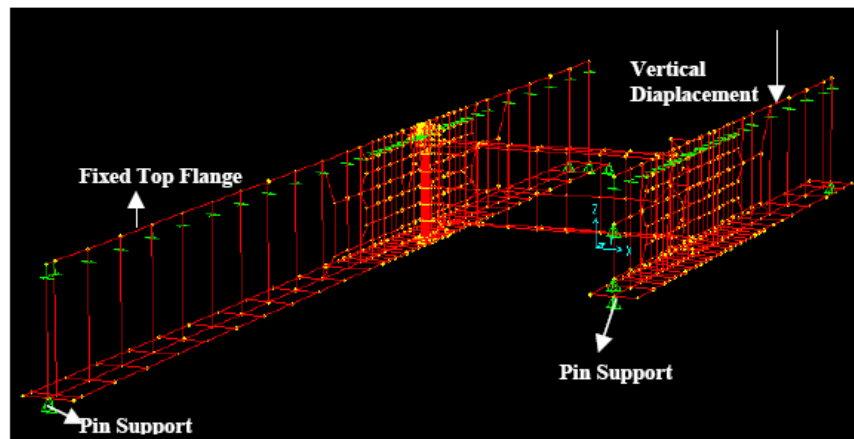


Figure 2.11 Micro model (Li and Schultz, 2005)

Another's commercial finite element software, ABAQUS was used by some researchers to model a steel I-beam bridge, as shown in figure 2.12, 2.13, and 2.14. The concrete deck was modeled by eight node shell element (ABAQUS S8R), while the steel girder is modeled by three nodes Timoshenko beam element (ABAQUS B32/B33). The full composite action between the centroid of the girder and the midsurface of the slab was modeled by rigid links (ABAQUS MPC). The bearing was modeled by assigning boundary conditions to the grounded spring elements (ABAQUS SPRING1) (Sotelino et al. 2004; Phuvoravan, 2006; and Chung et al, 2006)

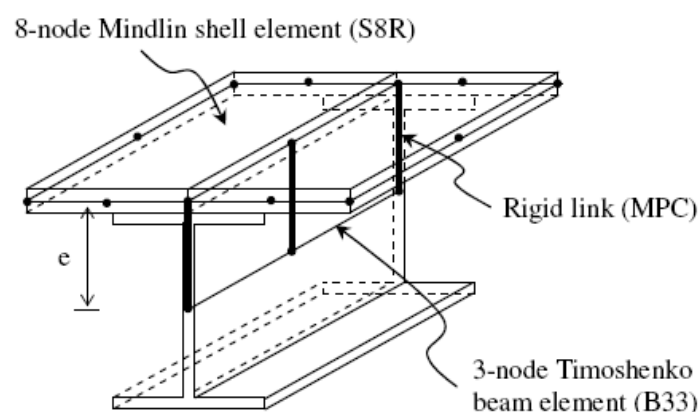


Figure 2.12 Finite element model (Phuvoravan, 2006)

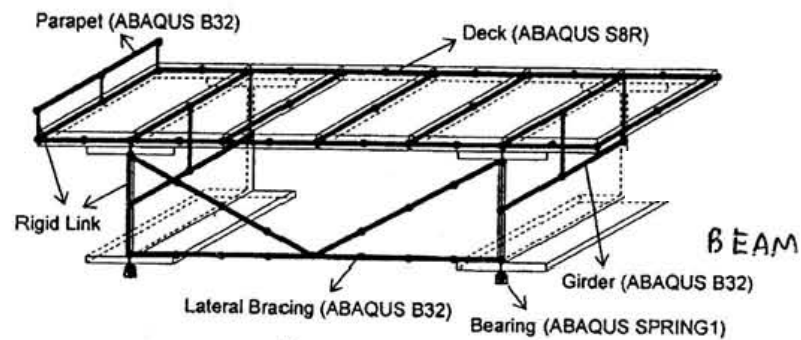


Figure 2.13 Finite element model (Chung et al, 2006)

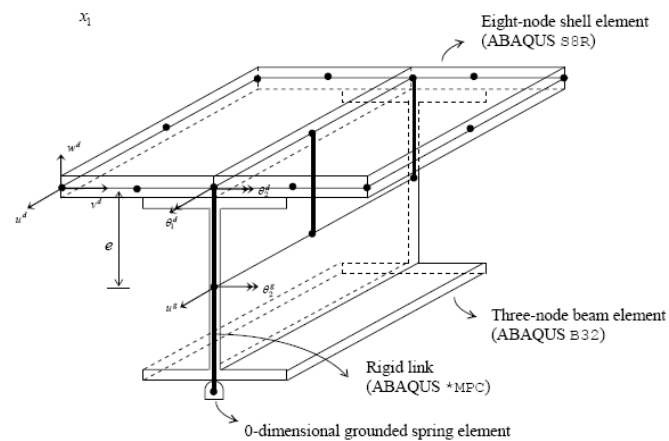


Figure 2.14 Finite element model (Sotelino et al, 2004)

Chung and Sotelino (2005) investigate the finite element model of composite bridge using ABAQUS. Four girder's modeling techniques were generated and comparison in displacement incompatibility and geometric modeling errors was investigated. The G1 model is a detailed model of a steel girder. The flanges and the web are modeled by shell elements as shown in figure 2.15 (a). The next model, G2, is similar to the G1 model except that the flange is modeled by beam elements instead of shell elements, as shown in figure 2.15 (b). As shown in figure 2.15 (c), the G3 model is proposed here to investigate the possible incompatibility at the element connection between web and flanges found in the previous two models. The G4 model is the simplest model and utilizes beam elements with the geometric properties of girder sections. This model is shown in figure 2.15 (d).

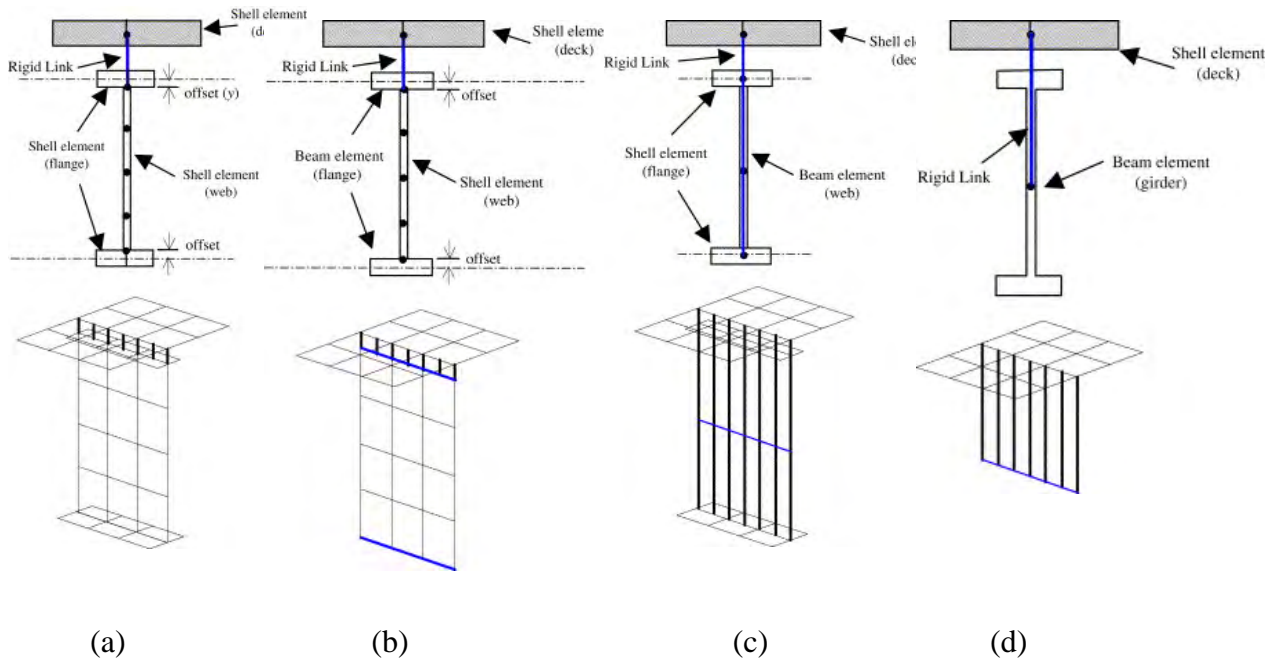


Figure 2.15 Girder's model techniques (Chung and Sotelino, 2006)

The study result the beam model (d) has been identified as the most economical model among all studied models, since this model is capable of accurately predicting the flexural behavior of girder bridges, including deflection, strain, and lateral load distribution.

Berglund and Schultz (2006) used SAP2000 Nonlinear to create a three dimensional model of the entire bridge with shell element was selected to idealize deck and girder webs and frame elements chosen to modeling girder flanges and integral concrete edge rails. Rigid links were used to connect members meant to exhibit composite behavior. As shown in figure 2.16, girder webs were modeled with two shell elements providing the joints on which the diaphragms could be connected. Deck mesh discretization was modified between different bridge models to accommodate the exact lateral location for lane loading.

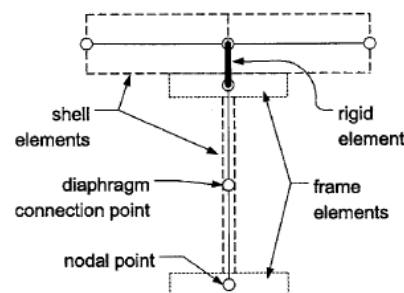


Figure 2.16 Partial cross section through FE model (Berglund and Schultz 2006)

CHAPTER III

THEORETICAL BACKGROUND

3.1 Introduction to Fatigue

Most of the structural components subjected to repeated fluctuating loads whose magnitude under monotonic loading is way below the fracture load. The process cumulative damage in environment that is caused by this load is called fatigue. Fatigue damage of the components subjected to normally elastic stress fluctuations occurs at regions of the stress (strain) raisers where the localized stress exceeds the yield stress of the material. After a certain number of load fluctuations, the accumulated damage causes the initiation and subsequent propagation of a crack, or cracks in the plastically damaged regions. The parameters affecting the fatigue performance include stress (load), geometry, and properties of the component, and external environment (Barsom and Rolfe, 1999).

LRFD Specifications categorizes fatigue as either “load induced” or “distortion induced”. Load induced is a “direct” cause of loading. Distortion induced is an “indirect” cause in which the force effect, normally transmitted by a secondary member, may tend to change the shape of, or distort, the cross section of a primary member.

3.1.1 Load-Induced Fatigue

LRFD Article 6.6.1.2 provides the framework to evaluate load-induced fatigue. Load-induced fatigue is determined by the following:

1. the stress range induced by the specified fatigue loading at the detail under consideration;
2. The number of repetitions of fatigue loading a steel component will experience during its 75-year design life. This is determined by using anticipated truck volumes; and
3. The nominal fatigue resistance for the Detail Category being investigated.

LRFD grouping details that is vulnerable to load-induced fatigue into eight categories base on fatigue resistance.

3.1.2 Distortion-Induced Fatigue

LRFD Article 6.6.1.3 provides specific detailing practices for transverse and lateral connection plates intended to reduce significant secondary stresses that could induce fatigue crack growth. The provisions of the *LRFD Specifications* are concise and direct requiring no mathematical computation.

Out of plane distortion-induced stresses are not quantified in the AASHTO design code. Unless appropriate finite-element analysis or field testing is conducted, secondary stress cannot be determined because the connection stiffener to girder flange and web intersection is under complex, three dimensional structural interaction, and the local geometry and relative stiffness of this detail are different for individual bridge (Roddis and Zhao, 2003).

3.2 Finite Element Types

This research is using SAP2000 (Computer and Structure, 2000) to construct the finite element model. SAP2000 is a general civil engineering finite element analysis package developed by Computers & Structures Inc.

3.2.1 3D Beam Element

3D element bar allows six degrees of freedom per node, three translations and three rotations as shown in figure 3.1. The w and θ_y degree of freedom account for lateral deflection in the zx plane. The θ_x is degree of freedom account for twist about the x axis. Which the stiffness coefficient is GK/L , where K is a property of the shape and size of the cross section.

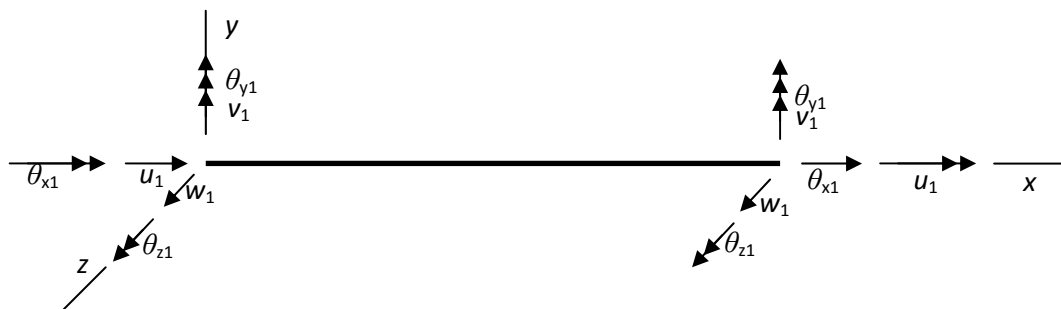


Figure 3.1 Beam element on the x axis of a rectangular coordinate system (Computer and Structure, 2000)

SAP2000 frame element uses as a general, three-dimensional, beam-column formulation includes the effects of biaxial bending, torsion, axial deformation, and biaxial shear deformation. A frame element is modeled as a straight line connecting two joints. Each element has its own local coordinate system for interpreting output

and defining section properties and loads. It normally activates all six degrees of freedom at both of its connected joints.

3.2.2 Shell Element

A shell structure carries loads in all directions, and therefore undergoing bending and twisting, as well as in-plane deformation. The most direct way to obtain a shell element is to combine a membrane element and a bending element. The membrane elements handle the *membrane* or in-plane effects, while the plate elements are used to handle *bending* or out-plane effects. The resulting element is flat and locally has five or six degrees of freedom per node, depending on whether or not the shell normal rotation at node present in the plane stress element, as shown in figure 3.2.

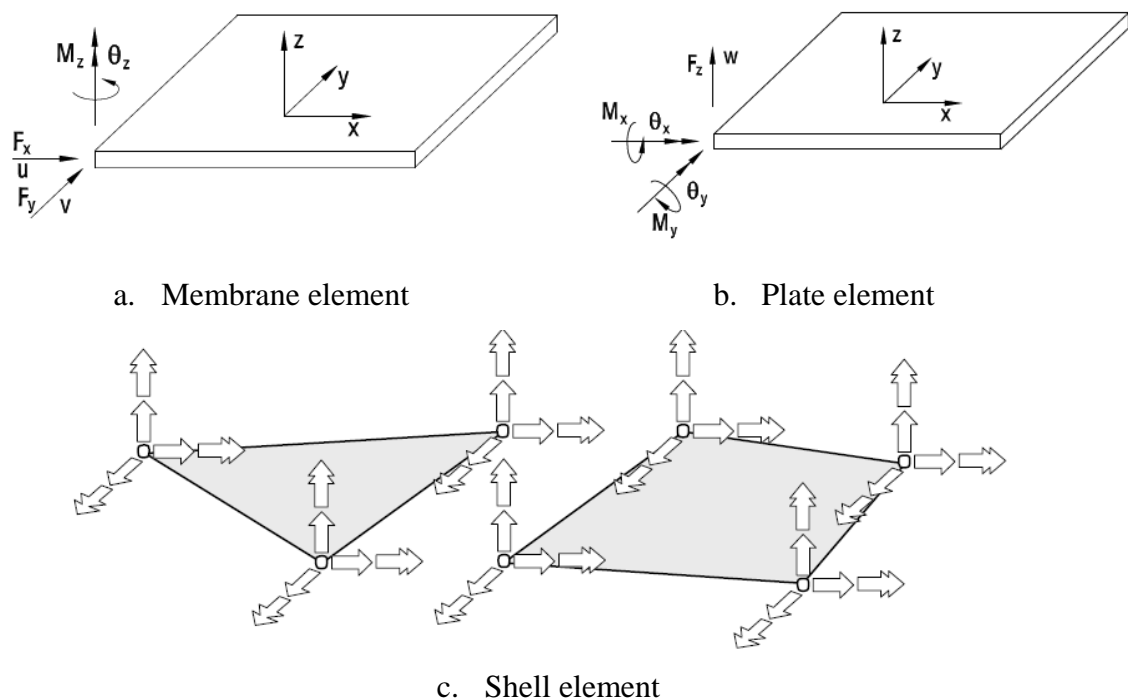


Figure 3.2 Degree of freedom (a) Membrane element (b) Plate element
(c) Shell element (Computer and Structure, 2000)

SAP2000 shell element is a three or four node formulation that combines separate membrane and plate-bending behavior. The membrane behavior uses an isoparametric formulation that includes translational in-plane stress stiffness component and a rotational stiffness component in the direction normal to the plane of the element. The plate-bending behavior includes two-way, out-of-plane, plate

rotational stiffness components and a translational stiffness component in the direction normal to the plane of the element. The shell element always activates all six degrees of freedom at each of its connected joints. Each shell element may have quadrilateral or triangular shapes.

3.3 Multiple Linear Regression in Matrix Form

The model of simple linear regression is

$$Y_i = \beta_0 + \beta_1 X_i + \varepsilon_i \text{ where } \varepsilon_i \text{ is independent } N(0, \sigma^2) \text{ and } i = 1, \dots, n$$

The model can be rewritten as

$$\begin{aligned} Y_1 &= \beta_0 + \beta_1 X_1 + \varepsilon_1 \\ Y_2 &= \beta_0 + \beta_1 X_2 + \varepsilon_2 \\ &\vdots \\ Y_n &= \beta_0 + \beta_1 X_n + \varepsilon_n \end{aligned} \tag{3.1}$$

In matrix terms, let $\mathbf{Y} = \mathbf{X}\boldsymbol{\beta} + \boldsymbol{\varepsilon}$, which is

$$\begin{bmatrix} Y_1 \\ Y_2 \\ \vdots \\ Y_n \end{bmatrix} = \begin{bmatrix} 1 & X_1 \\ 1 & X_2 \\ \vdots & \vdots \\ 1 & X_n \end{bmatrix} \begin{bmatrix} \beta_0 \\ \beta_1 \end{bmatrix} + \begin{bmatrix} \varepsilon_1 \\ \varepsilon_2 \\ \vdots \\ \varepsilon_n \end{bmatrix} = \begin{bmatrix} \beta_0 + X_1\beta_1 + \varepsilon_1 \\ \beta_0 + X_2\beta_1 + \varepsilon_1 \\ \vdots \\ \beta_0 + X_n\beta_1 + \varepsilon_1 \end{bmatrix} \tag{3.2}$$

Note $\mathbf{E}(\mathbf{Y}) = \mathbf{E}(\mathbf{X}\boldsymbol{\beta} + \boldsymbol{\varepsilon}) = \mathbf{E}(\mathbf{X}\boldsymbol{\beta}) + \mathbf{E}(\boldsymbol{\varepsilon}) = \mathbf{X}\boldsymbol{\beta}$ since $\mathbf{E}(\boldsymbol{\varepsilon}) = \mathbf{0}$ and $\mathbf{X}\boldsymbol{\beta}$ are constants.

It can be shown that β_0 and β_1 can be found from solving the “normal equations”:

$$n\beta_0 + \beta_1 \sum_{i=1}^n X_i = \sum_{i=1}^n Y_i \tag{3.3}$$

$$\beta_0 \sum_{i=1}^n X_i + \beta_1 \sum_{i=1}^n X_i^2 = \sum_{i=1}^n X_i Y_i \tag{3.4}$$

The normal equations can be rewritten as $\mathbf{X}^T \mathbf{X}\boldsymbol{\beta} = \mathbf{X}^T \mathbf{Y}$, where $\boldsymbol{\beta} = \begin{bmatrix} \beta_0 \\ \beta_1 \end{bmatrix}$.

It was shown that

$$\mathbf{X}^T \mathbf{Y} = \begin{bmatrix} 1 & 1 & \cdots & 1 \\ X_1 & X_2 & \cdots & X_n \end{bmatrix} \begin{bmatrix} Y_1 \\ Y_2 \\ \vdots \\ Y_n \end{bmatrix} = \begin{bmatrix} \sum_{i=1}^n Y_i \\ \sum_{i=1}^n X_i Y_i \end{bmatrix} \quad (3.5)$$

$$\mathbf{X}^T \mathbf{X} = \begin{bmatrix} 1 & 1 & \cdots & 1 \\ X_1 & X_2 & \cdots & X_n \end{bmatrix} \begin{bmatrix} 1 & X_1 \\ 1 & X_2 \\ \vdots & \vdots \\ 1 & X_n \end{bmatrix} = \begin{bmatrix} n & \sum_{i=1}^n X_i \\ \sum_{i=1}^n X_i & \sum_{i=1}^n X_i^2 \end{bmatrix} \quad (3.6)$$

Thus, $\mathbf{X}^T \mathbf{X} \boldsymbol{\beta} = \mathbf{X}^T \mathbf{Y}$ can be written as

$$\begin{bmatrix} n\beta_0 + \beta_1 \sum_{i=1}^n X_i \\ \beta_0 \sum_{i=1}^n X_i + \beta_1 \sum_{i=1}^n X_i^2 \end{bmatrix} = \begin{bmatrix} \sum_{i=1}^n Y_i \\ \sum_{i=1}^n X_i Y_i \end{bmatrix} \quad (3.7)$$

Suppose both sides of $\mathbf{X}^T \mathbf{X} \boldsymbol{\beta} = \mathbf{X}^T \mathbf{Y}$ are multiplied by $(\mathbf{X}^T \mathbf{X})^{-1}$ Then

$$(\mathbf{X}^T \mathbf{X})^{-1} \mathbf{X}^T \mathbf{X} \boldsymbol{\beta} = (\mathbf{X}^T \mathbf{X})^{-1} \mathbf{X}^T \mathbf{Y}$$

$$\mathbf{I} \boldsymbol{\beta} = (\mathbf{X}^T \mathbf{X})^{-1} \mathbf{X}^T \mathbf{Y}$$

$$\boldsymbol{\beta} = (\mathbf{X}^T \mathbf{X})^{-1} \mathbf{X}^T \mathbf{Y}$$

Therefore, using matrix algebra, $\boldsymbol{\beta} = (\mathbf{X}^T \mathbf{X})^{-1} \mathbf{X}^T \mathbf{Y}$

$$\boldsymbol{\beta} = \begin{bmatrix} n & \sum_{i=1}^n X_i \\ \sum_{i=1}^n X_i & \sum_{i=1}^n X_i^2 \end{bmatrix}^{-1} \begin{bmatrix} \sum_{i=1}^n Y_i \\ \sum_{i=1}^n X_i Y_i \end{bmatrix}$$

$$\boldsymbol{\beta} = \begin{bmatrix} \bar{Y} - \beta_1 \bar{X} \\ \frac{\sum (X_i - \bar{X})(Y_i - \bar{Y})}{\sum (X_i - \bar{X})^2} \end{bmatrix} \quad (3.8)$$

In order to validate the regression result, analysis of variance results is used. These can be rewritten using matrices:

$$SSTO = \text{Total Sum of Square} = \sum_{i=1}^n (Y_i - \bar{Y})^2 \quad (3.9)$$

$$SSE = \text{Error Sum of Square} = \sum_{i=1}^n e_i^2 = \sum_{i=1}^n (Y_i - \hat{Y})^2 \quad (3.10)$$

$$SSR = \text{Regression Sum of Square} = \beta' X' Y - \frac{1}{n} Y' J Y = SSTO - SSE \quad (3.11)$$

$$\text{Regression Coefficient of determination} = R^2 = \frac{SSR}{SSTO} \quad (3.12)$$

CHAPTER IV

FINITE ELEMENT STUDY

4.1 Overview

A linear finite element study of the bridge was undertaken to investigate the lateral moment distribution and differential deflection stress mechanism. The whole bridge was modeled in order to determine longitudinal moment in the girders and observe the stresses around web gap area. To accommodate both problems, dual level analysis was conducted. Two level of finite element analysis consist of global model as shown in figure 4.1, which is the modeled hole of the bridge, and submodel, which is a more detailed model of the bridge, was shown in figure 4.2. Both global model and submodel were studied using SAP2000 software package.

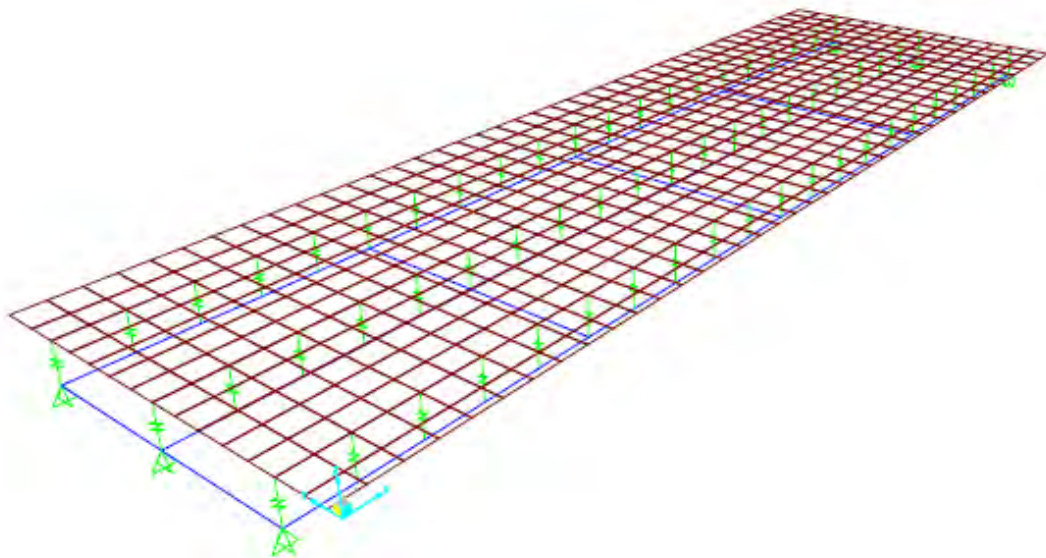


Figure 4.1 Global model

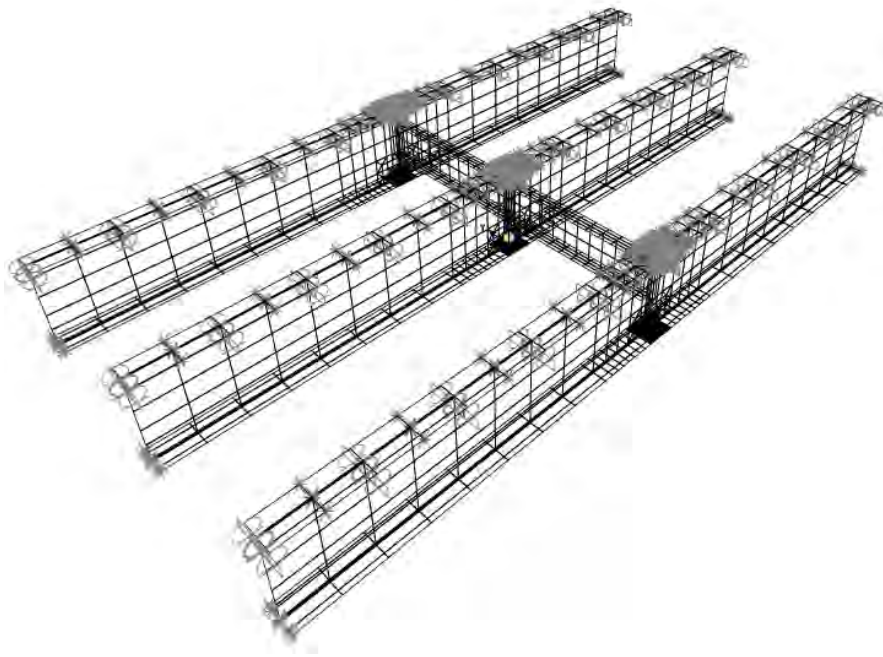


Figure 4.2 Sub model

4.2 Model Verification

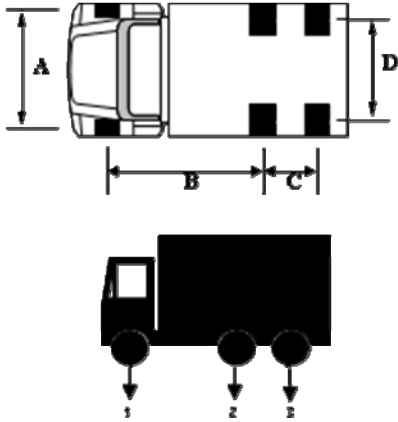
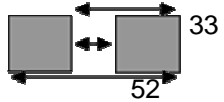
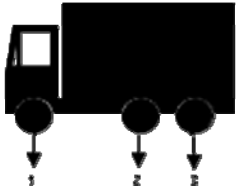
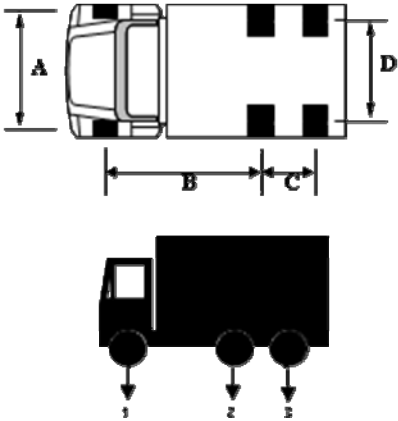
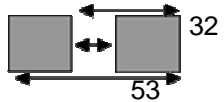
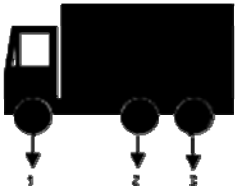
4.2.1 Field Test Data

4.2.1.1 Bridge Dimension

Field test data were collected from three highway bridges in Bangkok and all of them are a multi-girder composite I-girder. They are Prachanukul Bridge, Wongsawang Bridge, and Bangplad Bridge. However, the data from Wongsawang bridge were chosen in this study. The bridge span is 25 m with two traffic lanes and three girders. The concrete slab has a thickness of 200 mm with lane width 3.25 m. All three girders have the same dimension, built up wide flange 1450×450×12×22. This span has two types of lateral diaphragm, beam diaphragm and truss diaphragm as shown in figure 4.3.

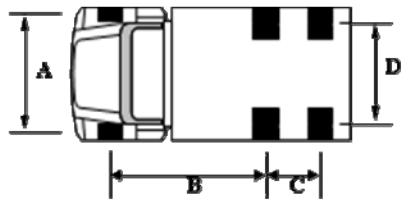
4.2.1.2 Truck Loadings

In the field test, three cases of static loadings were applied to the bridge. The truck moved and stopped every 5 m along the bridge span. Three cases are one truck on left lane, one truck on right lane, and two trucks on both lanes with same longitudinal position, as shown in figure 4.4. Approximately 25 ton truck weight was used in this field test. Distribution of wheel load is shown in table 4. 1.

Table 4.1 Truck Properties (Wongsawang In Bound)				
Truck Properties	Truck No.			
	Truck Dimension (m)	Wheel Dimension		
	A = 1.93	X = 0.21		
	B = 4.17	Y = 0.33		
	C = 1.30			
	D = 1.80			
	Weight (Tons)	Left	Right	
		Sum		
	Axle 1	3.005	3.005	6.01
	Axle 2	4.900	4.900	9.80
	Axle 3	4.675	4.675	9.35
	Total	25.16		Tons
	Truck Dimension (m)	Wheel Dimension		
	A = 1.93	X = 0.20		
	B = 4.18	Y = 0.32		
	C = 1.30			
	D = 1.85			
	Weight (Tons)	Left	Right	
		Sum		
	Axle 1	3.205	3.205	6.41
	Axle 2	4.930	4.930	9.86
	Axle 3	4.375	4.375	8.75
	Total	25.02		Tons

Truck Properties

Truck No. 3

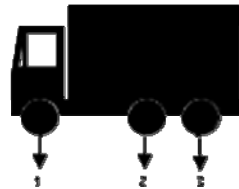
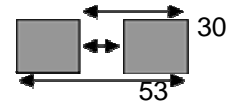


Truck Dimension (m)

A =	<u>1.78</u>
B =	<u>3.65</u>
C =	<u>1.33</u>
D =	<u>1.70</u>

Wheel Dimension

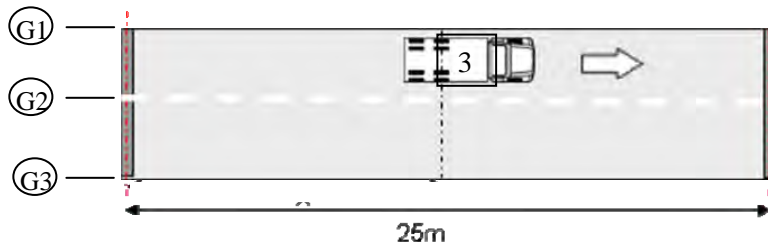
X =	<u>0.21</u>
Y =	<u>0.32</u>



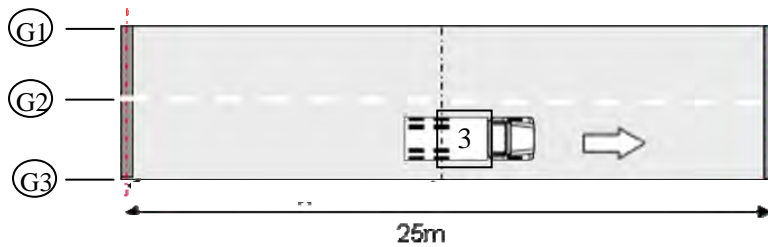
Weight (Tons)

	Left	Right	Sum
Axle 1	2.785	2.785	5.57
Axle 2	4.970	4.970	9.94
Axle 3	4.755	4.755	9.51
Total			25.02

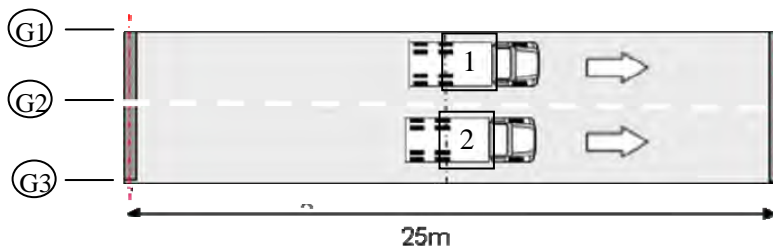
Tons



(a)



(b)



(c)

Figure 4.4 Truck loading cases in the field test (a) one truck on left lane (b) one truck on right lane (c) two trucks on both lanes.

4.2.1.3 Field Test Data

Static cases test results stresses in the girder's bottom flange. The strain gages placed in $\frac{1}{4}$ span, $\frac{1}{2}$ span, and $\frac{3}{4}$ span for the purpose of verifying the finite element model, static load results by a truck 10 m from the edge was considered, as shown in table 4.2.

Table 4.2 Field test data

Bridge	Truck loading case	Strain gage	Stress result (MPa)		
			G1	G2	G3
Wongsawang	Case (a) One truck on left lane	$\frac{1}{4}$ span	186	112	24
		$\frac{1}{2}$ span	242	144	38
		$\frac{3}{4}$ span	122	0	26
	Case (b) One truck on right lane	$\frac{1}{4}$ span	44	114	168
		$\frac{1}{2}$ span	60	144	226
		$\frac{3}{4}$ span	38	0	118
	Case (c) Two truck on both lanes	$\frac{1}{4}$ span	210	214	208
		$\frac{1}{2}$ span	274	280	290
		$\frac{3}{4}$ span	150	0	160

Web gap stress was also measured in field test. Because of the installation difficulties, the strain gage was placed around one inch from the end of stiffener, as shown in figure 4.5.

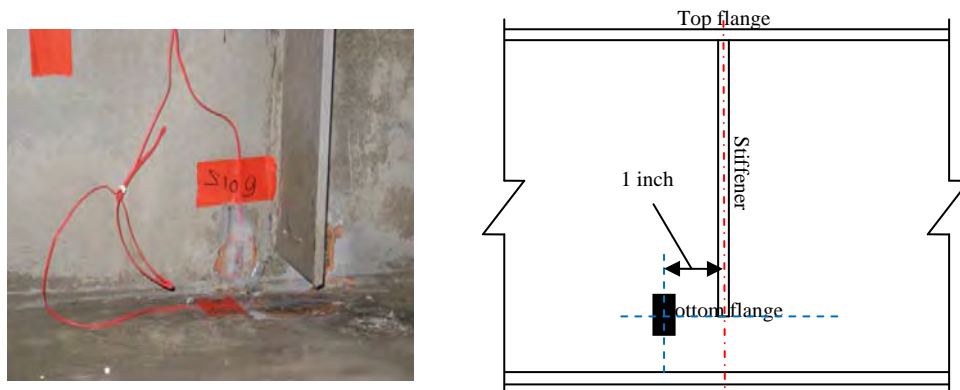


Figure 4.5 Strain gage position in web gap area.

4.2.2 Finite Element Model

4.2.2.1 Global Model

A three dimensional finite element model of the bridge was created using SAP2000 (Computer and Structures, 2000). A 25-m span of Wongsawang bridges, for which field test data were obtained, was modeled. This bridge has two types of transverse element, diaphragm as a beam element in the end and mid-span of the bridge and cross frame as a truss element in the quarter and third quarter span, as shown in figure 4.6. In the global model, the cross frame was modified to a beam element. The simple analysis is needed in order to replace the truss structure of cross frame with the frame structure having the appropriate displacement shape of the girder.

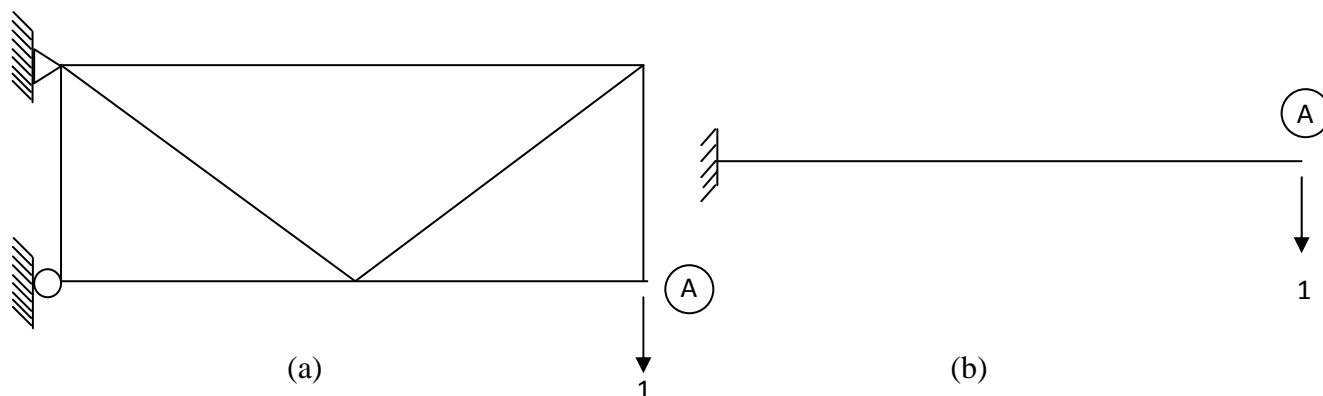


Figure 4.6 Two types of cross frame (a) Truss cross frame (b) Space frame

Figure 4.6(a) shows the cross frame of the bridge. A 1-ton static load is applied at the end of the truss. Direct stiffness method is used to determine the stiffness of the structure and the vertical displacement in joint A. This analysis only considers the vertical displacement since only this is applied in the model. Accordingly, the space frame, as shown in figure 4.6(b), must result the same value of vertical displacement. Assuming that the displacement and the loading from both structures are similar, the stiffness must be also same with the moment inertia determined. The software MATLAB 7.0 was used to analyze.

In this case, the cross frame between two girders is shown in Figure 4.7. The length for each member are $L_1 = 2880$ mm, $L_2 = 900$ mm, and $L_3 = 3017.35$ mm. The area of the section is $A_d = 1269.95$ mm², $A_h = 4101.94$ mm², and $A_v = 2000$ mm². Modulus of elasticity is 200000 MPa

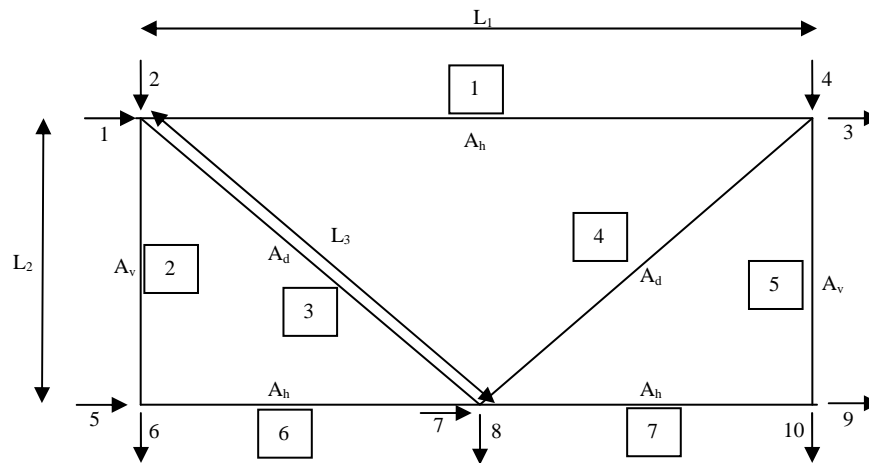


Figure 4.7 Model of truss cross frame

The cross frame structure has ten degrees of freedom, thus the stiffness of the structure becomes 10×10 matrix. The end supports of the structure are shown in Figure 4.6(a). Support in the left edge causes degree of freedom numbers 1, 2, and 5 to become zero. The reduced stiffness resulted to a smaller 7×7 matrix. The stiffness matrix of the cross frame, K_t , is

$$\mathbf{K}_t = \begin{array}{c} \begin{array}{ccccccc} & \color{red}{3} & \color{red}{4} & \color{red}{6} & \color{red}{7} & \color{red}{8} & \color{red}{9} & \color{red}{10} \\ \begin{array}{l} \color{red}{3} \\ \color{red}{6} \\ \color{red}{7} \\ \color{red}{8} \\ \color{red}{9} \end{array} \end{array} \\ \left[\begin{array}{ccccccc} \frac{A_h}{L_1} + \left(\frac{1}{2}L_1\right)^2 \frac{A_d}{L_3^3} & \frac{1}{2}L_1L_2 \frac{A_d}{L_3^3} & 0 & -\left(\frac{1}{2}L_1\right)^2 \frac{A_d}{L_3^3} & -\frac{1}{2}L_1L_2 \frac{A_d}{L_3^3} & 0 & 0 \\ \frac{1}{2}L_1L_2 \frac{A_d}{L_3^3} & \frac{A_v}{L_2} + \left(\frac{1}{2}L_1\right)^2 \frac{A_d}{L_3^3} & 0 & -\frac{1}{2}L_1L_2 \frac{A_d}{L_3^3} & \left(\frac{1}{2}L_1\right)^2 \frac{A_d}{L_3^3} & 0 & -\frac{A_v}{L_2} \\ 0 & 0 & \frac{A_v}{L_2} & 0 & 0 & 0 & 0 \\ -\left(\frac{1}{2}L_1\right)^2 \frac{A_d}{L_3^3} & -\frac{1}{2}L_1L_2 \frac{A_d}{L_3^3} & 0 & \frac{4A_h}{L_1} + 2\left(\frac{1}{2}L_1\right)^2 \frac{A_d}{L_3^3} & 0 & -\frac{2A_h}{L_1} & 0 \\ -\frac{1}{2}L_1L_2 \frac{A_d}{L_3^3} & \left(\frac{1}{2}L_1\right)^2 \frac{A_d}{L_3^3} & 0 & 0 & 2L_2^2 \frac{A_d}{L_3^3} & 0 & 0 \\ 0 & 0 & 0 & -\frac{2A_h}{L_1} & 0 & -\frac{2A_h}{L_1} & 0 \\ 0 & -\frac{A_v}{L_2} & 0 & 0 & 0 & 0 & \frac{A_v}{L_2} \end{array} \right] \begin{array}{l} \color{red}{3} \\ \color{red}{6} \\ \color{red}{7} \\ \color{red}{8} \\ \color{red}{9} \end{array}
 \end{array}$$

Based on the equilibrium equation, if 1 ton load is applied in the DOF_{10} the displacement in the DOF_{10} is 0.7535 mm.

Beam element was constructed to replace the cross frame. It was designed to have the same vertical displacement in one edge with the cross frame. Vertical displacement from analysis above was used to obtain the beam stiffness. Assume the beam with same length with L_1 , as shown in **figure 4.8**.

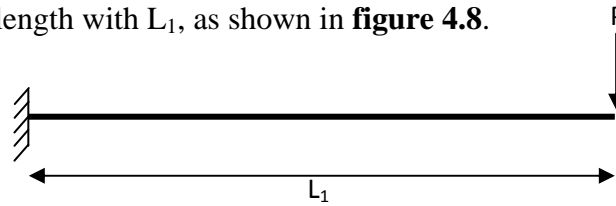


Figure 4.8 Beam element

The equilibrium of this equation is

$$P = \frac{3EI}{L_1^3} u_{10} \quad (4.1)$$

With u_{10} equal to 0.7535 mm, load 1 T and 20000 MPa modulus of elasticity result the moment inertia of the beam $5.1831 \times 10^8 \text{ mm}^4$. With trial and error the I-beam section $450 \times 190 \times 14 \times 26$ ($I = 5.182 \times 10^8 \text{ mm}^4$) was chosen to represent the truss cross frame section.

Global model consisting of main girders, diaphragms, and cross frames were idealized as frame elements and the concrete slab modeled with quadrilateral shell elements. As shown in figure 4.9, all three main girders (G1, G2, and G3) were simply supported with 2.8-m girder spacing. The bridge dimensions and material properties were similar to those of the real bridge.

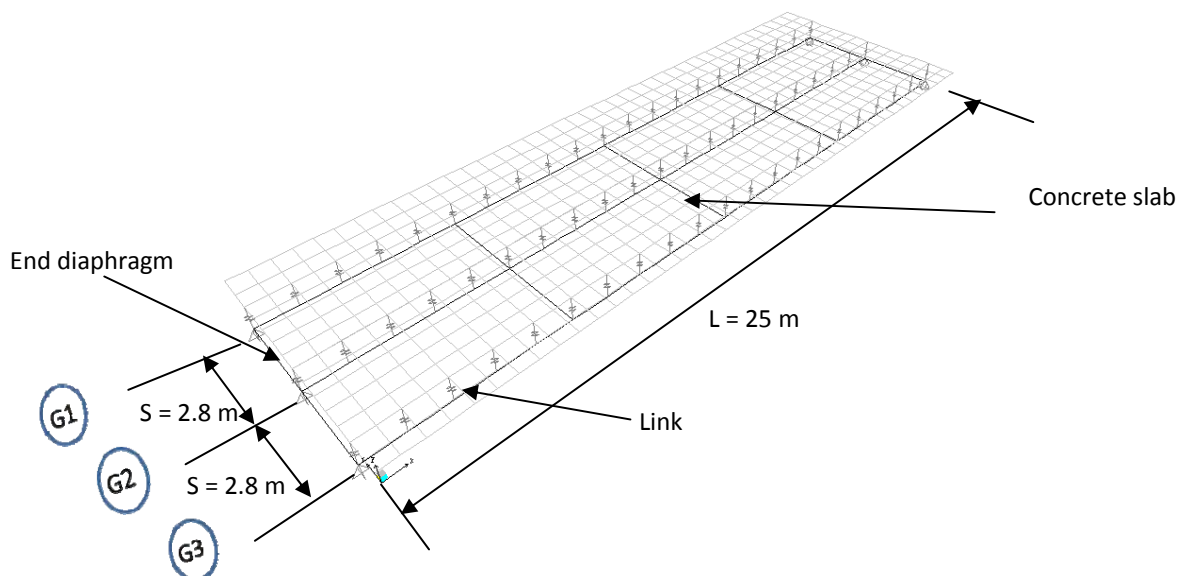


Figure 4.9 Global model of Wongsawang bridge

In the composite bridge, concrete deck and steel girder was designed to work together as one structure. All degrees of freedom of the concrete deck were distributed to the girder by shear studs.

Mabsout et al.(1997) and Chung and Sotelino (2005) used rigid links to idealize composite action of finite element model to accommodate the eccentricity between frame element and shell element as a concrete deck. This technique showed a good result for lateral distribution. The moment of the girder in this finite element model resulted to longitudinal stiffness of the structure consisting of the shell element and frame element working together. However, if shear studs do not work 100%, it means the longitudinal stiffness of the structure was reduced. The Wongsawang bridge has a concrete deck thickness of 200 mm and height of 1450 mm. Finite element model of this bridge used rigid link between shell element and frame element. Based on the real bridge design, the length of the links is 825 mm, as shown in figure 4.10.

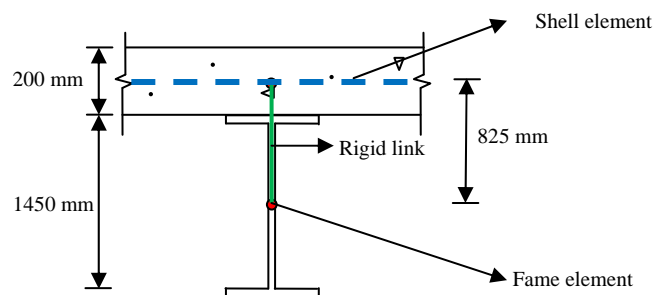


Figure 4.10 Partial bridge section

The field test data include the longitudinal stresses at the bottom flanges of girders G1, G2, and G3. The truck loading was idealized as point load vehicle load with similar value and configuration with the wheel truck in the field test, as shown from figure 4.11 to figure 4.13. All truck loading cases were modeled in multistep analysis that configures three cases of lane loading, as shown in figure 4.13 to figure 4.15. For the field test, Truck 3 was applied in the left lane and right lane in case (a) and case (b), respectively and truck 1 in the left lane and truck 2 in the right lane was modeled in case (c). The lane width is 1.8 m.

General Vehicle Data

Vehicle Name T1

Floating Axle Loads

	Value	Width Type	Axle Width
For Lane Moments	0.	One Point	
For Other Responses	0.	One Point	

Double the Lane Moment Load when Calculating Negative Span Moments

Usage

Lane Negative Moments at Supports
 Interior Vertical Support Forces
 All other Responses

Min Dist Allowed From Axle Load

Lane Exterior Edge 304.8
 Lane Interior Edge 609.6

Miscellaneous Parameters

Use BD 37/01 (2002) for Uniform Load Length Effects
 Vehicle Applies To Straddle (Adjacent) Lanes Only
 Straddle Reduction Factor

Loads

Load Length Type	Minimum Distance	Maximum Distance	Uniform Load	Uniform Width Type	Uniform Width	Axle Load	Axle Width Type	Axle Width
Leading Load	Infinite		0.	Fixed Width	1950.	6.	Two Points	1930.
Leading Load	Infinite		0.	Fixed Width	1950.	6.	Two Points	1930.
Fixed Length	4170.		0.	Fixed Width	1830.	10.	Two Points	1800.
Fixed Length	1300.		0.	Fixed Width	1830.	9.6	Two Points	1800.

Vehicle Remains Fully In Lane (In Lane Longitudinal Direction)

Units Ton, mm, C

OK Cancel

Figure 4.11 Modeling of truck 1

General Vehicle Data

Vehicle Name T2

Floating Axle Loads

	Value	Width Type	Axle Width
For Lane Moments	0.	One Point	
For Other Responses	0.	One Point	

Double the Lane Moment Load when Calculating Negative Span Moments

Usage

Lane Negative Moments at Supports
 Interior Vertical Support Forces
 All other Responses

Min Dist Allowed From Axle Load

Lane Exterior Edge 304.8
 Lane Interior Edge 609.6

Miscellaneous Parameters

Use BD 37/01 (2002) for Uniform Load Length Effects
 Vehicle Applies To Straddle (Adjacent) Lanes Only
 Straddle Reduction Factor

Loads

Load Length Type	Minimum Distance	Maximum Distance	Uniform Load	Uniform Width Type	Uniform Width	Axle Load	Axle Width Type	Axle Width
Leading Load	Infinite		0.	Fixed Width	1930.	6.4	Two Points	1930.
Leading Load	Infinite		0.	Fixed Width	1930.	6.4	Two Points	1930.
Fixed Length	4180.		0.	Fixed Width	1850.	10.	Two Points	1850.
Fixed Length	1300.		0.	Fixed Width	1850.	8.8	Two Points	1850.

Vehicle Remains Fully In Lane (In Lane Longitudinal Direction)

Units Ton, mm, C

OK Cancel

Figure 4.12 Modeling of truck 2

General Vehicle Data

Vehicle Name: T3

Load Plan

Load Elevation

Usage

Lane Negative Moments at Supports
 Interior Vertical Support Forces
 All other Responses

Min Dist Allowed From Axle Load

Lane Exterior Edge: 304.8
 Lane Interior Edge: 609.6

Miscellaneous Parameters

Use BD 37/01 (2002) for Uniform Load Length Effects
 Vehicle Applies To Straddle (Adjacent) Lanes Only
 Straddle Reduction Factor:

Load Length Type	Minimum Distance	Maximum Distance	Uniform Load	Uniform Width Type	Uniform Width	Axle Load	Axle Width Type	Axle Width
Leading Load	Infinite		0	Fixed Width	1780	5.6	Two Points	1780
Leading Load	Infinite		0	Fixed Width	1780	5.6	Two Points	1780
Fixed Length	3650		0	Fixed Width	1700	10	Two Points	1700
Fixed Length	1330		0	Fixed Width	1700	9.6	Two Points	1700

Vehicle Remains Fully In Lane (In Lane Longitudinal Direction)

Units: Ton, mm, C

OK Cancel

Figure 4.13 Modeling of truck 3

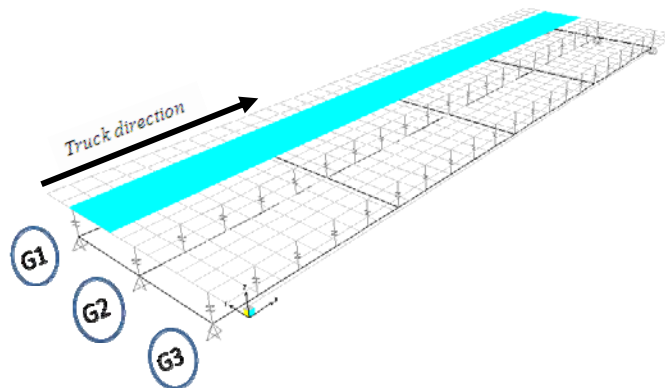


Figure 4.14 Truck loading lane of one truck on left lane case (case a)

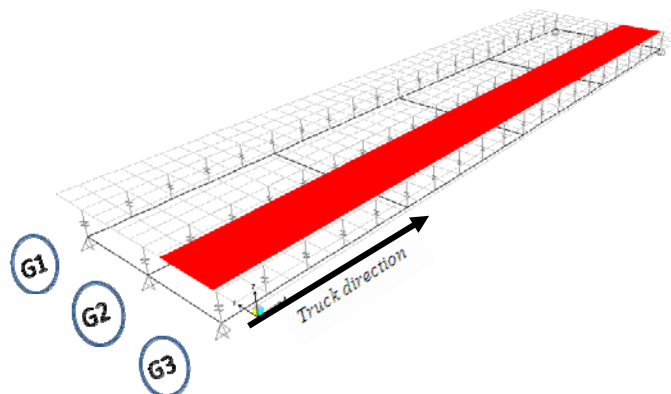


Figure 4.15 Truck loading lane of one truck on right lane case (case b)

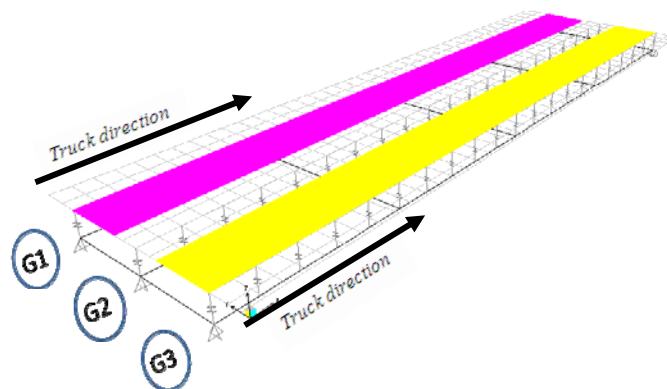


Figure 4.16 Truck loading lane of two trucks on both lanes case (case c)

The accuracy of finite element model depends significantly on both the geometric meshes and the algebraic solvers (Wang et al. 2005). The generation of finite element meshes focused on providing good results which the minimal errors on their solutions. The error was used to construct an economic mesh of finite element model (Becker and Vexler, 2004). In this study, the case of two trucks on both lanes was used. The data was for comparison is when truck stops in 10 m from the support. It compared with four finite elements with different discrete of shell elements and frame elements. Four discrete types of finite element models are: Type A with 70 frame elements and 160 shell element connected by 63 rigid links, Type B with 130 frame element and 560 shell element connected by 123 rigid links, Type C with 250 frame element and 2240 shell element connected by 243 rigid links, and Type D with 370 frame elements and 5040 shell element connected by 363 rigid links, as shown in figure 4.17 to figure 4.20. all node in girders are connected to the slab nodes via rigid links (all degree of freedom are coupled). The longitudinal moment from frame element output can be analyze to obtain longitudinal stresses in the bottom flanges at midspan are compared.

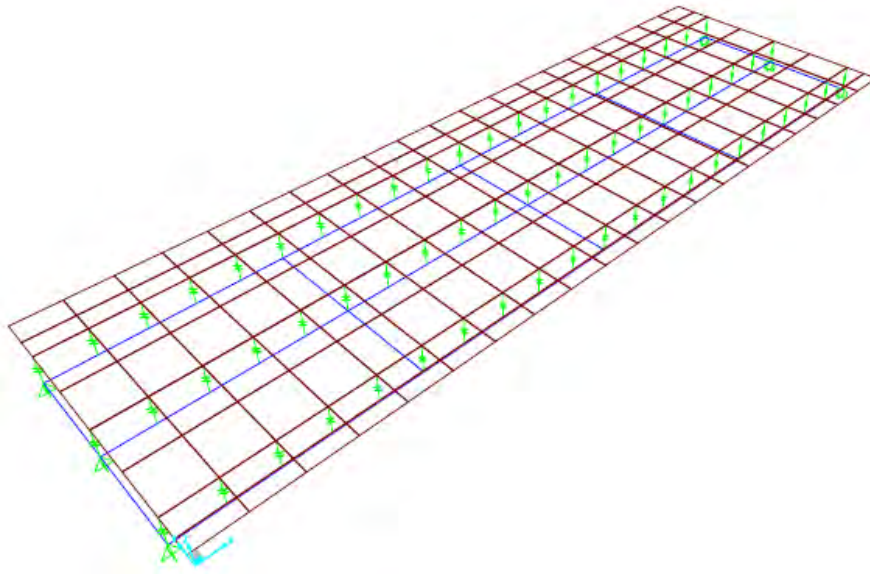


Figure 4.17 Global model for sensitivity study Type A (293 elements)

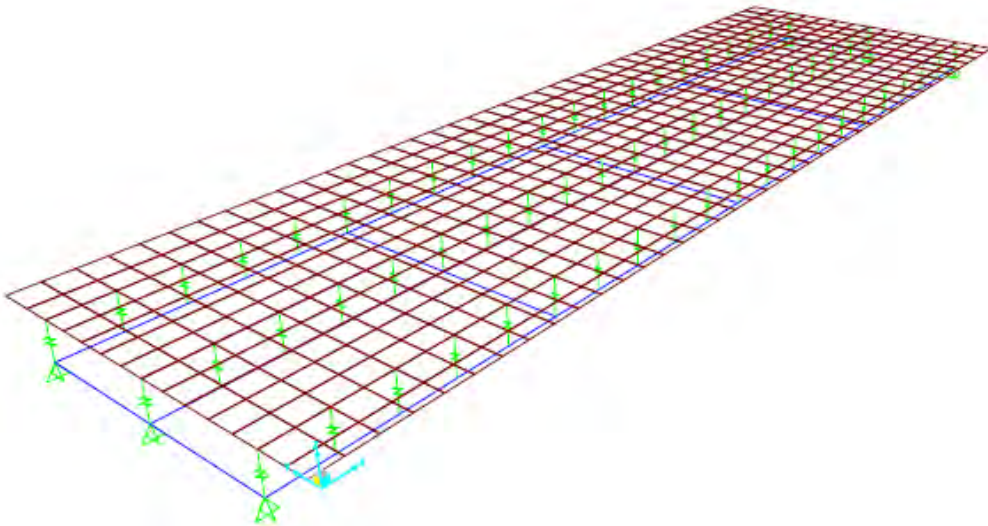


Figure 4.18 Global model for sensitivity study Type B (817 elements)

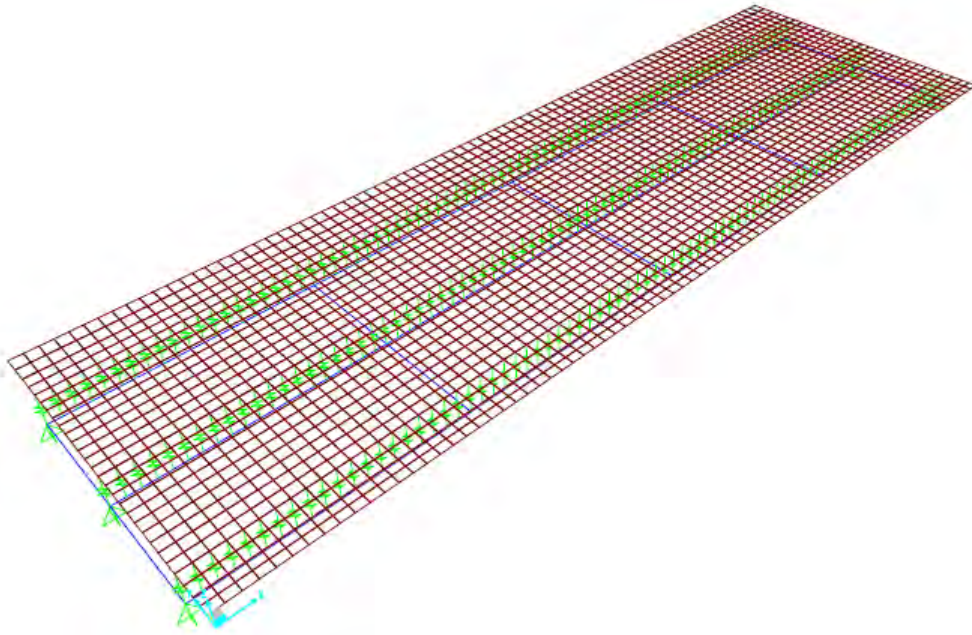


Figure 4.19 Global model for sensitivity study Type C (2773 elements)

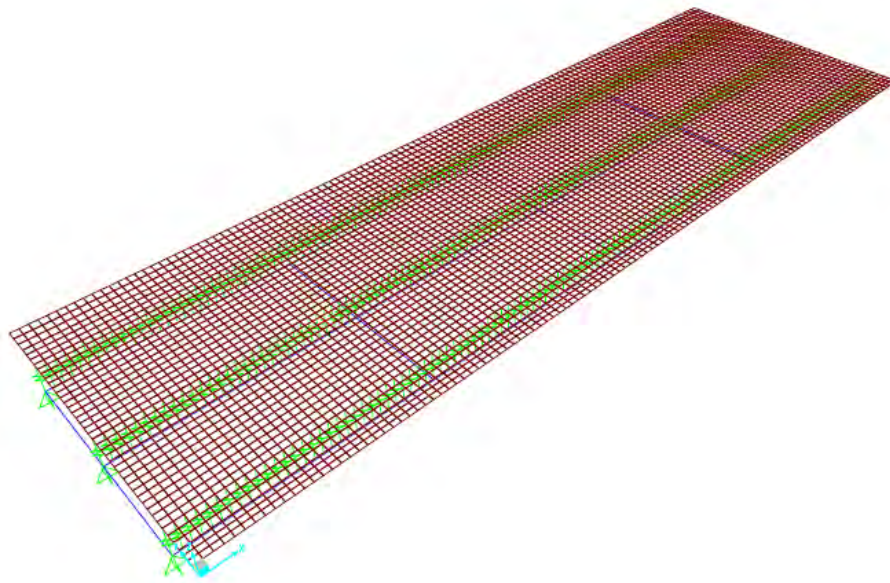


Figure 4.20 Global model for sensitivity study Type D (5772 elements)

Sensitivity study shows that the longitudinal stress in the midspan decreases with increasing amount of shell and frame elements. Figure 4.21 to figure 4.23 shows the convergence of longitudinal stress in the bottom flanges in the midspan. Based on the convergence trends of finite element model result, the mesh in global model type

C with 2773 element shows the best mesh because global model type D does not give significant difference result.

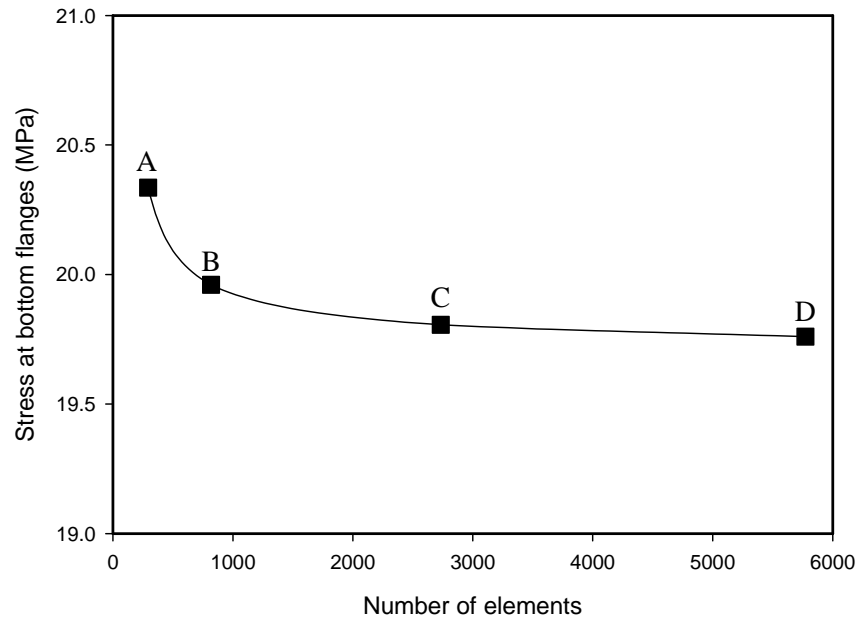


Figure 4.21 Longitudinal stress in G1 from sensitivity study result

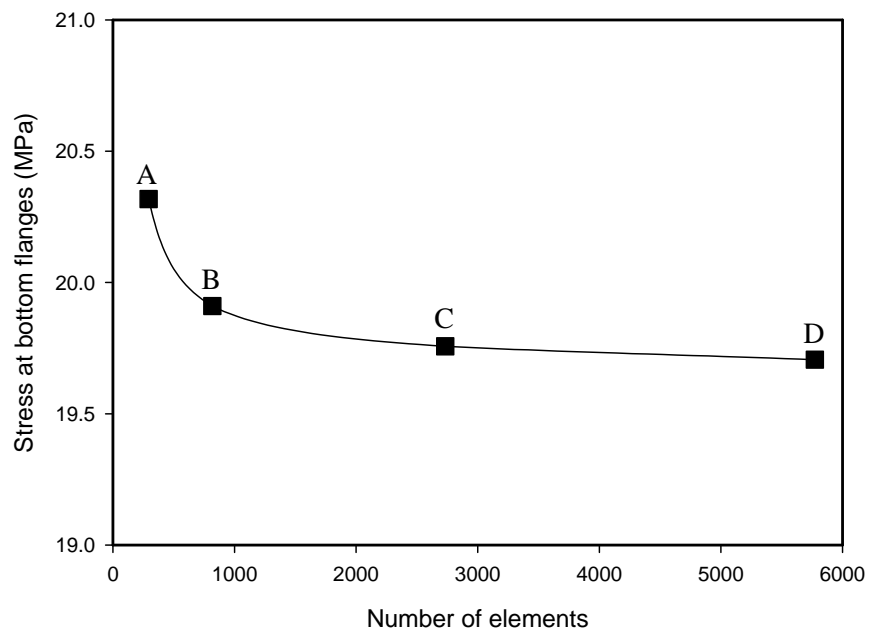


Figure 4.22 Longitudinal stress in G2 from sensitivity study result

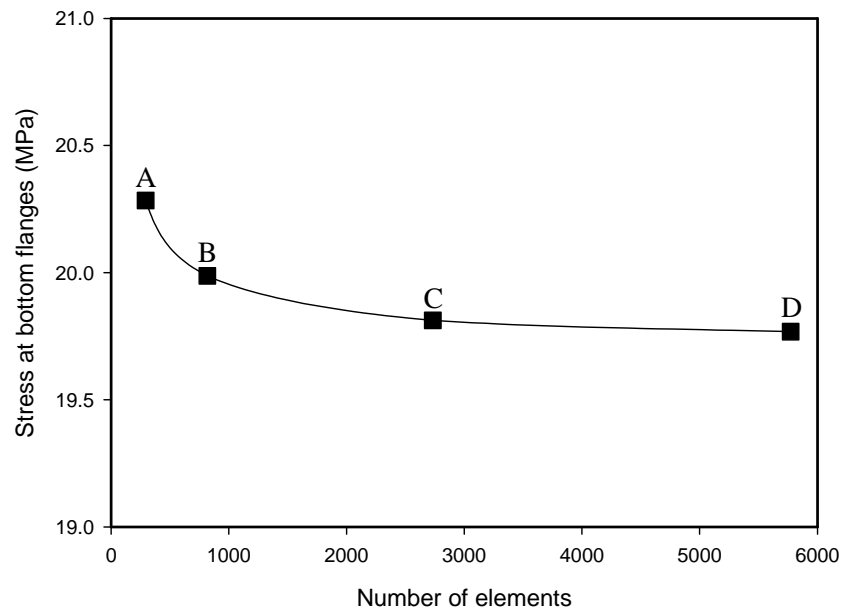


Figure 4.23 Longitudinal stress in G3 from sensitivity study result

Four global models were constructed and compared with field test data. However, the comparisons show the discrepancy between the field test result and the finite element model result. Global model type C shows the result underestimates the field test data by 30%, it can be ensue because degree of composite action in the real bridge is not 100%.

In this study, the modification of finite element model dimension was implemented in order to obtain the finite element model which is appropriate to the field test. The modification was needed in order to obtain smaller longitudinal stiffness. The way of modification is reduce the slab thickness until the height of the shear studs of the field test. This modification assumes the composite action is doing well in the height of shear studs or half of slab thickness, as shown in figure 4.24.

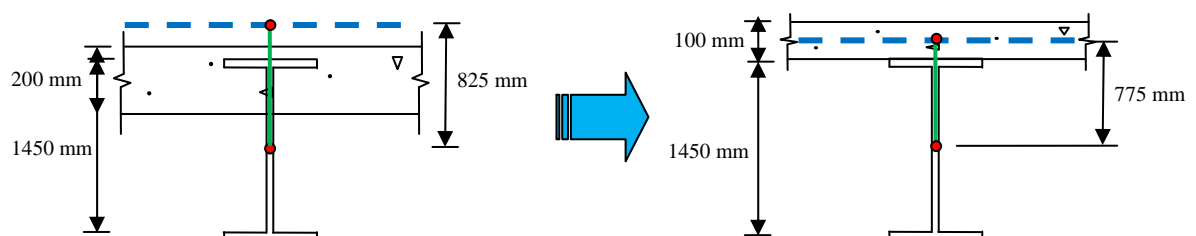


Figure 4.24 Global model modification

The modified finite element model results in higher longitudinal stress in the bottom flanges than unmodified model. The maximum difference between finite element model and field test data is 15%, as shown in figure 4.25.

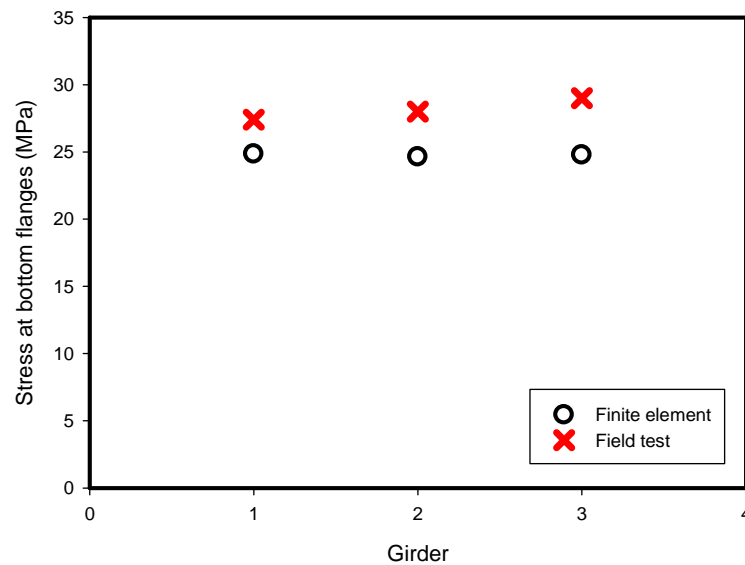


Figure 4.25 Modified longitudinal stress comparison

The vertical displacements of the girder from the modified finite element model were applied to the more detailed model, call submodel, in the next section.

4.2.2.2 Submodel

The second level model is called submodel, which is a detailed finite element model of the diaphragm-stiffener-web connection. Submodel consists of all shell elements. The portion of submodel is only half of girder span with full length diaphragm connect the girder, as shown in figure 4.26 (a). The model consists of three girders, connected by a diaphragm, as shown in figure 4.26 (b). All dimensions were taken directly from the bridge itself or from the design plans. Top flange of girders is free to move in the vertical direction and rotate in the longitudinal direction. However, it is restrained against transverse rotation to simulate the restraining effect of concrete slab. Vertical direction in the loading node is restrained to accommodate the applied displacement loading from the global model. At the support, the bottom flanges nodes are restrained in the longitudinal and transverse axis of the girder and free to move in longitudinal direction at the roller support.

The vertical displacements of girders from global model were applied to the top of the girder flanges along the length of the submodel. It caused the shape of the girder represents the global model displacement.

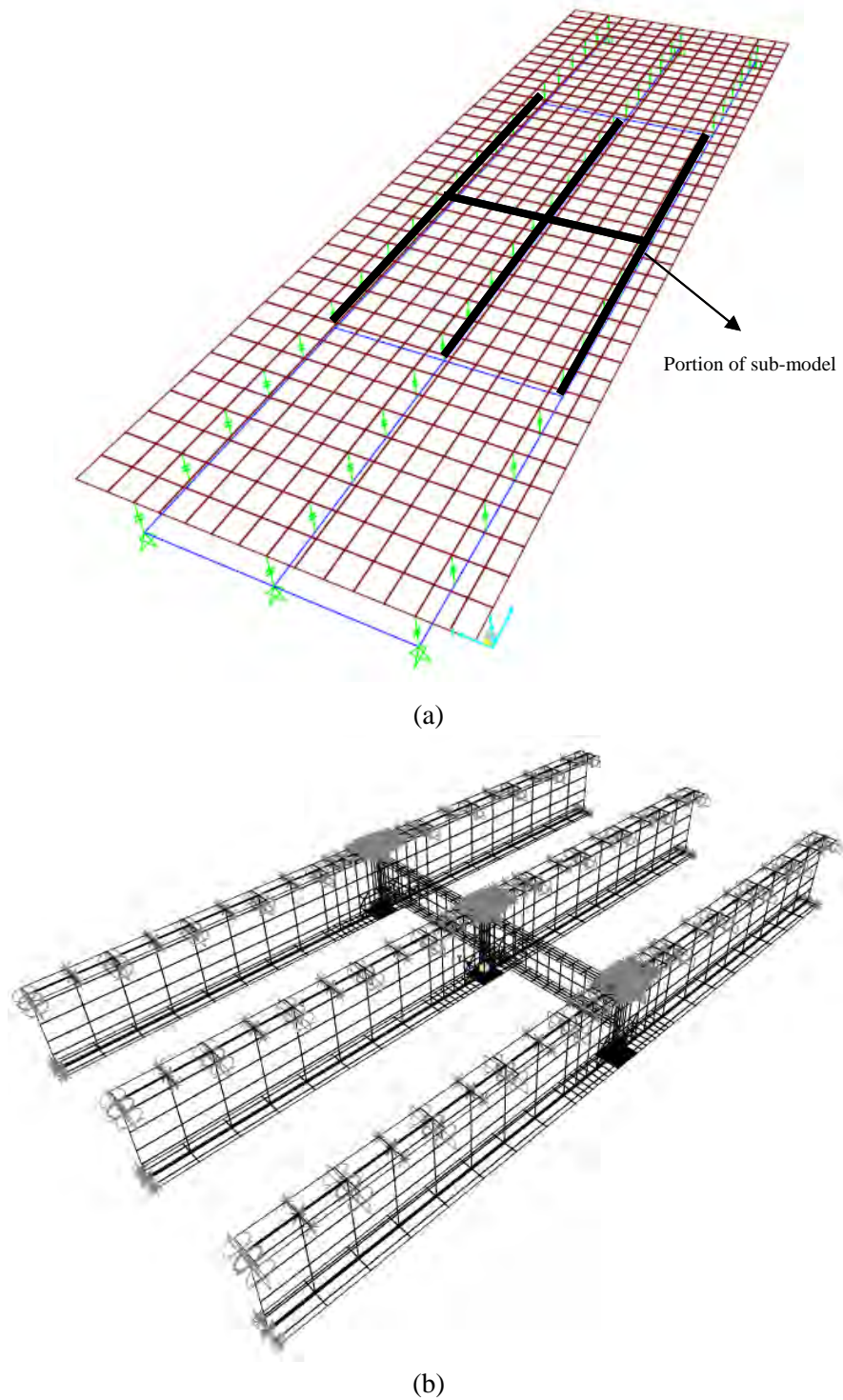


Figure 4.26 Finite element model (a) Global model (b) Submodel

The mesh in web gap area was refined in order to obtain local out-of-plane stresses. Because the size of the mesh in this area was much smaller than the mesh near the supports, a transition mesh was needed. To find the sufficient mesh, the convergence study is performed. The study used the case of one truck on left lane.

After the truck was applied in the global model, the vertical displacements in the girder in a portion of the submodel were applied to the top flanges in the submodel. Equal vertical displacement was applied to all the nodes in the same transverse direction in every longitudinal space.

Four types of mesh were chosen in the sensitivity study. All finite element models were constructed based on the girder and diaphragm of Wongsawang bridge dimension. Each model has a varying local mesh in the web gap area. The four types of mesh are: Type A with 3808 shell elements, type B with 4198 shell elements, type C with 8638 shell element, and Type D with 29418 shell elements. Figure 4.27 shows the mesh in the web gap area for every type of submodel.

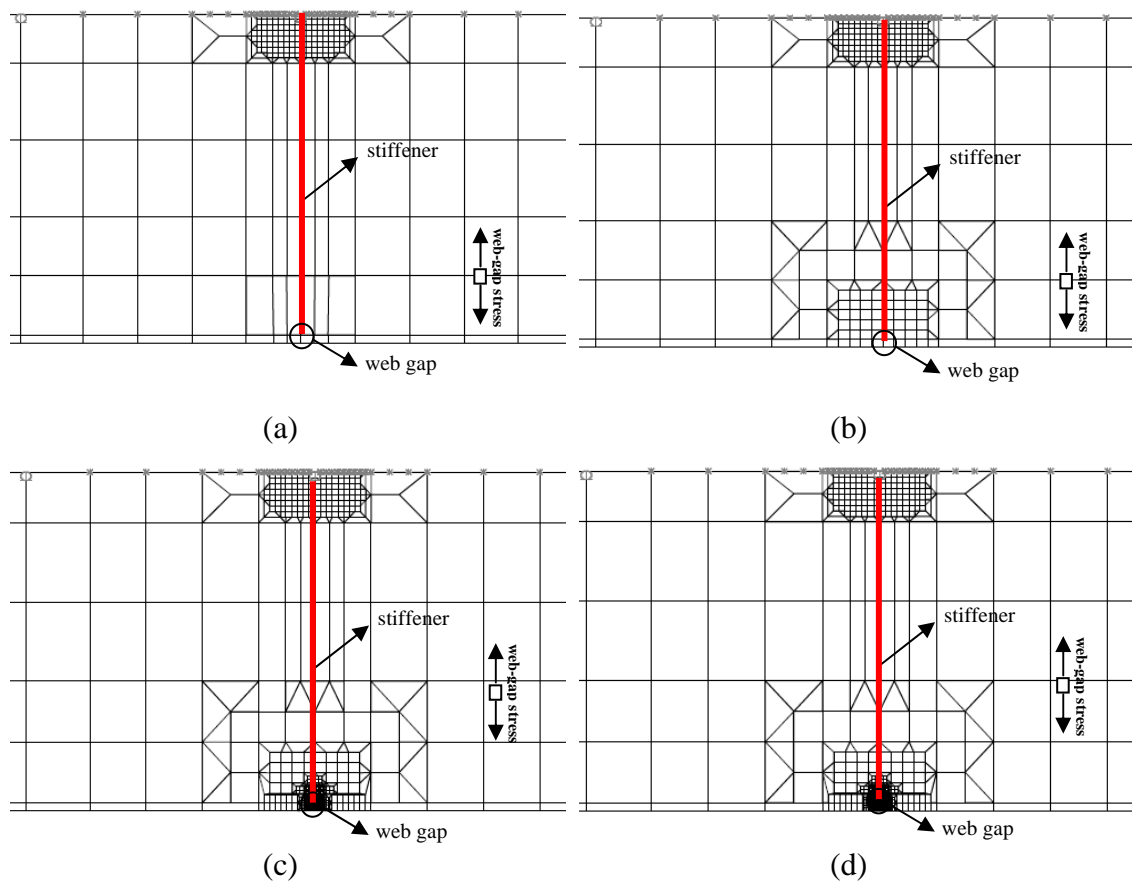


Figure 4.27 Mesh of Submodel for sensitivity study (a) Type A (b) Type B

(c) Type C (d) Type D

The vertical stress distribution along the web gap length was studied. The coarse mesh results show a lowest of the stress in the top and bottom of web gap. As the mesh gets finer, the stress in the top and bottom of the web-gap increase. The result converges as the mesh is refined. Figure 4.28 and figure 4.29 show the vertical

stresses comparison of four types submodel. The stress in top of web gap was considered in this sensitivity study. As shown in figure 4.28, submodel type C and D shows the stress in the end of stiffener is converging.

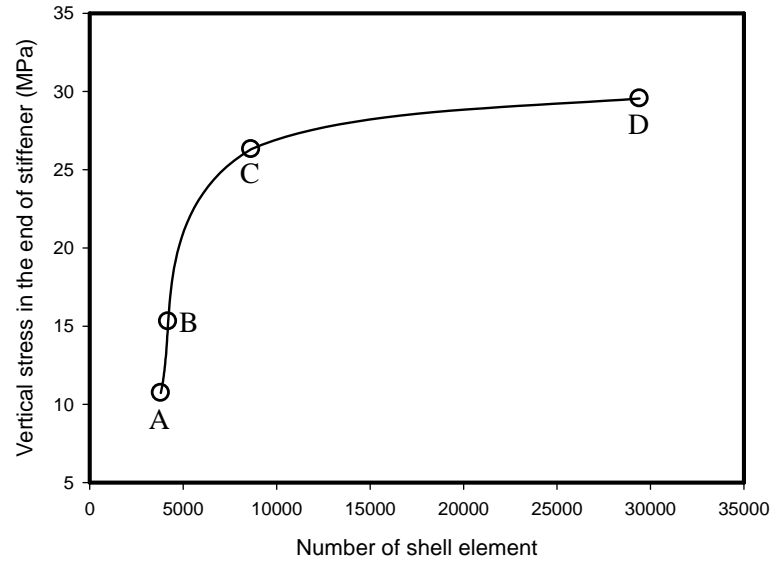


Figure 4.28 Convergence of submodel

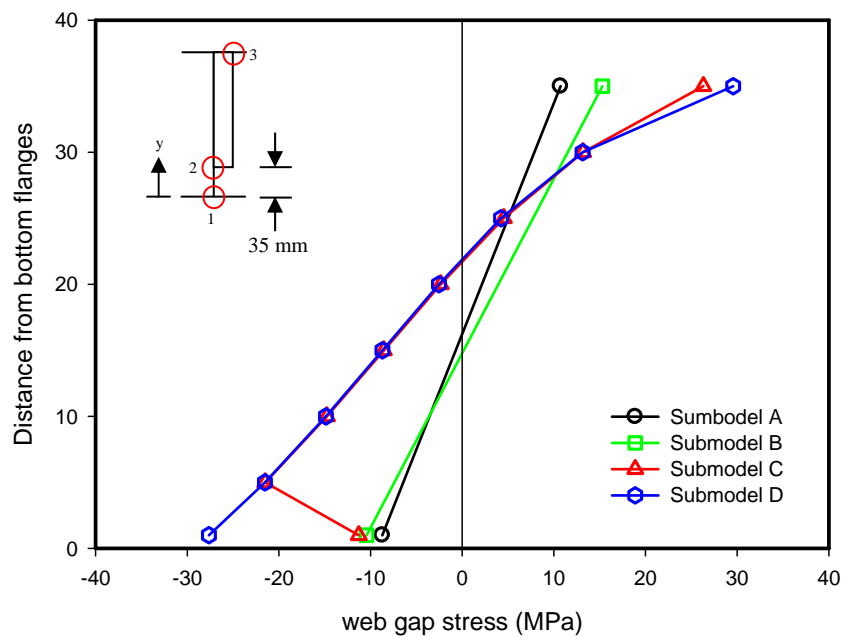


Figure 4.29 Stress distribution in vertical direction of web gap

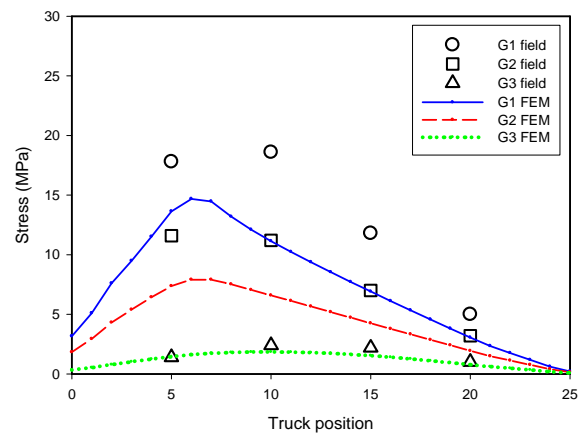
Distribution of vertical stress along the length of web gap found was shown in figure 4.29. Submodel type D is found more suitable than type C. After the mesh of global model and submodel were identified, data from field test was used to verify the model.

4.2.3 Verification of The Finite Element Model

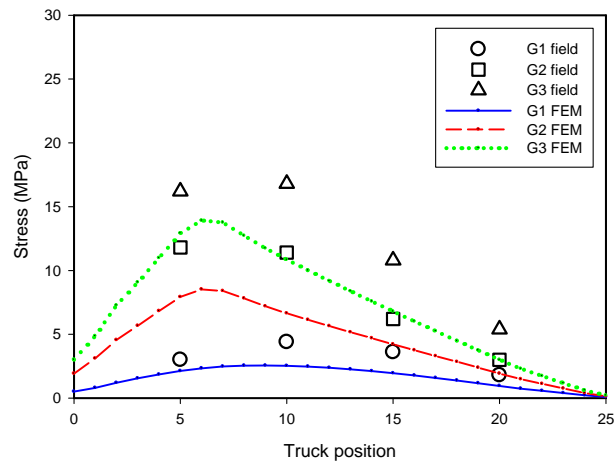
Model's validation is a necessary requirement for model application. In this study, multistep analysis was performed to calibrate the global model. To calibrate the bridge model, a set of truck loads equivalent to the truck axle weight was applied as a vehicle on the lanes set earlier. Longitudinal stresses in quarter-span, mid-span, and third-quarter spans in every 5 m truck stops were considered for comparison.

4.2.3.1 Global Model

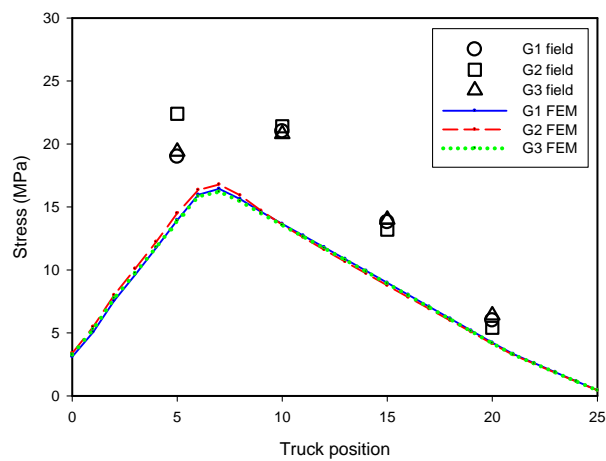
Three loading cases were applied to the finite element model. The comparison of longitudinal stress in the quarter-span, mid-span, and three-quarter-span in every truck loading cases in unmodified global model are shown in figure 4.30 to figure 4.32.



(a)

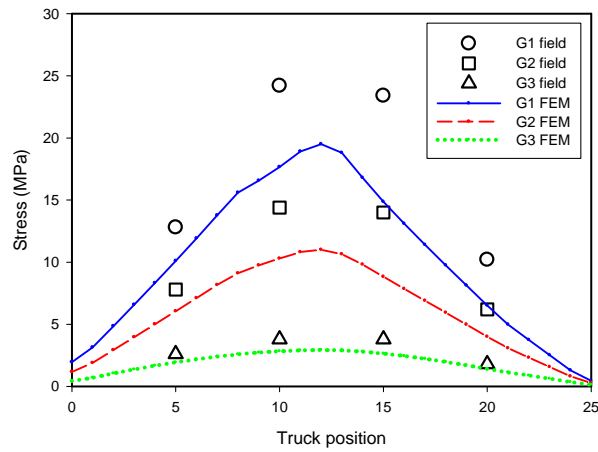


(b)

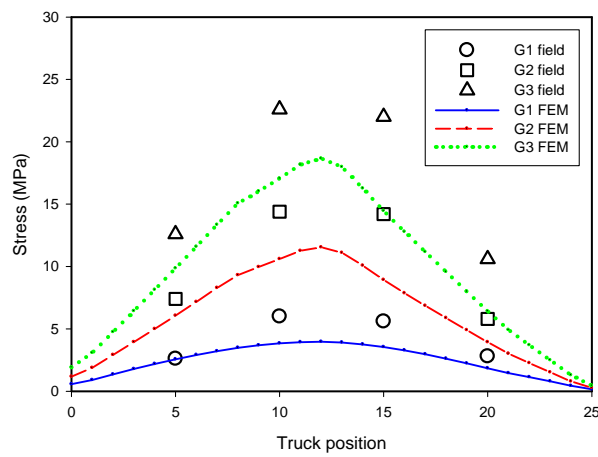


(c)

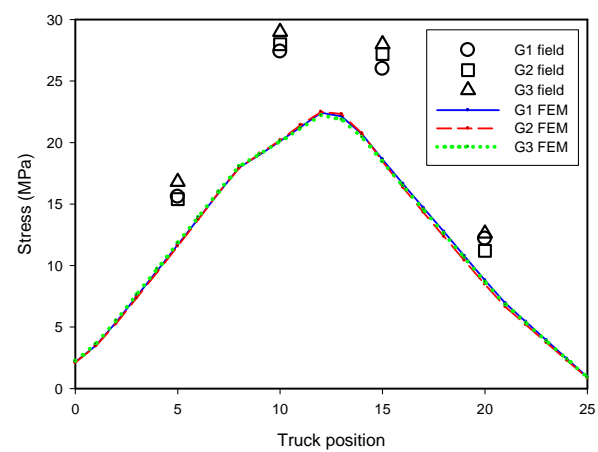
Figure 4.30 Comparison of longitudinal stresses in the bottom flange of all three girders at quarter span from unmodified global model (a) One truck on left lane (b) One truck on right lane (c) Two trucks on both lanes



(a)

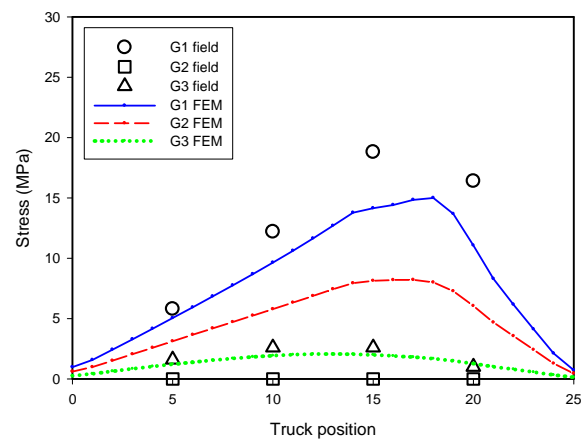


(b)

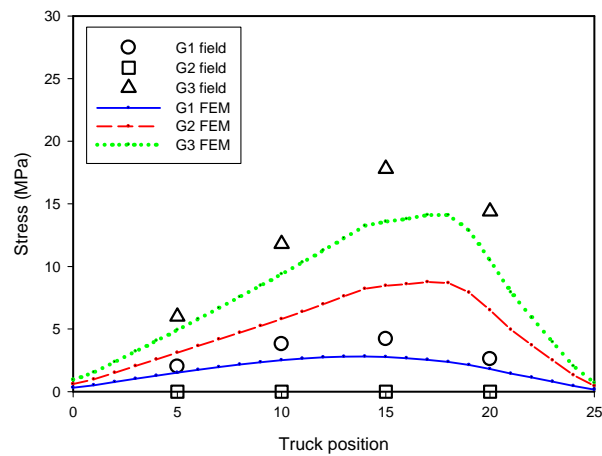


(c)

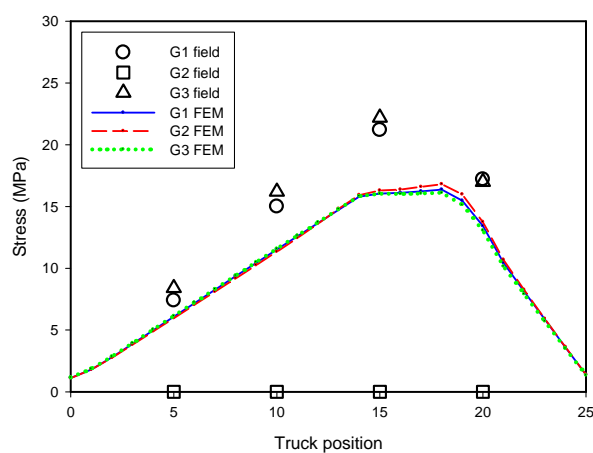
Figure 4.31 Comparison of longitudinal stresses in the bottom flange of all three girders at midspan from unmodified global model (a) One truck on left lane (b) One truck on right lane (c) Two trucks on both lanes



(a)



(b)



(c)

Figure 4.32 Comparison of longitudinal stresses in the bottom flange of all three girders at three quarter span from unmodified global model (a) One truck on left lane (b) One truck on right lane (c) Two trucks on both lanes

Figure 4.30 to figure 4.32 compare the differences between global model and field test. Overall, the difference between finite element result and field test data results is very high (more than 20%) because the unmodified global model is stiffer than real bridge.

In order to investigate the real bridge behavior, the modified global model was validated using the same field test data. The longitudinal stress comparison in modified global model is shown in figure 4.33 to figure 4.35.

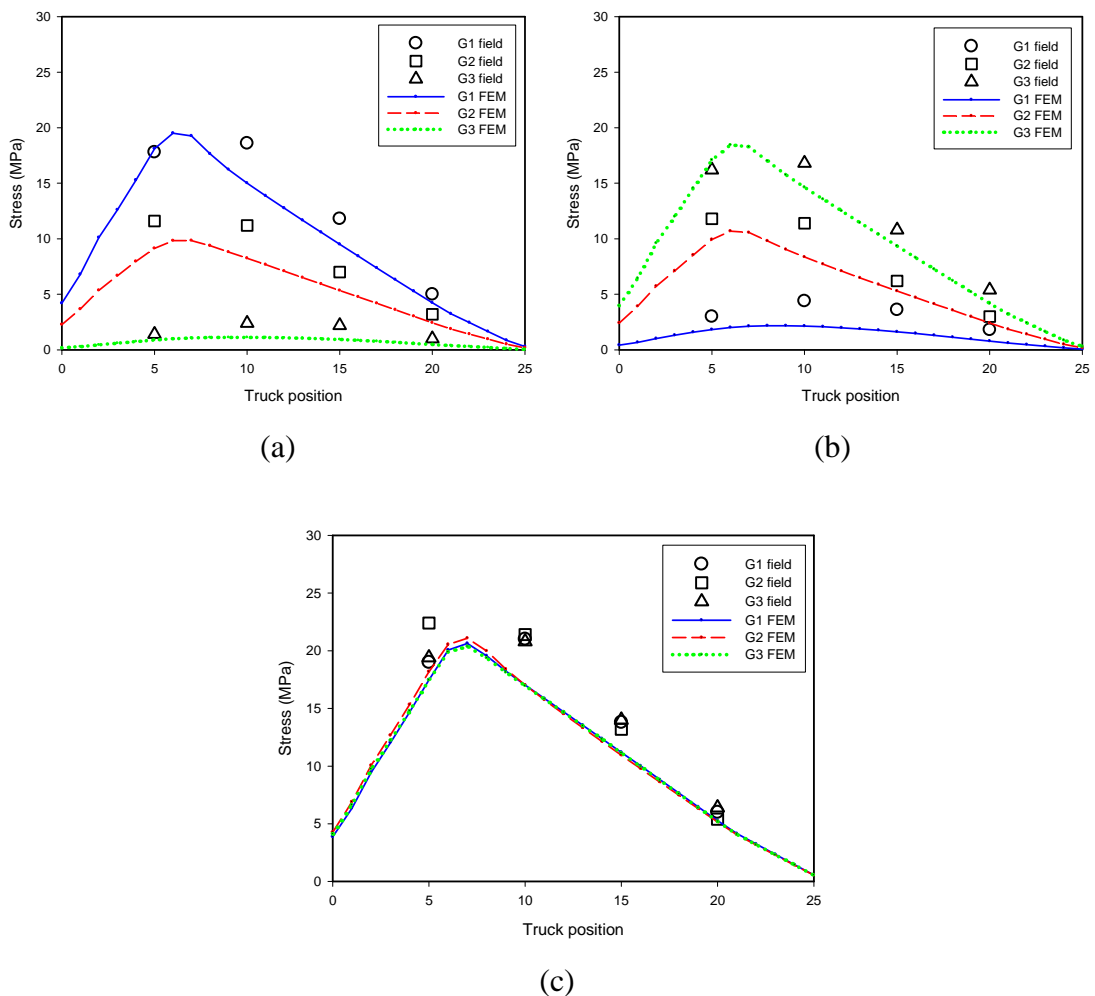


Figure 4.33 Comparison of longitudinal stresses in the bottom flange of all three girders at quarter span from modified global model (a) One truck on left lane (b) One truck on right lane (c) Two trucks on both lanes

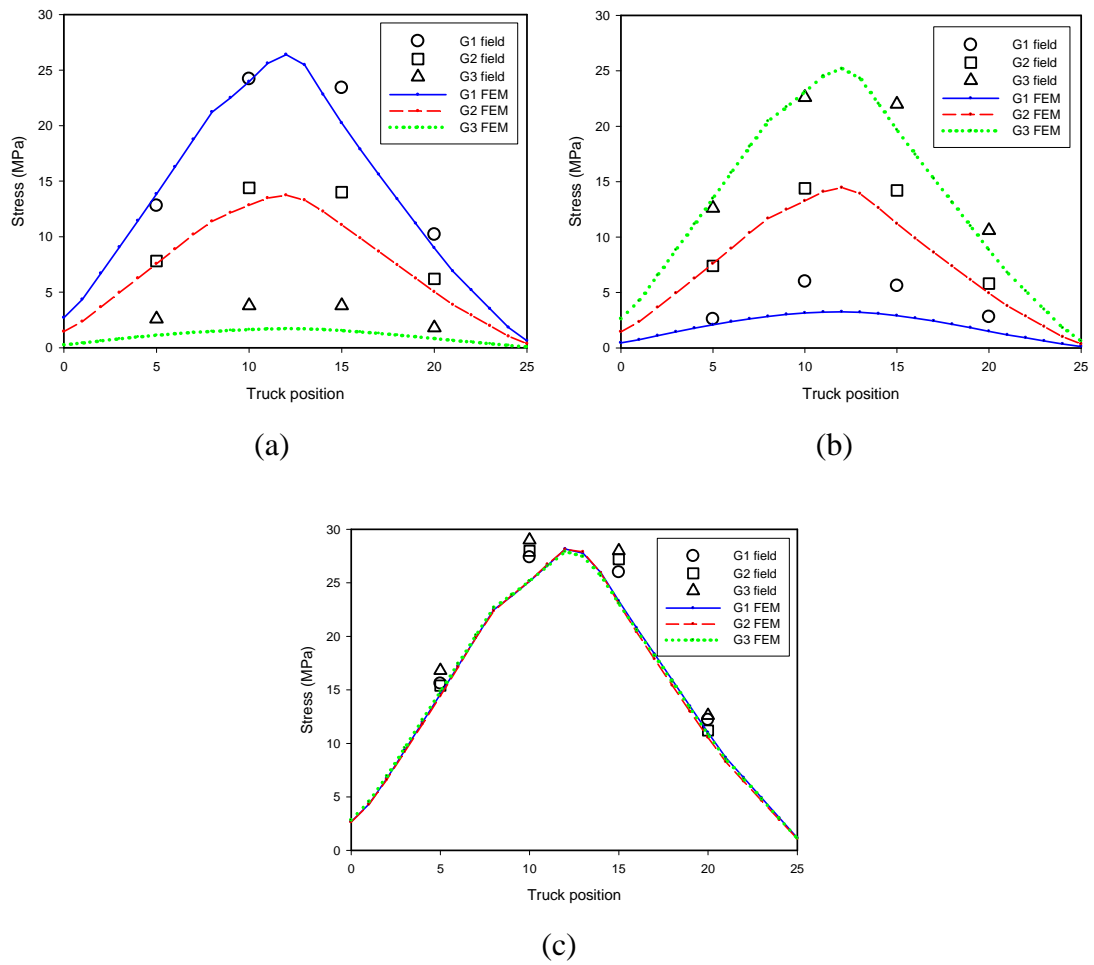


Figure 4.34 Comparison of longitudinal stresses in the bottom flange of all three girders at midspan from modified global model (a) One truck on left lane (b) One truck on right lane (c) Two trucks on both lanes

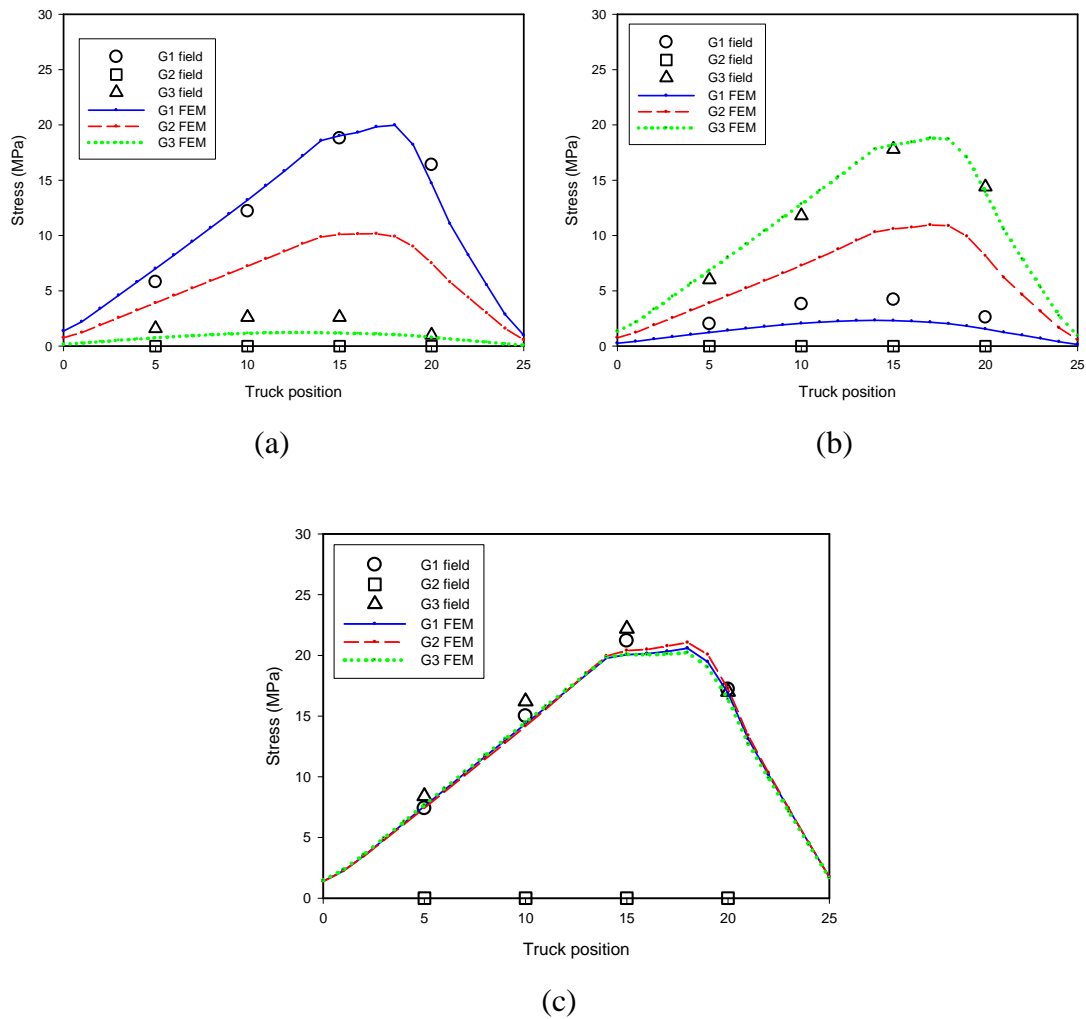


Figure 4.35 Comparison of longitudinal stresses in the bottom flange of all three girders at three quarter span from modified global model (a) One truck on left lane (b) One truck on right lane (c) Two trucks on both lanes

The comparison in figures 4.29 to figure 4.35 shows that the maximum stress occurs in the girder G1 when the truck locates on the left lane, case (a), because the girder locates under the truck wheel position. The stresses in girders G2 and G3 are lower than the girder G1 depending on the lateral load distribution. Similarly, when truck on right lane girder G3 experiences the highest stress followed by G2 and G1. In case of two trucks on both lanes, case (c), all girders share approximately the same stresses. For the quarter-span longitudinal stress comparison, the maximum stress occurred when the truck is on the quarter-span. Similarly, the maximum stresses on the mid-span and three-quarter-span occurred when the truck is on the mid-span and three-quarter-span, respectively. Lastly, the maximum stress in this bridge is obtained in the mid-span when truck position is in the mid-span.

Figure 4.33 compares the longitudinal stresses in the bottom flanges of girders G1, G2 and G3 in the quarter-span from the finite element analysis with the field test data cases (a), (b), and (c), respectively. The maximum stress in the field test occurred when truck is around quarter span. In this position, the maximum differences are 20% and 25% for girders G1 and G2, respectively in case (a). In the case (b), the maximum differences are 25% and 13% for girders G2 and G3, respectively. In the case (c), the difference is 19%, 20%, and 20% for girder G1, G2, and G3, respectively.

Figure 4.34 shows the comparison of longitudinal stress of bridge finite element model and the field test in the mid-span. Similar to the quarter-span, the maximum stress in the field test occurred when truck is in midspan. In case (a), the maximum difference is 1% for girders G1 and 10% for girder G2. Case (b) obtained maximum differences with 8% and 2% for girders G2 and G3, respectively. In the case (c), the maximum difference is 8%, 10%, and 13%, for girder G1, G2, and G3, respectively.

Comparison in figure 4.35 is between the longitudinal stresses of real bridge and finite element model in the three-quarter-span. The maximum stress in the field test occurred when the truck in three quarter span. 1.2% differences are shown in case (a) for girders G1. Case (b) rise maximum differences 2% for G3. In the case (c), the difference is 10% and 5% difference was occurred in G1 and G3.

4.2.3.2 Submodel

As mentioned above, the mesh in the submodel is refined in the web gap area, as shown in figure 4.36.

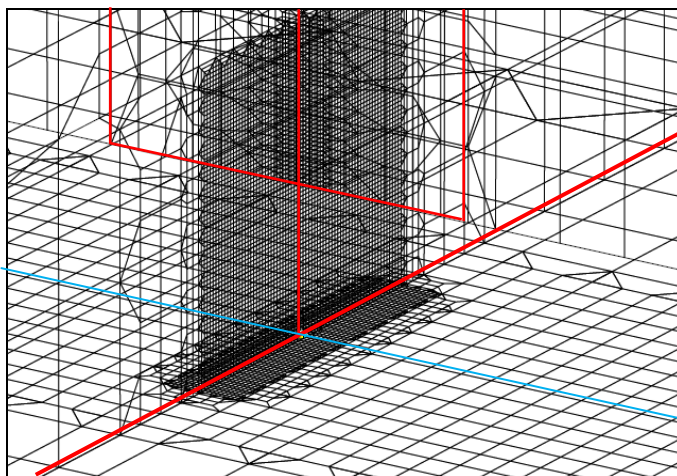


Figure 4.36 Web gap area mesh

In order to validate with field test, the displacement shape of modified global model was applied. Three cases of global model above have different vertical displacements in the girder. The vertical displacements in the girder that is result the shape of girder were applied as a load to the submodel. Stresses in the web gap area and in the bottom flanges of the girder are used on this comparison. When truck stop at 10 m from the edge, the comparison results for all cases are shown in table 4.3.

Table 4.3 Comparison stress in the bottom flanges in the mid-span between global model, submodel, and field test

Case	Girder	Field test	Global model	Submodel	Difference to Field
		(MPa)	(Mpa)	(Mpa)	(%)
a	G1	24.2	23.9	23.7	2
	G2	14.4	12.3	11.29	20
	G3	3.8	1.6	0.8	78
b	G1	6	3.1	2.4	15
	G2	14.4	13.3	12.2	7
	G3	22.6	23.1	24.2	6
c	G1	27.2	25.5	25.48	6
	G2	27	25.1	22.7	15
	G3	29	25.1	25.6	11

case (a) = one truck on left lane, case (b) = one truck on right lane c, and case (c) = two trucks on both lanes.

The comparison shows that the maximum stresses that occurred in the girder close to the truck wheel position. In case (a) and case (b), the exterior girder in unloading lane shows very small longitudinal stress in the bottom flanges. In case of two trucks on both lanes, case (c), all girders share approximately the same stresses. The comparisons also show a reasonable agreement between the submodel, global model and the field test data of longitudinal stress in the mid-span bottom flange of the girders.

4.2.3.3 Web Gap Stress

The finite element study is used to investigate the maximum stress at the web gap. After an examination of the web gap stress data, stress data of strain gage in the girder G1 when truck is in the left lane and stops at 10 m from the support. A stress value of 13.2 MPa was decided as a benchmark experimental value in comparing with the finite element results.

The finite element model predicted a maximum web gap stress (at the end of stiffener) of about 44.7 MPa. It is much higher than 13.2 MPa from field test data. It can be attributed to the position of the strain gage and the web-gap deformation

mechanism. Stress distribution along the girder length of the web gap is plotted in figure 4.37. The 34 mm position indicates the stress along the web-to-bottom-flange junction and the 0.0 mm position means the stress at the end of stiffener.

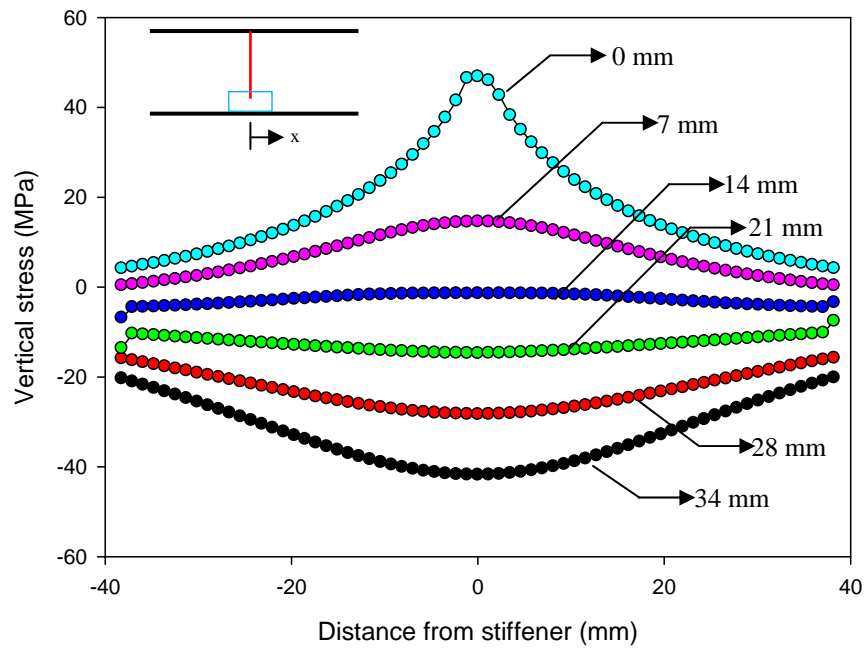


Figure 4.37 Distribution of web gap stress along the girder length

Figure 4.37 shows the stress changes in the horizontal section. It means that the stress field around the connection between girder web and stiffener changes quickly, even small differences in strain gage placement can give large variations in strain readings (Jajich et al, 2000)

Because of the installation difficulties in the real bridge, the strain gage placement was modified as shown in figure 4.38.

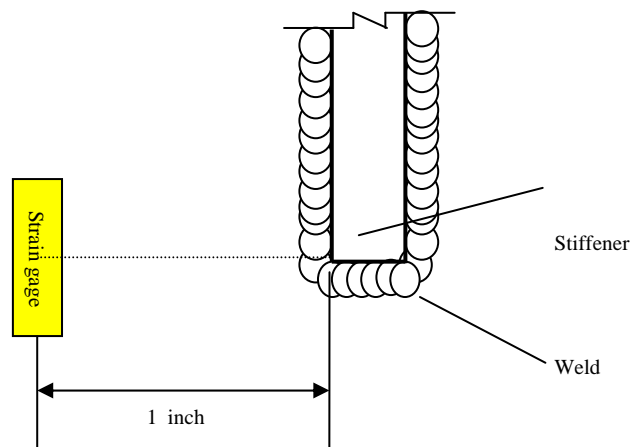


Figure 4.38 Strain gage placement

When the actual strain gage position is overlaid on the finite element stress distribution, as shown in figure 4.39, the finite element model predicted the stress to be 9.3 MPa at the strain gage location. Measured web gap strain shows $66 \mu\epsilon$, means the stress is 13.2 MPa. Therefore, the finite element result underestimates the field test result by 30%, but the quick stress gradient, the human error, and also the possibility of gage error also needs consideration (Jajich et al. 2000)

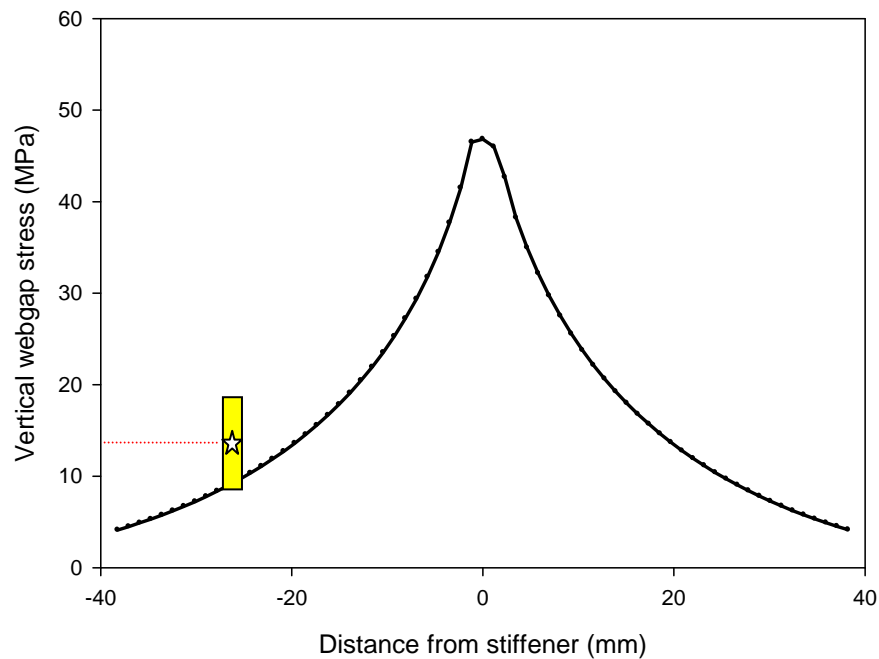


Figure 4.39 Comparison between measured web gap stress and prediction from results

Another important issue is the web gap deformation. It guides to the stress in the top of web gap. The deformation shape was shown in figure 4.40. It shows the double curvature shape of web gap because the rotation and the horizontal occurred in both end of web gap.

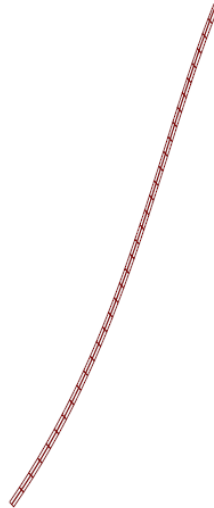


Figure 4.40 Web gap deformed shape

The finite element model showed the nodal rotation and displacement of web gap as shown in Figure 4.41. Assume the force is applied to the web gap only from the diaphragm rotation, if the vertical displacement is neglected, the direct stiffness method can be used to get the moment in the top of web gap.

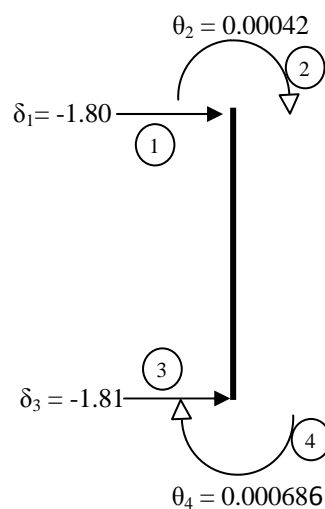


Figure 4.41 Displacement of web gap

Using the simple equilibrium equation of the beam, the moment in the top of web-gap can be obtained.

$$\begin{bmatrix} P_1 \\ M_2 \\ P_3 \\ M_4 \end{bmatrix} = \frac{EI}{L^3} \begin{bmatrix} 12 & -6L & -12 & -6L \\ -6L & 4L^2 & 6L & 2L^2 \\ -12 & 6L & 12 & 6L \\ -6L & 2L^2 & 6L & 4L^2 \end{bmatrix} \times \begin{bmatrix} \delta_1 \\ \theta_2 \\ \delta_3 \\ \theta_4 \end{bmatrix} \quad (4.2)$$

Assume the web gap to be applied by M_2 moment only. With L = web gap length (35 mm), $E = 20000$ MPa, thus:

$$M_2 = \frac{-6EI}{L^2} \delta_1 + \frac{4EI}{L} \theta_2 + \frac{6EI}{L^2} \delta_3 + \frac{2EI}{L} \theta_4 \quad (4.3)$$

$$M_2 = 7.689796Nmm$$

Assume y = half of girder web thickness, thus stress in the web gap:

$$\sigma = \frac{My}{I} \quad (4.4)$$

$$\sigma = 46.14MPa$$

Refer to figure 4.39, the calculation above gives underestimates the measured strain in the web gap within 2 %. This simple calculation assumes that the web gap undergo rotation and horizontal translation at both ends of web gap.

Distortion-induced stress is influenced by relative displacement between adjacent girders (Fisher et al. 1990). The increasing of relative displacement will generate the higher distortion induced stress.

The calibration and examination in the web gap area with many cases shows that the assumptions and the methods used in finite element model are appropriate to represent the behavior of the real bridge. In other words, the finite element model can be used in the parameter study.

CHAPTER V

PARAMETRIC STUDY

5.1 Overview

The objective of this parametric study is to investigate the influence of the bridge parameters on the relative girder deflections and maximum web gap stress. Dual level analysis was used in parametric study. Both global model and submodel were modeled using software package SAP2000. Parametric study was done by varying one parameter and fixing the other parameter. AASHTO standard truck HS20 was applied in multistep analysis. The truck was modeled to move in the line with a certain speed and stop in a certain time. Multistep analysis in global model results the maximum relative differential between adjacent girders. The girder's deformation shape was applied as loading to the submodel. Maximum relative displacement in the global model and the maximum tension web gap stress is studied.

5.2 Description on Finite Element Model

Both global model and submodel were made based on the finite element mesh in chapter III with some modifications. The global model consists of concrete slab, three main girders, and diaphragms at midspan, quarter spans and end spans of the bridge. This parametric study assumes a fully composite action. Thus, rigid links with all degree of freedom between the shell elements and frame elements coupled. The superstructure had two lanes with no sidewalk and the lanes width is as the same as girder spacing. Similarly, submodel portion, boundary and mesh of the submodel were made based on the finite element study in chapter III. A total 56 of Global model and submodel with 234 cases were analyzed in this study.

5.3 Bridge Parameters

The parameters chosen in the study are the bridge length (L), girder spacing (S), slab thickness (t_s), and girder stiffness (I_g). These parameters are shown in figure 5.1.

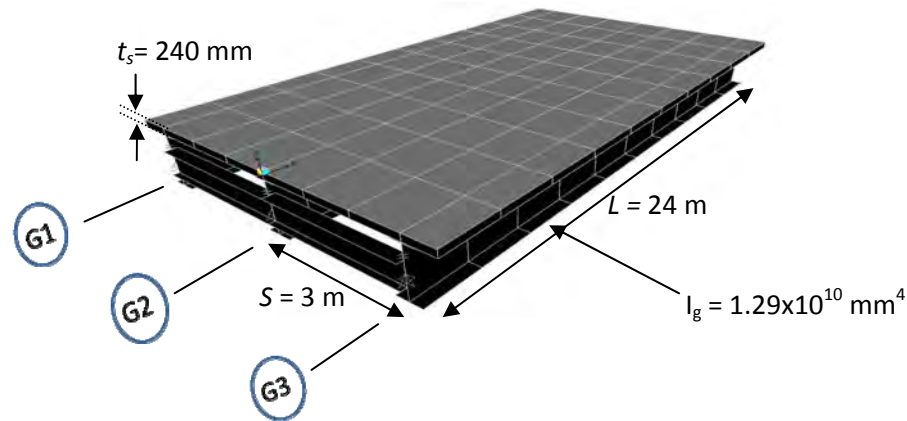


Figure 5.1 Typical FEM with base bridge parameter

The range of parameters was based on the applicability range in the AASHTO LDF equation. For example, the bridge length (L) varied from 18 m to 36 m, girder spacing (S) varied from 2.1 m to 3.0 m, and slab thickness (t_s) varied 210 mm to 300 mm. The range of girder stiffness (I_g) was based on the real bridge design. It varied from 1.1×10^{10} mm⁴ to 1.7×10^{10} mm⁴. To study the effect of a specific parameter, other parameters are fixed in the finite element analysis. The basic parameter values are as follows: bridge length = 24 m, girder spacing = 3.0 m, slab thickness = 240 mm, girder frame is I section 1450×450×12×22 with inertia stiffness = 12.9×10^9 mm⁴ and diaphragm I section 678×253×12×16 with inertia stiffness = 1.6×10^9 mm⁴. Sixteen variations were modeled in the parametric study. All of the bridge parameters are shown in table 5.1.

Table 5.1 Bridge's finite element model parameter

Girder spacing (m)	Slab Thickness (mm)	Girder stiffness (mm ⁴)	Bridge length (m)
2.1	240	1.2×10^{10}	24
2.4	240	1.2×10^{10}	24
2.7	240	1.2×10^{10}	24
3.0	240	1.2×10^{10}	24
3.0	210	1.2×10^{10}	24
3.0	240	1.2×10^{10}	24
3.0	270	1.2×10^{10}	24
3.0	300	1.2×10^{10}	24
3.0	240	1.0×10^{10}	24
3.0	240	1.2×10^{10}	24
3.0	240	1.5×10^{10}	24
3.0	240	1.7×10^{10}	24
3.0	240	1.2×10^{10}	18
3.0	240	1.2×10^{10}	24
3.0	240	1.2×10^{10}	30
3.0	240	1.2×10^{10}	36

5.4 Truck Loading

AASHTO HS20-44 standard truck was used in the parametric study. The truck load configuration is shown in figure 5.2. Two general types of loading are one truck on left lane and two trucks on both lanes.

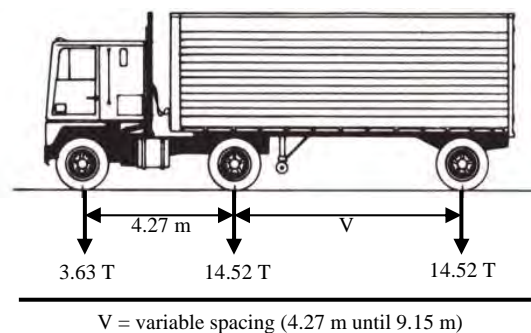
**Figure 5.2** AASHTO truck configuration (HS20-44)

Figure 5.3 shows the possible combinations for two trucks on both lanes. The outer-outer loading combination is when one truck moved in the left edge of left lane and another truck on right edge of right lane, as shown in Figure 5.3 (a), center-center loading combination is when both trucks moved in the center of the left and right lanes, as shown in Figure 5.3 (b), and inner-inner loading combination is when one truck moved in the right edge of left lane and another truck on left edge of the right lane, as shown in Figure 5.3 (c). Other transverse loading combinations include the outer-center, outer-inner, and center-inner are shown in Figure 5.3 (d), (e), and (f), respectively.

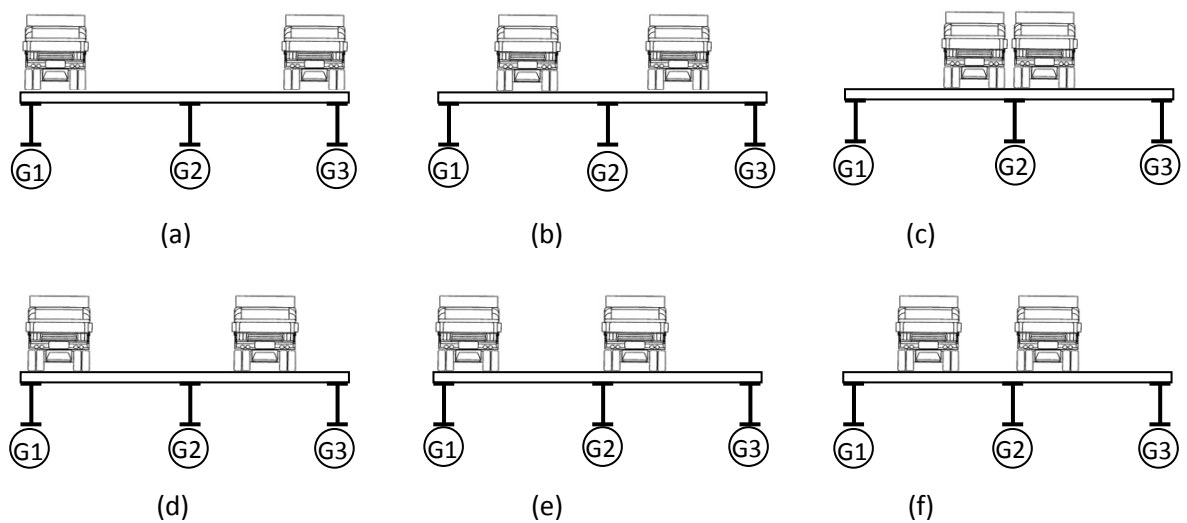


Figure 5.3 Transverse loading combination (a) Outer-outer (b) Center-center (c) Inner-inner (d) Outer-center (e) Outer-inner (f) Center-inner

5.5 Discussion on Finite Element Model Result

5.5.1 Critical Longitudinal and Transverse Positions of Truck Loading

In this parametric study, the truck was modeled to move along the bridge with speed 1 mm/s and to stop in every 100 second. It means the data from the truck load was collected in every 0.1 m. The first wheel of the truck was read by SAP2000 at the pivot point or the position of the truck load based on the first wheel. After examining the vertical displacement data, truck loading around midspan (first wheel 17.9 m from the support) causes the highest relative displacement between adjacent girders. It is also found in bridge length 18 m, 30 m, and 36 m that the maximum relative displacement occurs when truck around midspan. The same results were observed from both general types of loading.

In the two truck cases, the variations of transverse position were also combined. The examination shows the O-I (outer-inner) configuration, as shown in figure 5.3 (e). It results in the highest maximum relative displacement between adjacent girders rather than other transverse configuration. One of the trucks is on the outer lane above girder G1 and G2 and the other one is on the inner lane above girder G2 and G3. Both trucks move together along the bridge.

5.5.2 Maximum Relative Displacement Between Adjacent Girders (Global model)

5.5.2.1 Effect of Girder Spacing

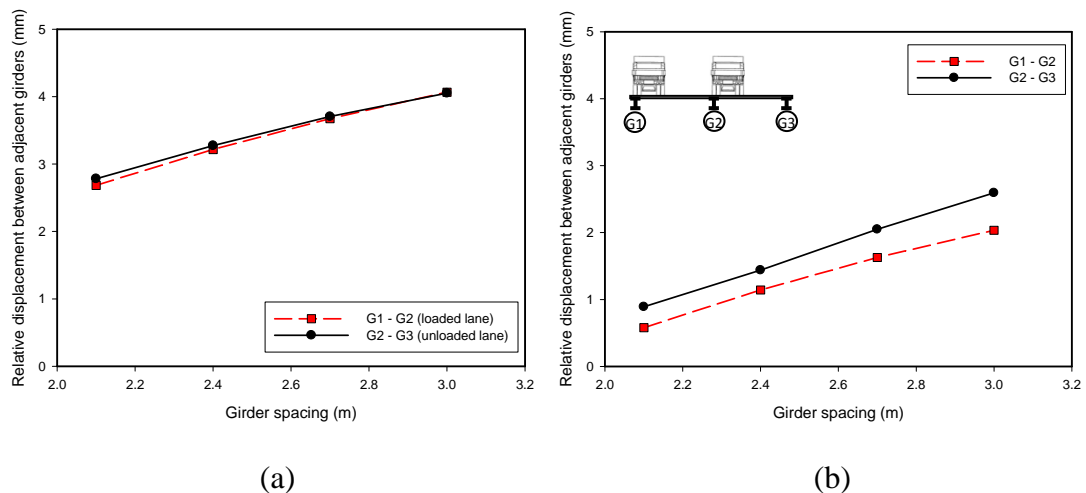


Figure 5.4 Girder spacing effect (a) One truck on left lane (b) Two trucks on both lanes

Figure 5.4 shows that the maximum relative deflections between adjacent girders as a function of the girder spacing. As the girder spacing increases, the length of diaphragm increases, thus, reducing the diaphragm stiffness and resulting to the increase of relative deflection. For the case of one truck loading, the difference between relative displacements between girders under loaded lane and unloaded lane is insignificant, as shown in figure 5.4 (a). The maximum relative deflection occurs when the truck is on the left end of the left lane (outer of the lane). Similar trend was also found in the case of two trucks, as shown in figure 5.4 (b), and the critical transverse truck combination is outer-inner. The maximum vertical deflection is in the girder G1, followed by girders G2 and G3, with relative displacement between G2 and G3 higher. Maximum relative displacement between adjacent girders for one truck loading is more critical than two trucks loading.

5.5.2.2 Effect of Slab Thickness

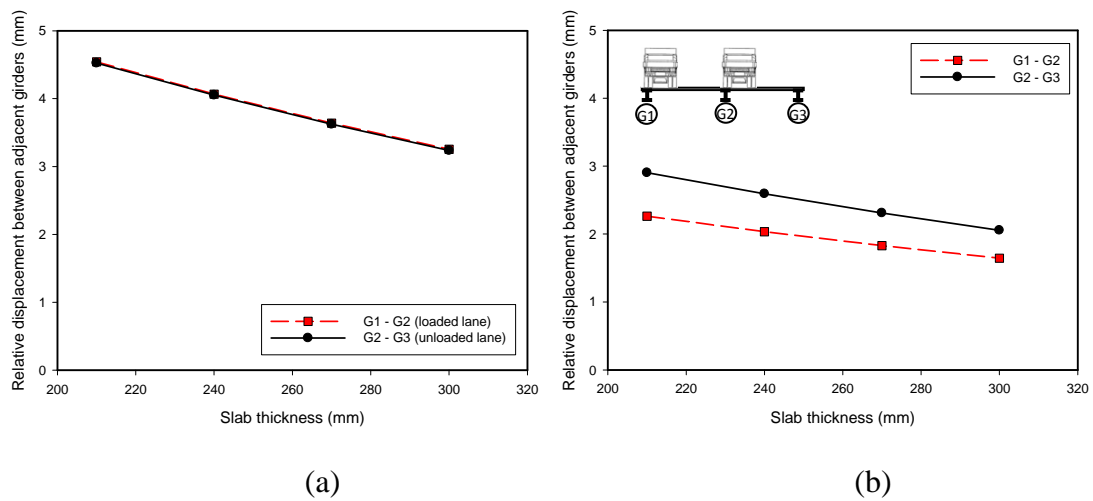


Figure 5.5 Slab thickness effect (a) One truck on left lane (b) Two trucks on both lanes

As shown in figure 5.5, the relative deflection decreases as slab thickness increases and comparison of both cases shows one truck case is more critical than two truck case. Figure 5.5 (a) shows the similarity relative displacement between girder under loading and unloading lane. Both show decreasing trend. Increasing the slab thickness causes the slab become more rigid and the unity of the slab become higher. It means that when the slab is very thick, live load in every position will cause the entire slab to deflect together as a unit. Moreover, slab thickness will transfer homogeneity to all girders and relative deflections between girders will become equal. Figure 5.5 (b) shows the similar results for the case of two trucks. The critical transverse position in two truck case is outer-inner.

5.5.2.3 Effect of Girder Stiffness

Girder is the main element of the bridge as it provides the longitudinal stiffness to the whole superstructure. If all girders are very stiff, the relative deflection between adjacent girders will be small, as shown in the trend in figure 5.6. In case of one truck loading, figure 5.6(a) shows that the relative deflection decreases as the girder becomes stiffer. For the two trucks loading, figure 5.6(b) shows that the outer-inner combination is a critical combination and the trend observed is similar to the case of one truck. The relative displacement of girder G2 and G3 is higher than G1 and G2. One truck case results higher critical relative displacement between adjacent girders than two truck case.

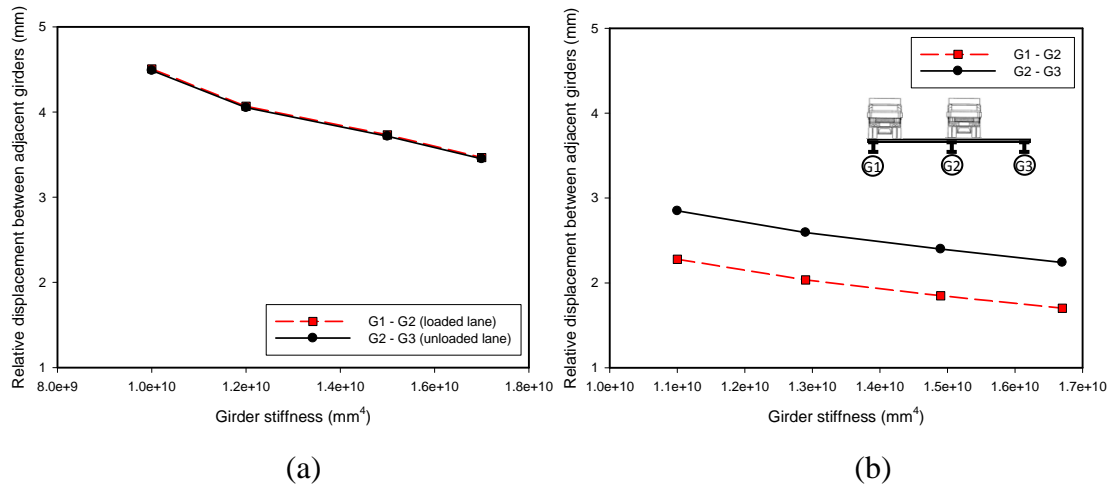


Figure 5.6 Girder stiffness effect (a) One truck on left lane (b) Two trucks on both lanes

5.5.2.4 Effect of Bridge Length

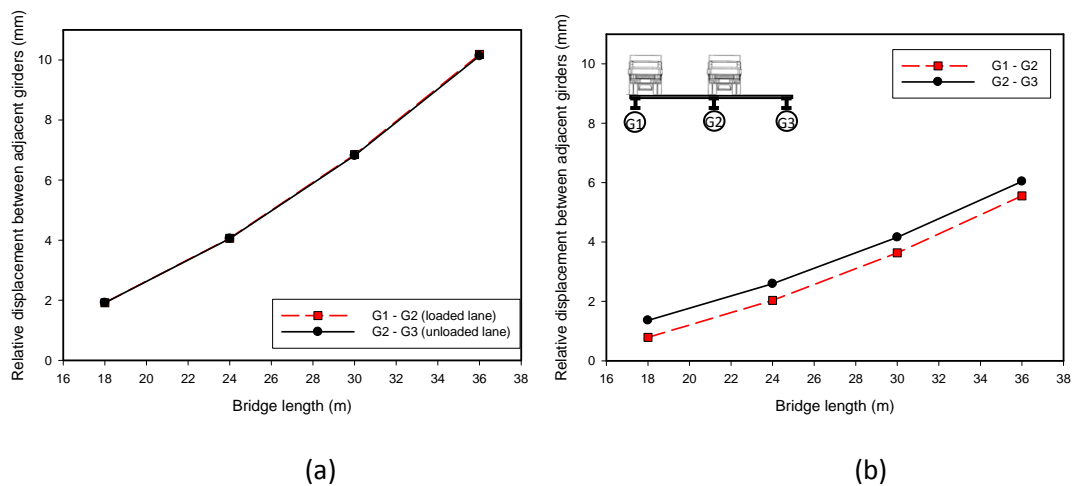


Figure 5.7 Bridge length effect (a) One truck on left lane (b) Two trucks on both lanes

Figure 5.7 shows the maximum relative deflections between adjacent girders as a function of the bridge length. The results show that the relative girder deflection becomes higher when the bridge length increases. Figure 5.7 (a) shows the results for the case of one truck on left lane. At a specific bridge length, the maximum value between the girders G1 and G2 is almost similar to the girders G2 and G3. Figure 5.7 (b) shows the results for the maximum relative deflection in case of two trucks and the outer-inner combination. In the case of two trucks, the relative displacement between G2 and G3 is higher than G1 and G2. For the case of two trucks, the maximum relative deflection was lower than the case of one truck.

5.5.3 Maximum Web Gap Stress

Figure 5.8 shows the transverse section of the bridge with determined web gap sides. After vertical displacement was applied in the submodel, midspan transverse section's deformed shape of finite element model with 3m girder spacing was shown in figure 5.9 and figure 5.10 for one truck case and two truck case, respectively.

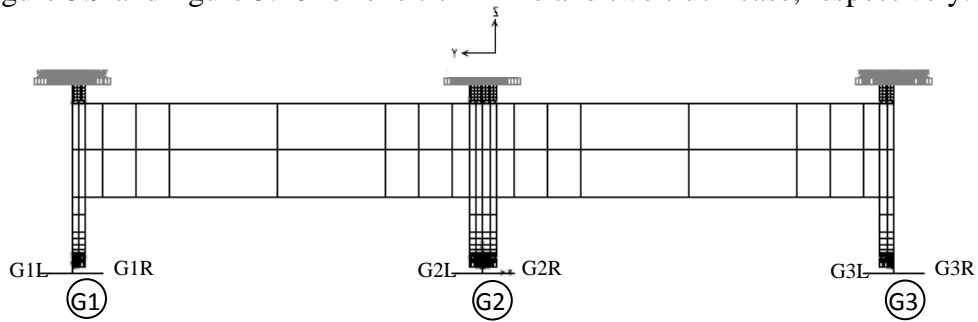


Figure 5.8 Web gap sides

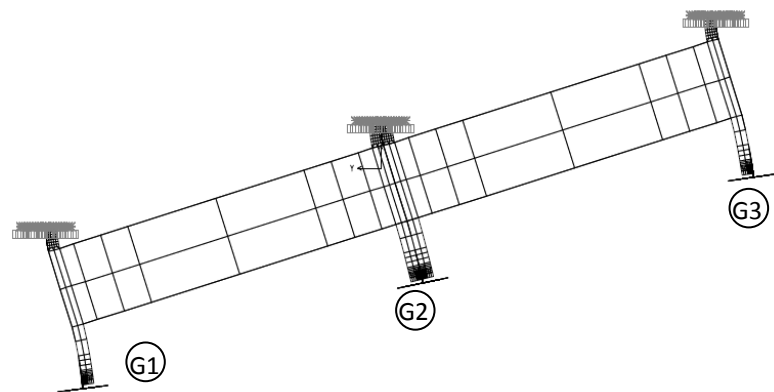


Figure 5.9 Midspan transverse section deformation shape in case of one truck loading

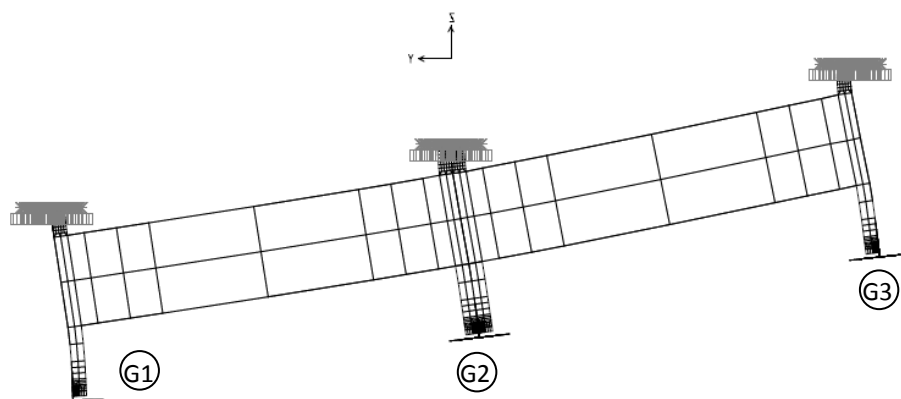
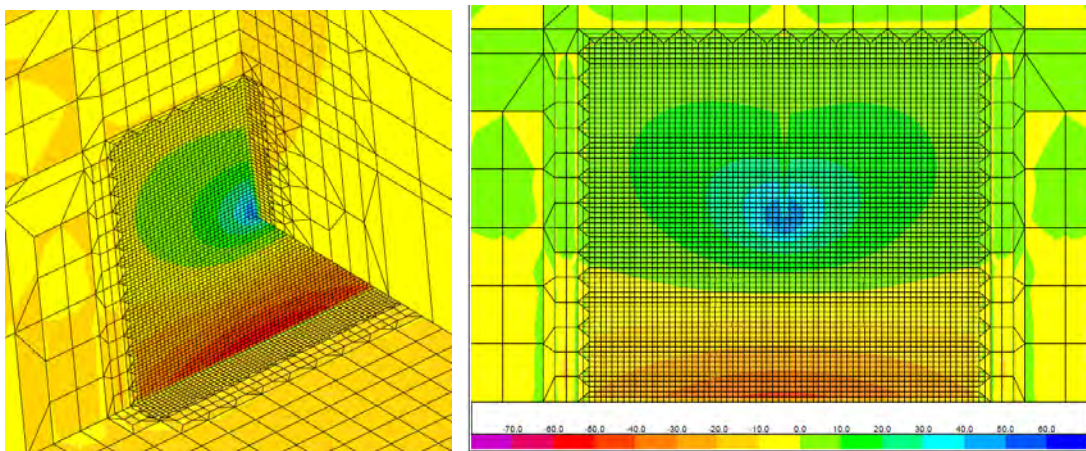


Figure 5.10 Midspan transverse section deformation shape in case of two truck loading

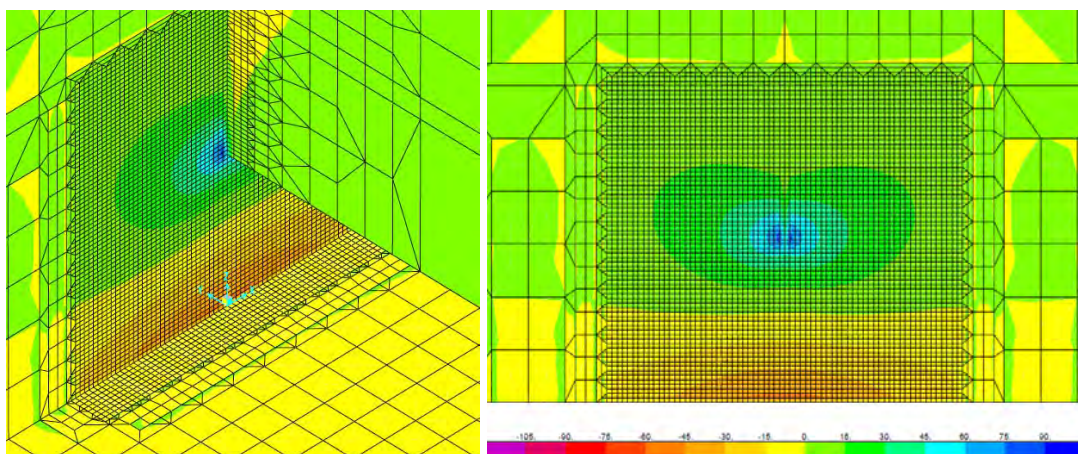
Using the refined finite element model, the peak web gap stress can be investigated. Figure 5.11 and figure 5.12 shows the vertical stress contour in the web gap area in the midspan of girder G1 and G2 in one truck case, respectively. It shows the stress field decays rapidly in both longitudinal and vertical directions away from end of stiffener. Stress distribution in the web gap area for all submodel shows the critical vertical stress occur in the top of web gap at the end of stiffener as shown in figure 5.13.



(a)

(b)

Figure 5.11 Stress distributions in web gap area of girder G1 (a) 3D view (b) Girder web view



(a)

(b)

Figure 5.12 Stress distributions in web gap area of girder G2 (a) 3D view (b) Girder web view

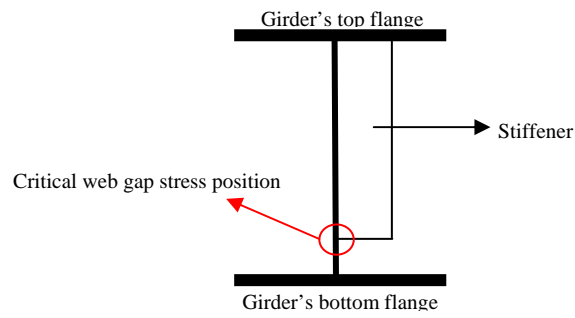


Figure 5.13 Critical vertical web gap stress position

5.5.3.1 Effect of Girder Spacing

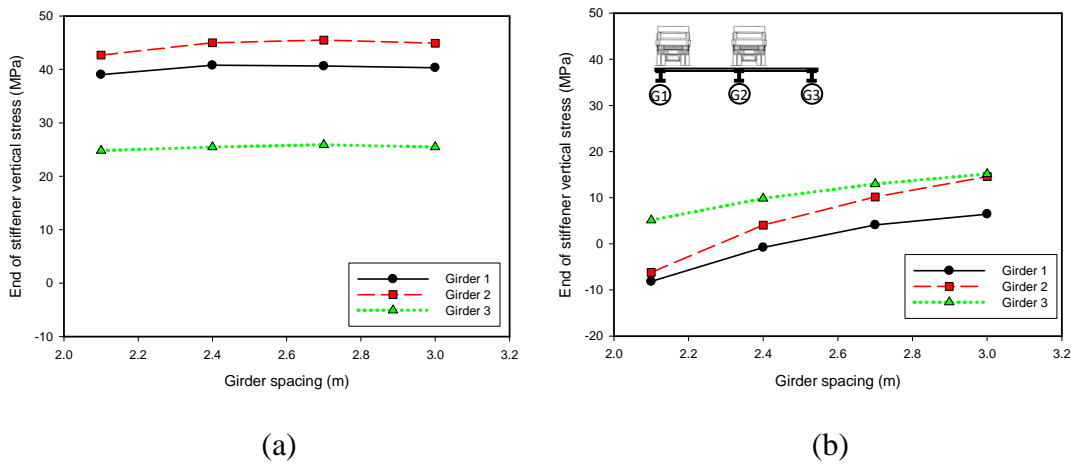


Figure 5.14 End of stiffener stress (a) One truck case (b) Two trucks case

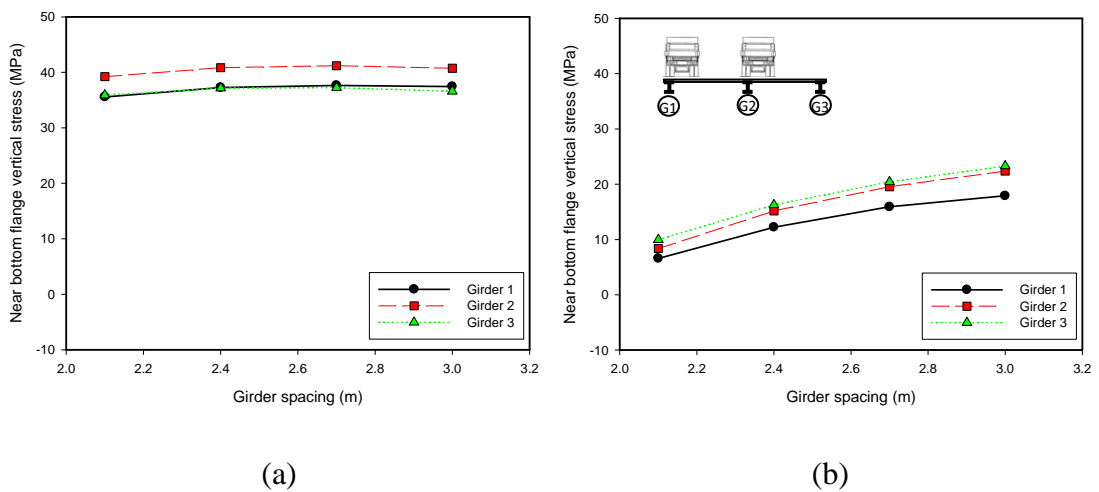


Figure 5.15 Near bottom flange stress (a) One truck case (b) Two trucks case

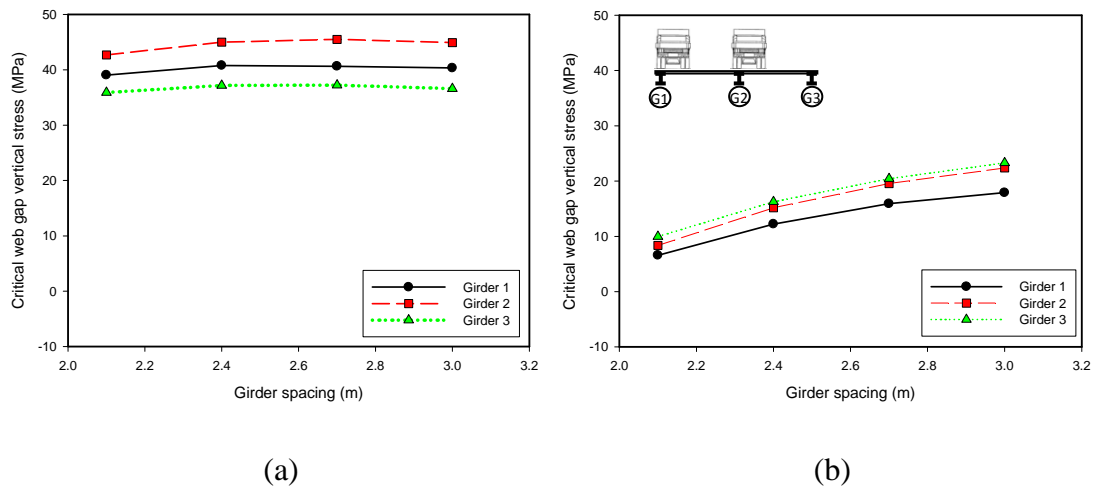


Figure 5.16 Girder spacing affect (a) One truck case (b) Two trucks case

Figure 5.14 shows the maximum web-gap stress as a function of the girder spacing in the end of stiffener and Figure 5.15 shows the maximum web-gap stress near bottom flanges. As shown in these figure, the critical web gap stress occurred in the end of stiffener of G2 in case of one truck and two truck case results the critical web gap stress in the area near bottom flanges. This result was obtained in all case of parameter. The critical web gap stress was shown in figure 5.16. All of the web-gap stresses occurred in the right side because girder G1 deflected the most. It was followed by girder G2 and G3, which shows that the tension area is in the right side of the web gap. In the case of one truck, the maximum web-gap stress occurred at the end of right stiffener of girder G2 (G2R side). Figure 5.16(a) shows that the maximum web gap stress does not change as the girder spacing increases. In the case of one truck, the rotation of diaphragm of every girders spacing, which was identified in dividing the relative displacement by the girder spacing, is almost equal. It result the critical web gap stress getting identical in every girder increasing. This assumption is accordance with Jajich et al.(2000) which is determined the web-gap stress by using the rotation of diaphragm. In two trucks loading, the maximum web-gap stress is higher as the girder spacing increasing and this is demonstrated in figure 5.16(b). The maximum web gap stress in the G2R and G3R is higher than G1R because the relative displacement between girder G2 and G3 is higher than between girder G1 and G2. Similar with relative displacement, comparison between two case shows one truck case result more critical vertical web gap stress in the end of stiffener than two truck case.

5.5.3.2 Effect of Slab Thickness

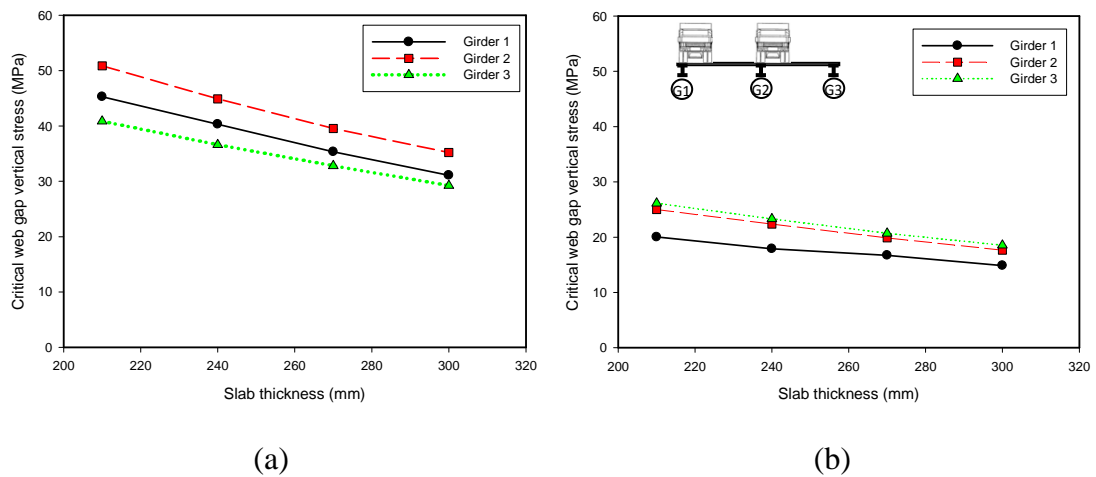


Figure 5.17 Slab thickness effect (a) One truck case (b) Two trucks case

As shown in figure 5.17, the maximum web gap stress decreases as slab thickness increases. Figure 5.17 (a) shows the results from one truck when the truck moves on the left edge of the left lane. It shows the maximum web-gap occurs in the G2R. Figure 5.17 (b) shows the similar results for the case of two trucks. The critical transverse position is the outer-inner combination. The relative displacement when the two trucks moves between girder G2 and G3, and it is higher than between G1 and G2. It causes the web-gap stress in the G2R and G3R identical and higher than G1R maximum web-gap stress. Comparison between two cases shows critical vertical web gap stress in the end of stiffener in one truck case is more critical than two truck case. It appropriates to the relative displacement comparison.

5.5.3.3 Effect of Girder Stiffness

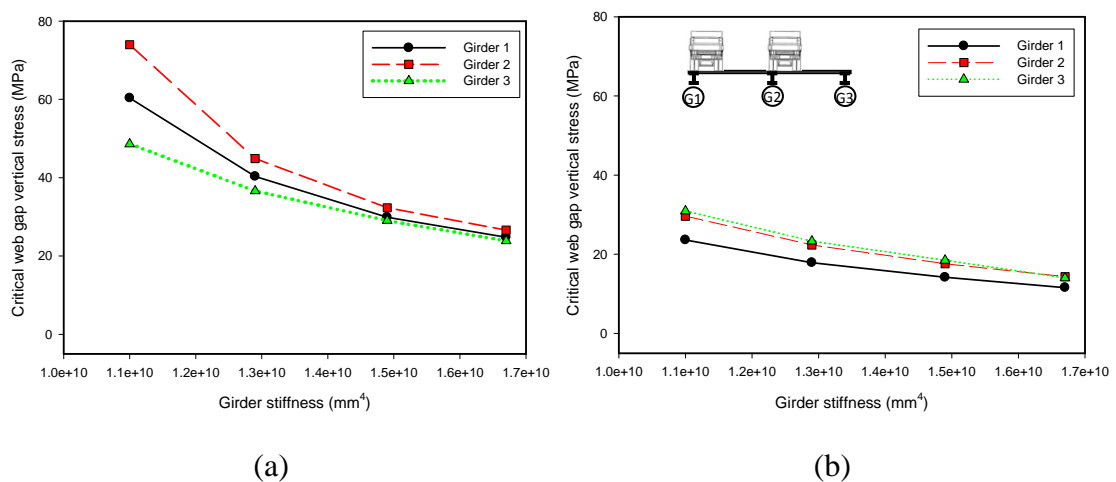


Figure 5.18 Girder stiffness effect (a) One truck on case (b) Two trucks case

If all girders are very stiff, the relative deflection between adjacent girders will be very small and the maximum web-gap stress reduces in both sides. Figure 5.18(a) shows that the relative deflection decreases as the girder becomes stiffer. The maximum web-gap stress occurs in the end of stiffener of G2R side and follow by G1R and G3R. Figure 5.18(b) shows the results for the case of two trucks and the outer-inner combination, which is a critical combination. The trend is similar to the case of one truck. In this parametric study, girder web and flanges were made thicker every increasing of girder stiffness. It cause web gap area become more stiff and result web gap stress decrease in girder stiffness increasing. Maximum web gap stress in the G2R and G3R is almost same and G1R result lower web-gap stress. It can be occur because of the differences of relative displacement. Similar with relative displacement comparison, one truck case shows more critical result than two truck case.

5.5.3.4 Effect of Bridge Length

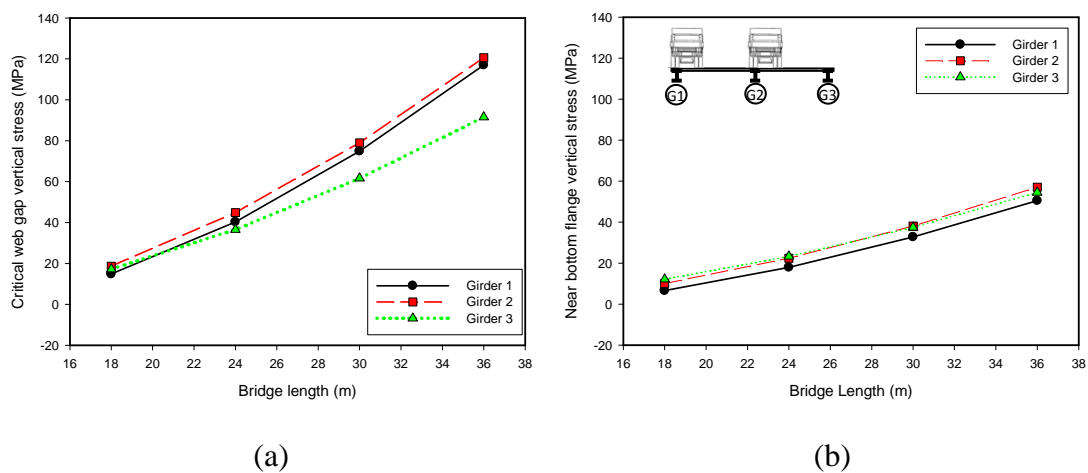


Figure 5.19 Bridge length effect (a) One truck case (b) Two trucks case

Figure 5.19 shows the maximum web gap stress as a function of the bridge length. The results show that the web-gap stress becomes higher as the bridge length increases. Figure 5.19 (a) shows the results for the case of one truck on left lane. At a specific bridge length, the maximum web gap stress in G2R and G1R is almost similar, and both are higher than G3R. Figure 5.19(b) shows the results for the maximum relative deflection in case of two trucks and the outer-inner combination. In case of two trucks, the relative displacement between G2 and G3 is higher than G1

and G2, but the finite element model (submodel) shows the critical web-gap stress to occur in the G2R, G1R and G3R consecutively. It contradicts with the relative displacement result where the relative displacement between G2 and G3 is higher than between G1 and G2. This happened probably because the relative displacement is very high and it led the stress in the stiffener side (inside side) to be higher than the outer side of external girder. Overall case of two trucks shows the maximum relative deflection to be lower than the case of one truck.

5.5.4 Lateral Load Distribution Factor

Another important issue of bridge design is lateral load distribution factor. It shows the maximum moment and shear of each girder because of the live load in concrete slab. Distribution factor was calculated by applying the finite element model with the truck positioned at the longitudinal location to produce the maximum moment. The trucks were then moved transversely across the width of the girder until it resulted to the largest moment in the girder section. The ratio of this moment to the moment from simple beam loading with one truck wheel line represents the distribution factor as demonstrated by Mabsout et al (1998) and Zokaie et al (2000). In this study, the lane was assumed as the same as girder spacing and applied by one truck each lane. Truck does not move to the other lane.

5.5.4.1 SAP2000 Result

The SAP2000 beam result are illustrate in figure 5.20. In this figure, P is the axial forces, M2 and M3 are the bending moments about the local axes 2 and local axes 3. The local tangent along the beam element, local axis 1, is defined as a vector from the node i to j. The local axis 3 direction is perpendicular to the local axes 1 and the local axes 2. These three axes follow the right-hand-rule. The result from the beam element that used in the load distribution factor analysis is P and M33.

The shells result was obtained using *section cut* ability in SAP2000. Section cut results of shell are illustrate in figure 5.21. The result from the section cut that used in the load distribution factor analysis is F2 and M2.

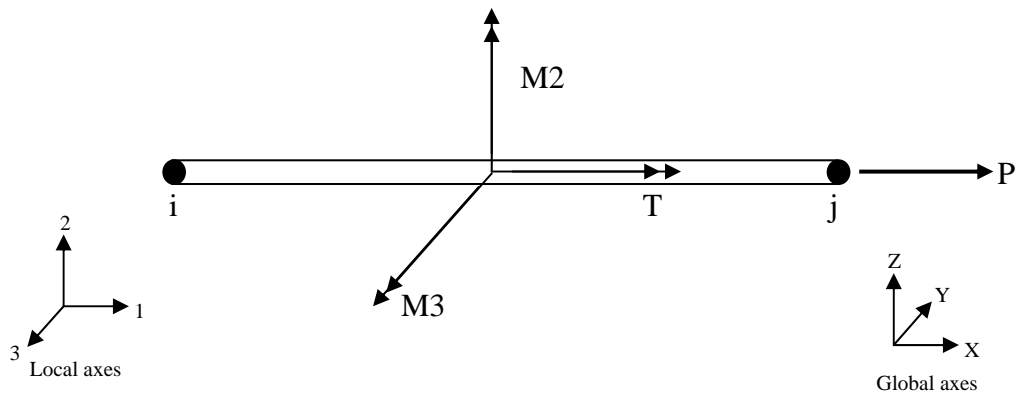


Figure 5.20 Notation of beam element result

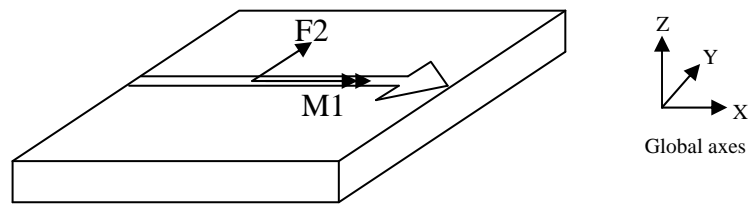


Figure 5.21 Notation of *section cut* result

5.5.4.2 Effective Width

The *section cut* length was built base on the effective width of the deck. The effective width of the deck was recommended by AISC. The effective width of slab is distance a plus distance b , as shown in figure 5.22. Value of a and b is the smallest value of:

- One-eighth of the effective span length;
- Half of spacing of adjacent beams.
- The width of the overhang.

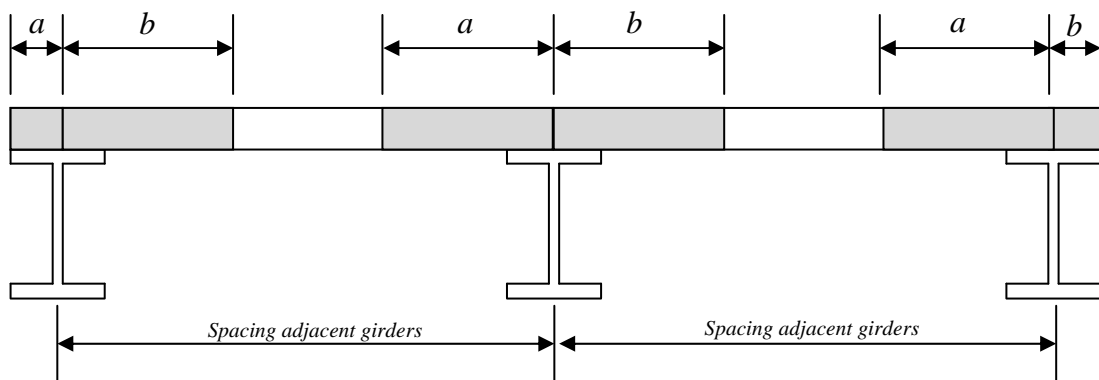


Figure 5.22 Effective width

5.5.4.3 Moment in The Girder Section

In order to calculate the load distribution factor from the finite element model, the moment in the girder section has to be determined. The moment in the girder section is the resultant of girder moment in the beam element, deck moment in the shell element, and moment from the axial forces, as shown in figure 5.23.

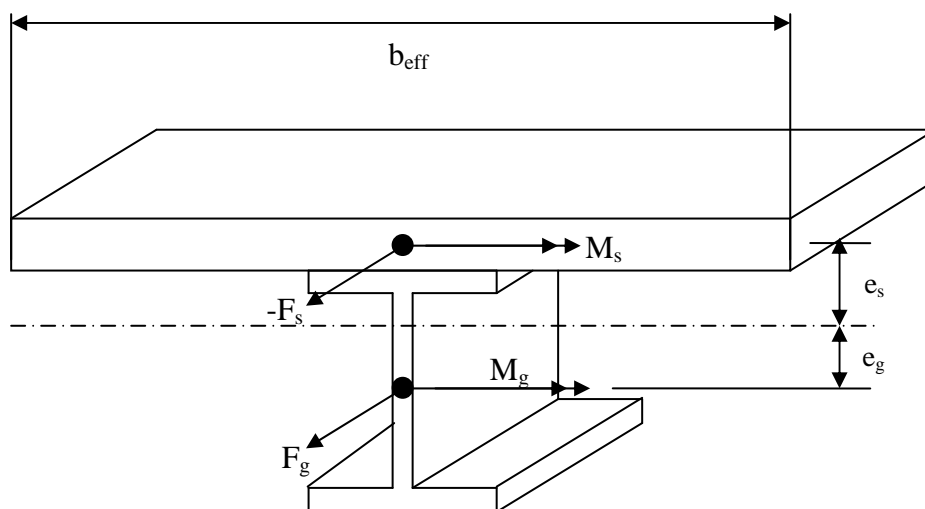


Figure 5.23 Notation of *section cut* result

a) Girder moment

The girder moment is the moment in the beam element. The girder moment in the midspan is obtained from the output of SAP2000. Moment M3 of the frame element is the longitudinal moment output.

$$M_g = M3(\text{frame element}) \quad (5.2)$$

b) Deck moment

The deck moment is the moment in shell element. It is generated by the *section cut* in SAP2000, as shown in figure 5.24. Moment in axes 1 was determined as deck moment. moment is the moment in the beam element. The girder moment in the midspan is obtained from the output of SAP2000. Moment M3 of the frame element is the longitudinal moment output.

$$M_s = M1(\text{section cut}) \quad (5.3)$$

Section Cutting Line

	X	Y	Z
Start Point	12000.	3000.	0.
End Point	11997.28	1358.77	0.

Resultant Force Location and Angle

	X	Y	Z	Angle (X to 1)
	11998.64	2179.385	0.	269.9051

Include Frames Shells Asolids Planes Solids INLLINK

Integrated Forces

	Right Side			Left Side		
	1	2	Z	1	2	Z
Force	-1.5431	61.5627	1.196	1.5431	-61.5627	-1.196
Moment	-1316.831	455.4528	-6769.64	1316.8309	-455.4528	6769.64

Buttons: Save Cut, Save Cut, Close, Refresh

Figure 5.24 Section cut form in SAP2000

c) Moment produced by axial force

After the force and moment in the girder are known, the neutral axis of the girder can be determined. The neutral axis is where the strain and the corresponding stress in the beam element are zero. The eccentricity from the neutral axis to the centroid of the girder is calculated as follows:

$$e_g = \frac{F_g \times I_g}{A_g \times M_g} \quad (5.4)$$

and

$$e_s = e - e_g \quad (5.5)$$

Then the moment due to the axial force can be calculated as follows:

$$M_{axial} = F_g \times e_g + -F_s \times e_s \quad (5.6)$$

Where A_g and I_g are the girder area and moment inertia, respectively, F_g is the girder axial force, F_s is the integrated axial force in the shell element, e is the distance between the centroids of the girder and the deck, e_g and e_s are the eccentricity from the section's neutral axis to the centroids of the girder and the deck, and M_{axial} is the moment from the axial force.

5.5.4.4 Moment From Beam Analysis

In this study, a simple beam model was constructed. To accommodate the finite element model in parametric study, four simple beam models with different length was constructed. The length is 18 m, 24 m, 30 m, and 36 m. The length and the mesh of the beam is the same as the three dimension finite element model. The loading is one lane of wheel loads move along the length of the beam. This was modeled in SAP2000 as shown in figure 5.25.

Figure 5.25 One lane wheel load in SAP2000

Simple beam analysis results showed that the maximum moment occurred in the mid-span area when the first wheel of truck is 16.4 m from edge of the 24 m beam. One line wheel truck on 13.4 m, 19.4 m, and 22.4 m caused the maximum moment for 18 m, 30 m, and 36 m beam length, respectively. Beam 18 m has the maximum moment 5.4×10^8 N-mm. Beam 24 m has the maximum moment 7.86×10^8 N-mm. The 30 m beam result the maximum moment 1.03×10^9 N-mm. Maximum moment 1.28×10^9 N-mm occurred in 36 m beam.

5.5.4.5 LDF Calculation

In the calculation of the load distribution factor, moment in the girder section from the finite element model results and the maximum moment from one dimensional beam analysis were compared. The moment in the girder section from

the finite element analysis is composed by girder moment, deck moment, and moment from the axial force.

One truck in left case and two trucks on both lanes case were analyzed using the finite element model. Each lane was divided in transverse direction into three in order to get the maximum moment with the same longitudinal position of truck. For one truck case, the maximum moment occurred when the truck move in the outer lane. The outer-inner combination of truck shows the maximum moment result in case of two trucks. The LDF is determined using the moment in the girder section divided by the maximum moment from the one-dimensional beam analysis. The load distribution factors of external girder for every model are shown in figure 5.26 until figure 5.29.

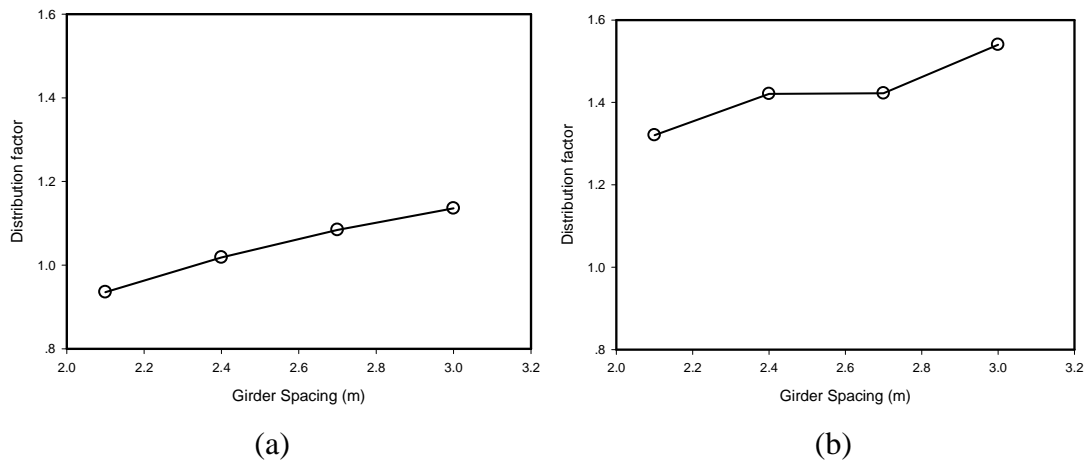


Figure 5.26 Girder spacing effect (a) One truck on left lane (b) Two trucks on both lanes

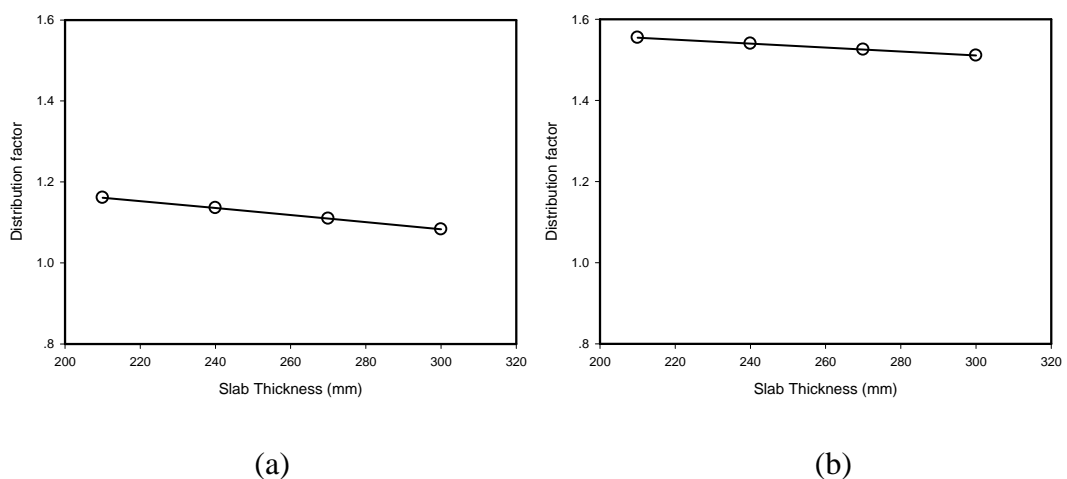


Figure 5.27 Slab thickness effect (a) One truck case (b) Two trucks case

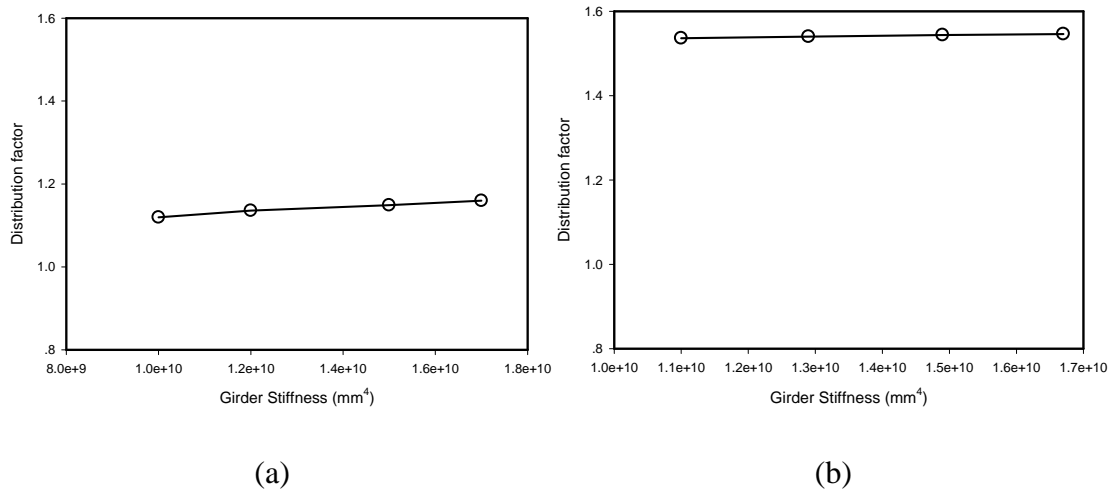


Figure 5.28 Girder stiffness effect (a) One truck case (b) Two trucks case

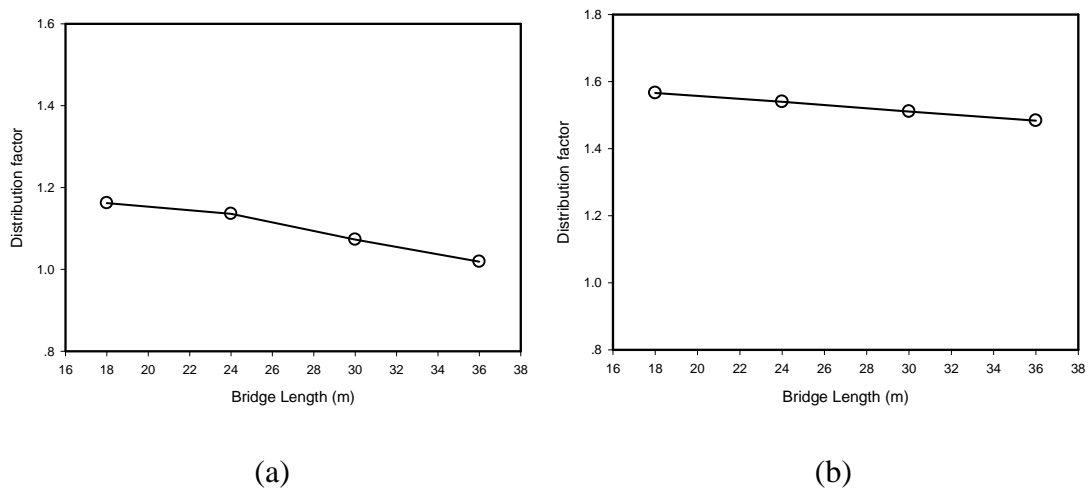


Figure 5.29 Bridge length effect (a) One truck case (b) Two trucks case

Four key parameter of lateral load distribution was investigated in the parametric study. The parameters are girder spacing (S), slab thickness (t_s), girder stiffness (I_g), and bridge length (L). Figure 5.26 to figure 5.29 shows the effect of each parameter on the distribution factor using the global model. The distribution factors decreases as the girder spacing and girder stiffness increase. This observation was also demonstrated in figure 5.26 and figure 5.28, respectively. However, the distribution factor increases as the slab thickness and bridge span increases. It can be verified by referring to figure 5.27 and figure 5.29, respectively. This result is in accordance with Zokaie's study.

5.6 Comparison Between AASHTO and Thai Trucks

5.6.1 Lateral Load Distribution Factor

Two different trucks, AASHTO truck and Thai truck, were evaluated using the finite element model. The properties of both trucks are shown in figure 5.30. For comparative purpose, a base finite element model from parametric study was used. The finite element model was evaluated with one truck and two truck case and load distribution in external girder was compared.

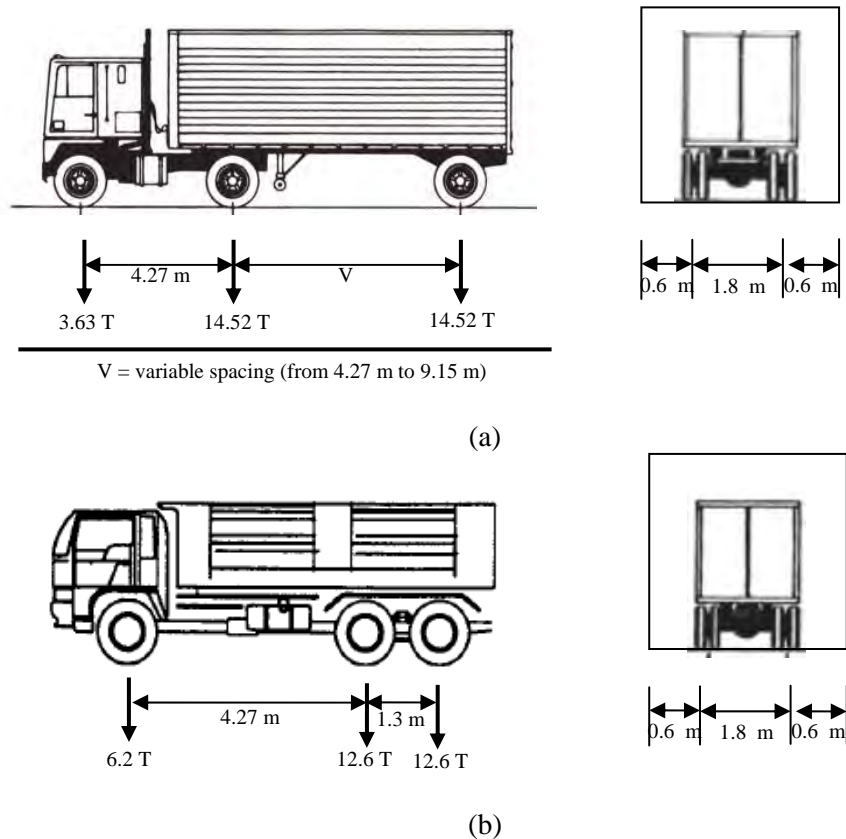


Figure 5.30 Characteristic of truck (a) AASHTO truck (b) Thai truck

Simple beam model was constructed in order to obtain the maximum moment by both AASHTO truck and Thai truck load. Simple beam model was constructed according the length of base finite element model, which is 24 m. The mesh of beam was made according the girder in global model. In a one dimension analysis, the truck load was modeled as one wheel load. The configuration of one lane vehicle load from SAP2000 is shown in figure 5.31. Simple beam analysis showed that the maximum moments occurred in the mid-span area when the first wheel of truck is 16.4 m from edge for AASHTO truck, and 16.3 m for Thai truck loading. One lane wheel of

AASHTO truck had a maximum moment 7.9×10^8 Nmm and Thai truck's one lane loading had a maximum moment 8.4×10^8 Nmm.

General Vehicle Data

Vehicle Name: HSn-44-1

Floating Axle Loads

	Value	Width Type	Axle Width
For Lane Moments	0.	One Point	
For Other Responses	0.	One Point	

Double the Lane Moment Load when Calculating Negative Span Moments

Usage

Lane Negative Moments at Supports
 Interior Vertical Support Forces
 All other Responses

Min Dist Allowed From Axle Load

Lane Exterior Edge: 304.8
 Lane Interior Edge: 609.6

Miscellaneous Parameters

Use BD 37/01 (2002) for Uniform Load Length Effects
 Vehicle Applies To Straddle (Adjacent) Lanes Only

Straddle Reduction Factor: _____

Loads

Load Length Type	Minimum Distance	Maximum Distance	Uniform Load	Uniform Width Type	Uniform Width	Axle Load	Axle Width Type	Axle Width
Leading Load	Infinite		0.	Fixed Width	3048.	1.8144	One Point	
Leading Load	Infinite		0.	Fixed Width	3048.	1.8144	One Point	
Fixed Length	4267.2		0.	Fixed Width	3048.	7.2575	One Point	
Variable Length	4267.2	9144.	0.	Fixed Width	3048.	7.2575	One Point	

Vehicle Remains Fully In Lane (In Lane Longitudinal Direction)

Units: Ton, mm, C

(a)

General Vehicle Data

Vehicle Name: Thai Truck-1

Floating Axle Loads

	Value	Width Type	Axle Width
For Lane Moments	0.	One Point	
For Other Responses	0.	One Point	

Double the Lane Moment Load when Calculating Negative Span Moments

Usage

Lane Negative Moments at Supports
 Interior Vertical Support Forces
 All other Responses

Min Dist Allowed From Axle Load

Lane Exterior Edge: 304.8
 Lane Interior Edge: 609.6

Miscellaneous Parameters

Use BD 37/01 (2002) for Uniform Load Length Effects
 Vehicle Applies To Straddle (Adjacent) Lanes Only

Straddle Reduction Factor: _____

Loads

Load Length Type	Minimum Distance	Maximum Distance	Uniform Load	Uniform Width Type	Uniform Width	Axle Load	Axle Width Type	Axle Width
Leading Load	Infinite		0.	Zero Width		3.1	One Point	
Leading Load	Infinite		0.	Zero Width		3.1	One Point	
Fixed Length	4200.		0.	Zero Width		6.3	One Point	
Fixed Length	1300.		0.	Zero Width		6.3	One Point	

Vehicle Remains Fully In Lane (In Lane Longitudinal Direction)

Units: Ton, mm, C

(b)

Figure 5.31 Characteristic of truck loadings in SAP2000 (a) AASHTO truck (b) Thai truck

The truck longitudinal position obtained from simple beam model was used with varying transverse position. According to the previous sub-chapter the critical transverse position is when truck move in the outer lane for one truck case and one truck in the outer lane plus one truck in the inner lane is the the critical transverse position for two trucks case

The maximum moment occurred in G1 because it is below the truck lane. The controlling moment was then selected. Similar method with chapter 5.5.4 was used to obtain the longitudinal moment in the composite bridge as shown in figure 5.21. The load distribution factor of external girder in one truck case results 1.14 for AASHTO truck and 1.11 for Thai truck, while two AASHTO truck and Thai truck result 1.54 and 1.44 load distribution factor, respectively.

The distribution factor from AASHTO truck was overestimated the Thai truck. However, the difference is only 10% and can be neglected. This is as the same as Chaisombob and Larshima (2000) study, which is a result of Thai truck distribution factor, it is smaller than the distribution factor from the AASHTO HS20-44 trucks.

5.6.2 Web Gap Stress

In order to obtain the maximum web-gap stress with the same bridge dimension, the maximum relative displacement between adjacent girders must be predicted. The truck on the outer lane of left lane was chosen on this analysis because it results the critical maximum relative displacement in the midspan. From the global model AASHTO truck in 17.9 m and Thai truck in 16.2 m longitudinal position, the maximum relative displacement for both truck cases is 4.1 mm for one truck in the outer lane that is occurred in the girder under loading and unloading lane. Afterward, 2.6 mm relative displacement under the truck in move in the inner lane was occurred in two truck case. The girder shape of all three girders from quarter-span until three-quarter span was applied from the load to the submodel. After the deformed shape of girder was applied to the submodel, SAP2000 analysis shows that the maximum web gap stress occurred in the end of stiffener for the two types of truck load. Maximum web gap stress in every girder was obtained from G1R, G2R, and G3R where the tension stress occurred. All maximum web gap results are shown in figure 5.32.

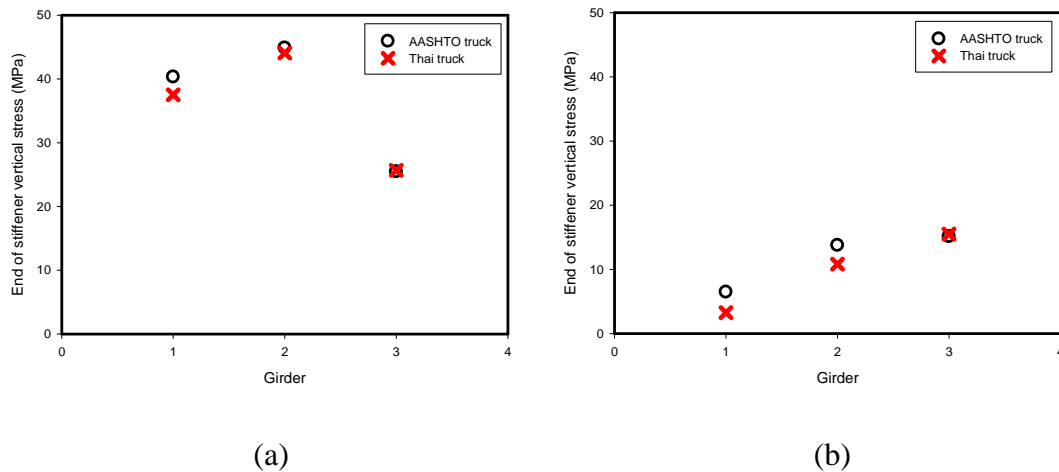


Figure 5.32 End of stiffener vertical web gap stress in each girder (a) One truck case
(b) Two truck case

Figure 5.32 shows the web gap stresses at the end of stiffener of every girder. It shows that the critical web gap stress occurred in the G2R area in case of one truck and G3R area in case of two trucks. Figure 5.32 shows the maximum web-gap stress of AASHTO truck loading to be slightly an overestimate of the Thai truck loading. The difference critical web gap stress of two truck loading types is 1% for one truck case and 2% for two truck case, which occurred in G1R and can be neglected.

CHAPTER VI

DEVELOPMENT OF THE FORMULA FOR RELATIVE DISPLACEMENT BETWEEN ADJACENT GIRDER AND WEB GAP STRESSES

6.1 Ranking of The Influencing Bridge Parameters

Chapter 5.5 explains the study on the effect of the bridge's parameters on the relative displacement and web gap stress. The most influenced parameter yields the highest deviation of result in the same increasing. However, the units of these parameters cause a problem in determining the most influential parameter. In order to eliminate the parameter's unit, the increasing from the smaller value of the parameters (%) needs to be used. Increasing parameters means the different of the next parameter to the first parameter divide by the first parameter and multiplied by 100%. The dependent value (relative displacement between adjacent girder of or maximum web-gap stress) was modified to the deviation to the first parameter. In other words, the smallest value of each parameter increasing should be equal to zero and the next parameter as the increasing of the second, third, and fourth value in percent.

6.1.1 Relative Displacement Between Adjacent Girders.

The effect of the parameter increasing on the deviation relative displacement between adjacent girders is shown in figure 6.1 until figure 6.4.

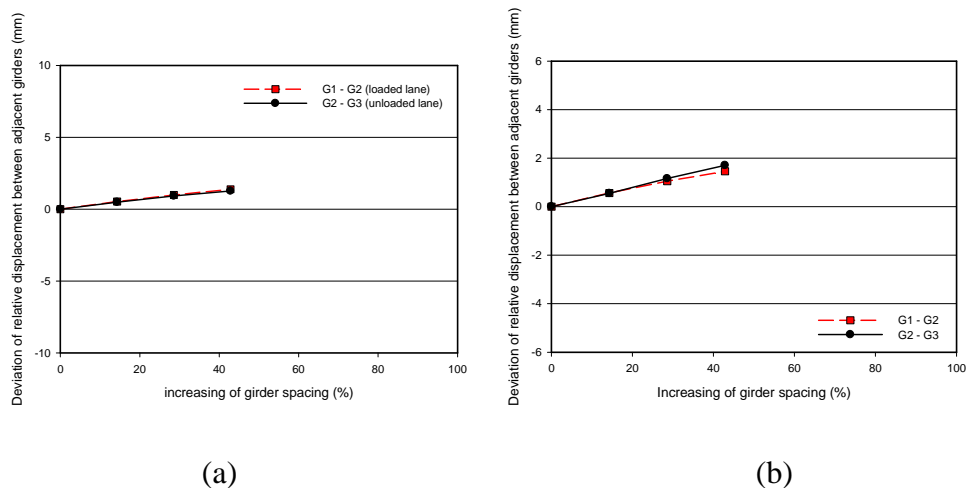
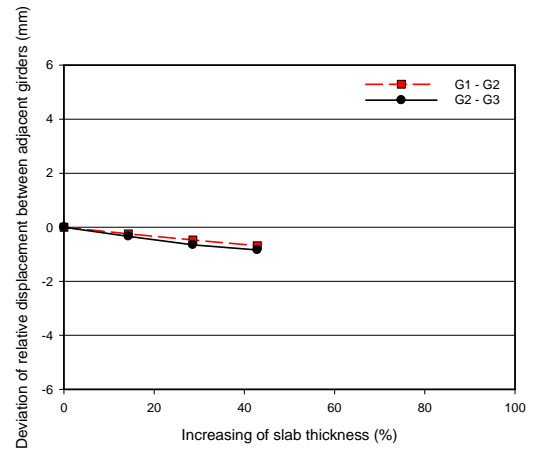
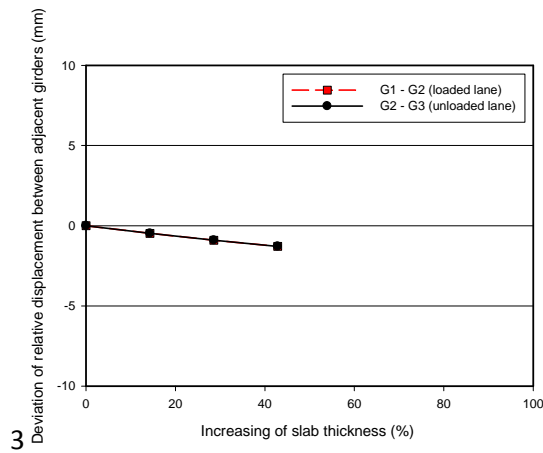


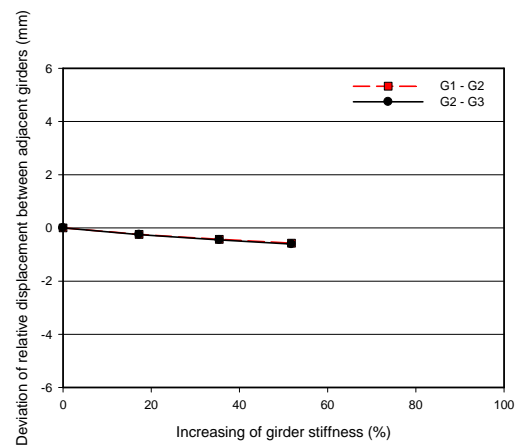
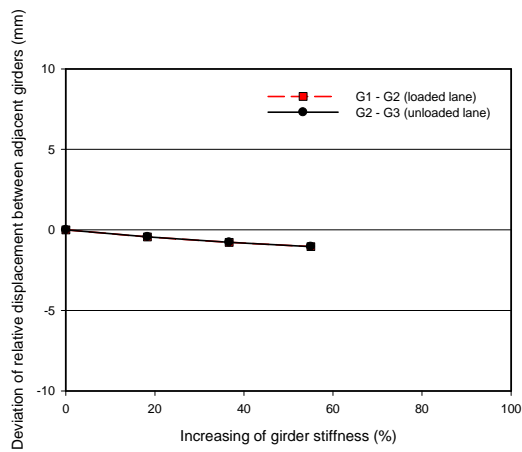
Figure 6.1 Girder spacing effect (a) One truck case (b) Two trucks case



(a)

(b)

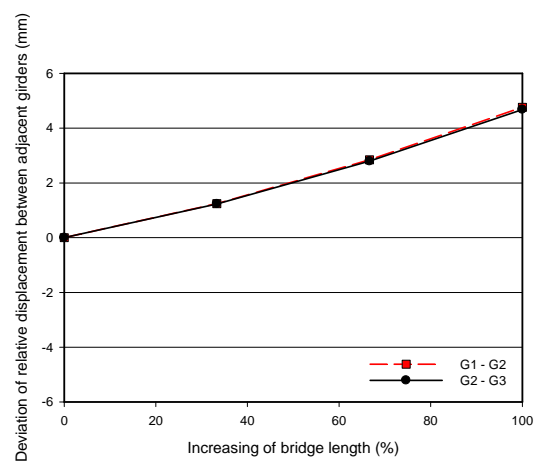
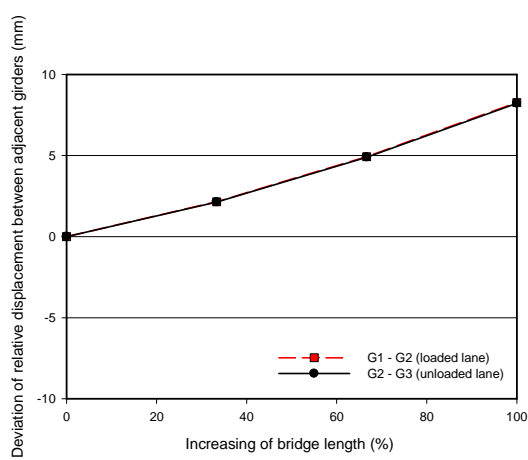
Figure 6.2 Slab thickness effect (a) One truck case (b) Two trucks case



(a)

(b)

Figure 6.3 Girder stiffness effect (a) One truck case (b) Two trucks case



(a)

(b)

Figure 6.4 Bridge length effect (a) One truck on case (b) Two trucks case

Figure 6.1 until figure 6.4 plot the deviation of critical relative displacement between adjacent girders with increasing of parameter. Positive slope means the relative displacement gets higher with increasing bridge parameter and vice versa. Figure 6.1 (a) shows the regression line slope for a one case truck to be lower than two truck case, as shown in figure 6.1(b). It means the range of the relative displacement of two truck cases is higher than a one truck case. From figure 6.1 to figure 6.4, a one truck case slope of linear regression shows that the highest slope occurred in comparison of bridge length parameter then followed by slab thickness, girder spacing, and the lowest slope as the girder stiffness comparison. For comparison, in 40% increasing of bridge length result 3 mm deviation of relative displacement, slab thickness result 1.3 mm, girder spacing result 1.2 mm, and when girder stiffness increasing 40%, the relative displacement decrease 0.8 mm. It shows the sensitivity rank of parameter to the relative displacement between adjacent girders in one truck case is bridge length, slab thickness, girder spacing, and girder stiffness. Similarly for the two truck case, the highest slope occurs in bridge length, but in this case followed by girder spacing, slab thickness, and girder stiffness. For comparison, 40% increasing of bridge length, girder spacing, slab thickness, and girder stiffness result 1.8 mm, 1.6 mm, 0.9 mm, and 0.5 mm deviation of relative displacement, respectively. Overall the most influential bridge parameter to the relative displacement between adjacent girders is the bridge length, while the smallest influence was observed from the girder stiffness.

6.1.2 Web Gap Stress.

The effect of each parameter increasing in maximum web gap stress is shown in figure 6.5 until figure 6.8.

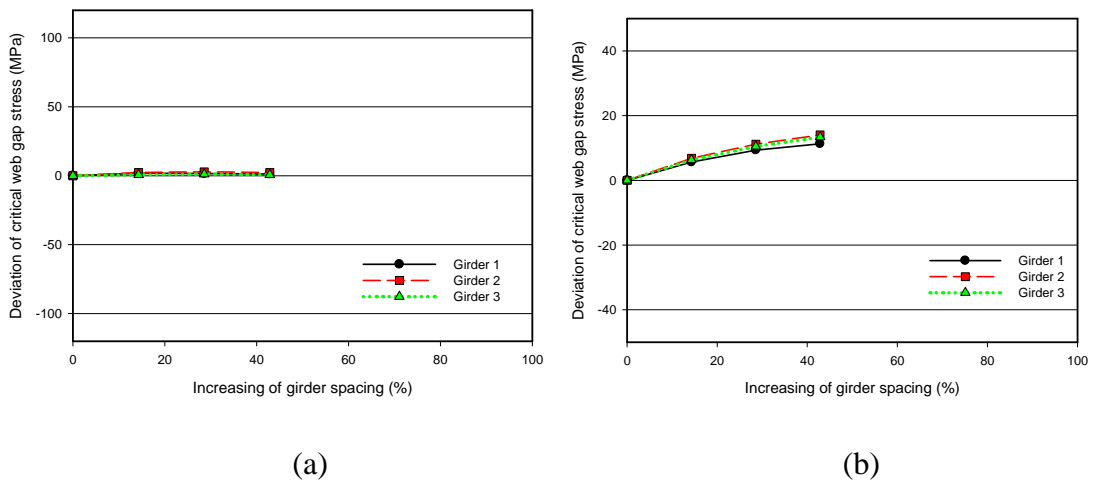


Figure 6.5 Girder spacing effect (a) One truck case (b) Two trucks case

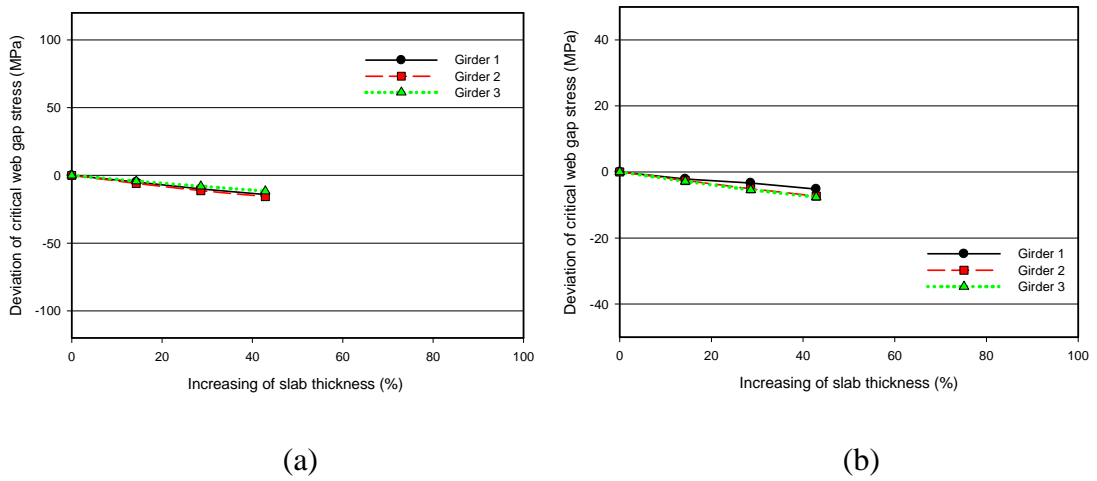


Figure 6.6 Slab thickness effect (a) One truck case (b) Two trucks case

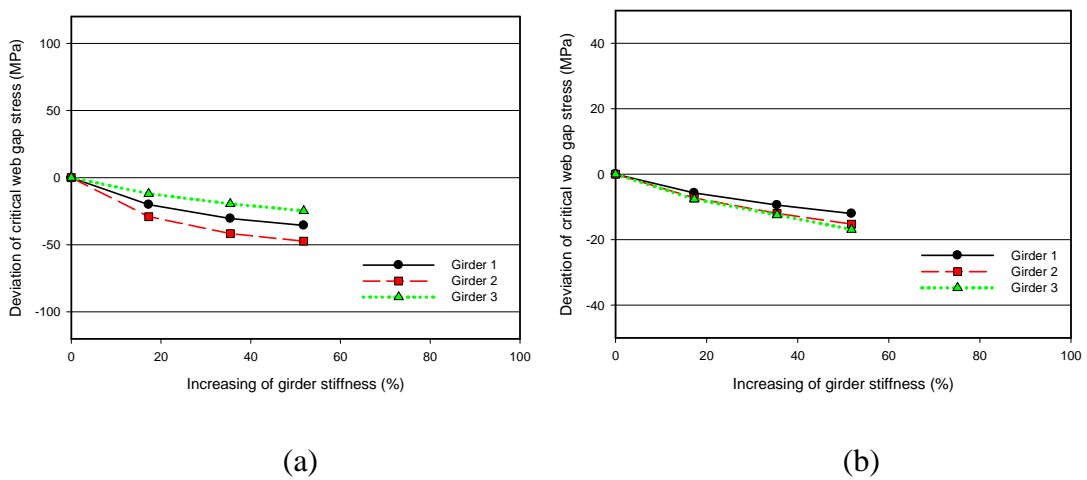


Figure 6.7 Girder stiffness effect (a) One truck case (b) Two trucks case

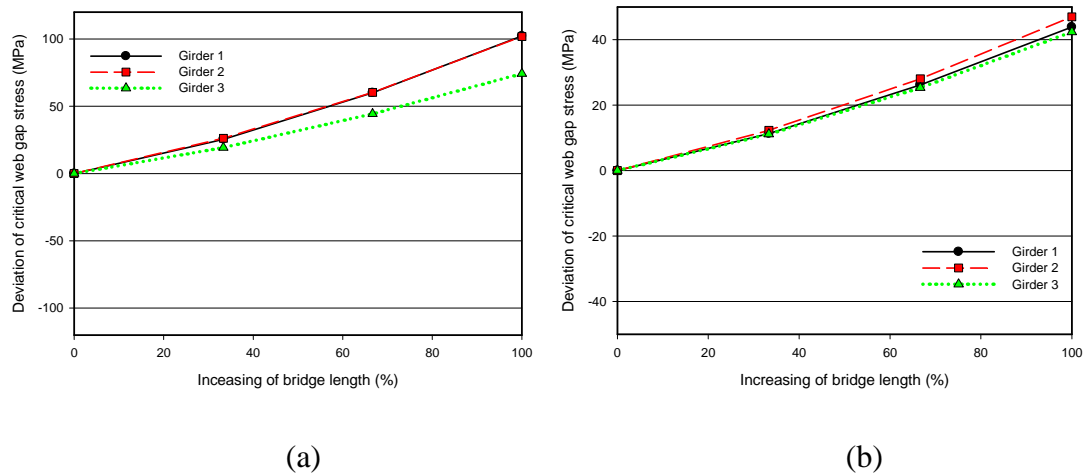
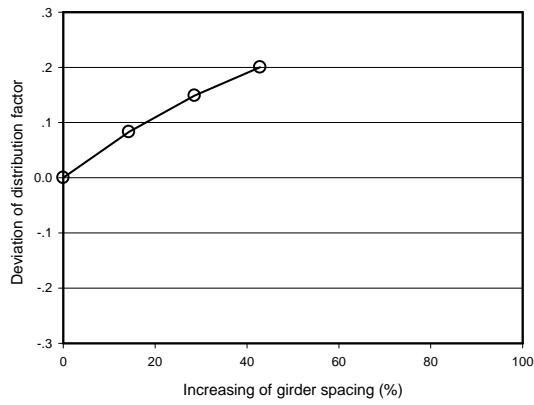


Figure 6.8 Bridge length effect (a) One truck case (b) Two trucks case

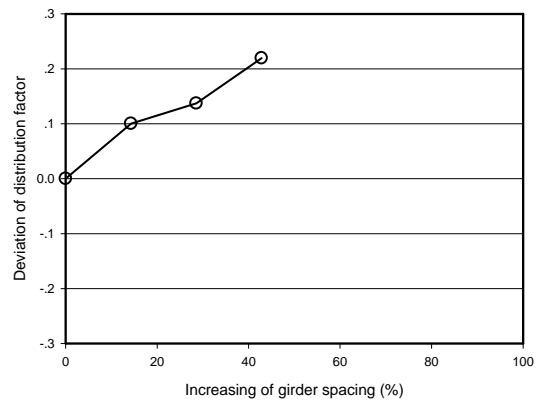
Figure 6.5 until figure 6.8 shows the quadratic polynomial regression of relative displacement between adjacent girders and bridge parameter comparison. Similar sensitivity analysis method is also adopted in the web gap stress comparison. The difference of critical web gap stress in case of one truck from figure 6.5 until figure 6.8 shows that the highest difference occurred in comparison of girder stiffness parameter. It is then followed by bridge length, slab thickness, and the lowest slope is occur comparison girder spacing. Girder stiffness can be give more influence than the girder spacing because the variation of girder stiffness was done with varying thickness of girder flanges and web. Comparison between influences of girder spacing and slab thickness were determined by the influence of these parameters in relative displacement as the relative displacement also governs the maximum web gap stress (Fisher et al (1990)). In relative displacement, slab thickness is more influence than girder spacing in one truck on left case but in case of two trucks, girder spacing has more influence than slab thickness. In case of two trucks, the two most influential parameters is bridge length then followed by girder stiffness, girder spacing, and slab thickness.

6.1.3 Lateral Load Distribution Factor.

The effect of each parameter increasing in deviance of lateral load distribution factor is shown in figure 6.9 until figure 6.12.

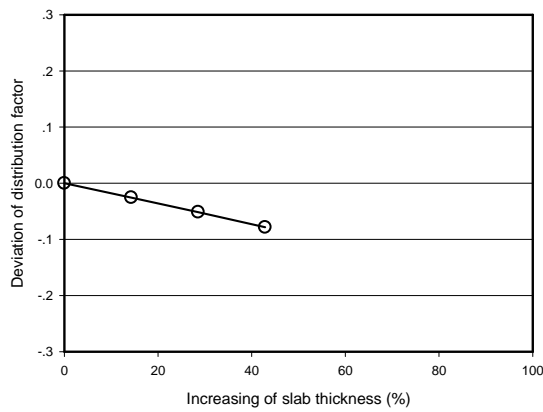


(a)

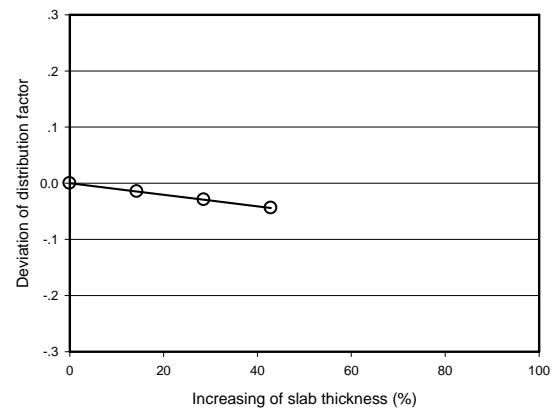


(b)

Figure 6.9 Girder spacing effect (a) One truck case (b) Two trucks case

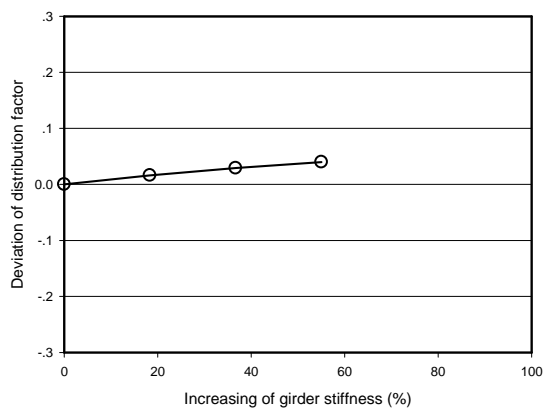


(a)

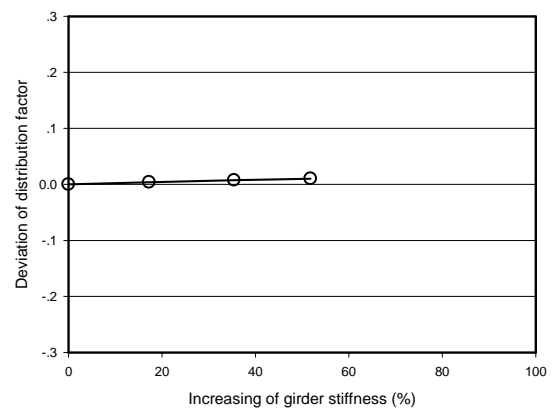


(b)

Figure 6.10 Slab thickness effect (a) One truck case (b) Two trucks case



(a)



(b)

Figure 6.11 Girder stiffness effect (a) One truck case (b) Two trucks case

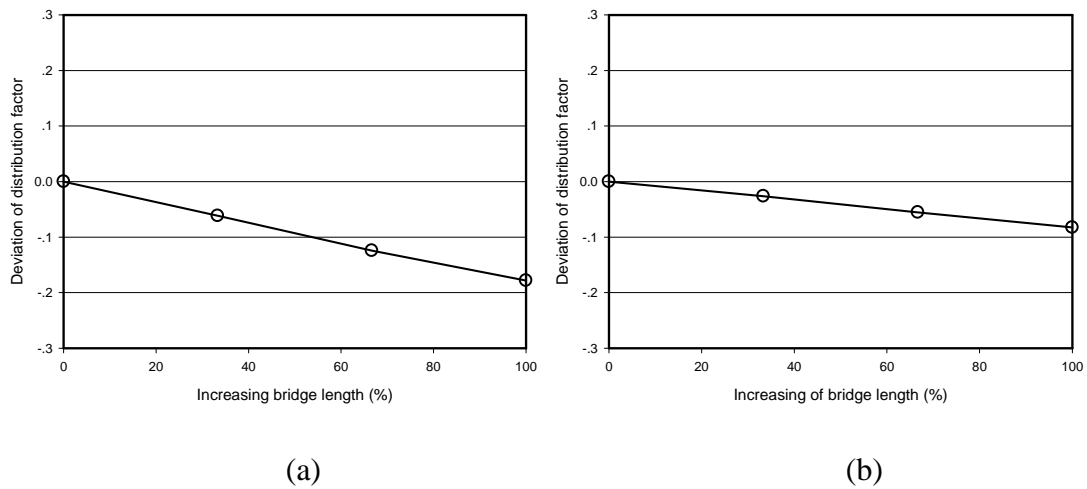


Figure 6.12 Bridge length effect (a) One truck case (b) Two trucks case

Figure 6.9 until figure 6.12 shows the regression of lateral distribution factor difference and bridge parameter increasing comparison. Similar sensitivity analysis method is also adopted in the web gap stress comparison. In case of one truck, with 40% increasing of girder spacing, bridge length, slab thickness, and girder stiffness result the difference 0.2, 0.08, 0.07, and 0.03, respectively and 0.2, 0.04, 0.04, and 0.01 deviation in case of two truck, respectively. It shows the girder spacing have the most influence then follow by bridge length, slab thickness, and girder spacing for both case.

6.2 Development of Formula

All the comparison of bridge parameters with relative displacement between adjacent girders and maximum web gap stress shows the bridge parameter effect to be linear. It can lead to the formulation based on this linear regression from each parameter effect. Subsequently, all the parameter formulas are combined by multiple linear regression to generate the formulation of maximum relative displacement.

Assuming that the effect of each key parameter can be modeled by functions $f(L)$, $f(S)$, $f(t_s)$, and $f(I_g)$, respectively, the equation of bridge parameter effect can be expressed in the form of:

$$Y_i = \beta_0 + \beta_1 S + \beta_2 t_s + \beta_3 I_g + \beta_4 L + \varepsilon \quad (6.1)$$

The model can be rewritten as

$$\begin{aligned}
 Y_1 &= \beta_0 + \beta_1 S_1 + \beta_2 t_{s1} + \beta_3 I_{g1} + \beta_4 L_1 + \varepsilon_1 \\
 Y_2 &= \beta_0 + \beta_1 S_2 + \beta_2 t_{s2} + \beta_3 I_{g2} + \beta_4 L_2 + \varepsilon_2 \\
 &\vdots \\
 Y_n &= \beta_0 + \beta_1 S_n + \beta_2 t_{sn} + \beta_3 I_{gn} + \beta_4 L_n + \varepsilon_n
 \end{aligned} \tag{6.2}$$

In the parametric study, 16 finite element models were constructed with varying bridge parameters. Bridge length (m), girder spacing (m), and slab thickness (mm) varied in the parametric study. Girder stiffness is converted to m^4 to avoid the singular matrix. In matrix terms, the independent variable is:

$$X = \begin{bmatrix}
 1 & 2.1 & 0.24 & 0.013 & 24 \\
 1 & 2.4 & 0.24 & 0.013 & 24 \\
 1 & 2.7 & 0.24 & 0.013 & 24 \\
 1 & 3.0 & 0.24 & 0.013 & 24 \\
 1 & 3.0 & 0.21 & 0.013 & 24 \\
 1 & 3.0 & 0.24 & 0.013 & 24 \\
 1 & 3.0 & 0.27 & 0.013 & 24 \\
 1 & 3.0 & 0.30 & 0.013 & 24 \\
 1 & 3.0 & 0.24 & 0.011 & 24 \\
 1 & 3.0 & 0.24 & 0.013 & 24 \\
 1 & 3.0 & 0.24 & 0.015 & 24 \\
 1 & 3.0 & 0.24 & 0.017 & 24 \\
 1 & 3.0 & 0.24 & 0.013 & 18 \\
 1 & 3.0 & 0.24 & 0.013 & 24 \\
 1 & 3.0 & 0.24 & 0.013 & 30 \\
 1 & 3.0 & 0.24 & 0.013 & 36
 \end{bmatrix} \tag{6.3}$$

The dependent variable in this study is the result of the parametric study. This parametric study showed that the maximum relative displacement between adjacent girders in case of one truck on left and two trucks on both lanes and maximum web gap stress in both cases. The dependent variable for maximum relative displacement between adjacent girders in case of one truck is the relative displacement under loading lane is:

$$\Delta_{1T} = \begin{bmatrix} 2.78 \\ 3.27 \\ 3.7 \\ 4.07 \\ 4.54 \\ 4.07 \\ 3.64 \\ 3.25 \\ 4.5 \\ 4.07 \\ 3.73 \\ 3.46 \\ 1.92 \\ 4.09 \\ 6.85 \\ 10.18 \end{bmatrix} \text{ mm} \quad (6.4)$$

Dependent variable of maximum relative displacement between adjacent girders in two trucks case is the relative displacement under truck in the inner side of the lane:

$$\Delta_{2T} = \begin{bmatrix} 0.89 \\ 1.44 \\ 2.05 \\ 2.59 \\ 2.9 \\ 2.59 \\ 2.3 \\ 2.06 \\ 2.85 \\ 2.59 \\ 2.39 \\ 2.24 \\ 1.36 \\ 2.59 \\ 4.16 \\ 6.04 \end{bmatrix} \text{ mm} \quad (6.5)$$

Dependent variable of maximum web gap stress in one truck case is the critical vertical stress:

$$\sigma_{wg1T} = \begin{bmatrix} 42.68 \\ 44.98 \\ 45.49 \\ 44.89 \\ 50.84 \\ 44.89 \\ 39.54 \\ 35.2 \\ 73.96 \\ 44.89 \\ 32.32 \\ 26.61 \\ 18.69 \\ 44.89 \\ 78.96 \\ 120.59 \end{bmatrix} \text{ MPa} \quad (6.7)$$

Dependent variable of maximum web gap stress in two trucks case is the vertical stress in the end of stiffener in G3R side:

$$\sigma_{wg2T} = \begin{bmatrix} 9.95 \\ 16.26 \\ 20.42 \\ 23.29 \\ 30.68 \\ 26.3 \\ 23.29 \\ 18.52 \\ 30.92 \\ 23.29 \\ 18.48 \\ 14.01 \\ 12.13 \\ 23.29 \\ 35.84 \\ 54.5 \end{bmatrix} \text{ MPa} \quad (6.7)$$

β is determined based on the variation of these parameters distribution. Multiple linear regression analysis results use \mathbf{X} and \mathbf{Y} matrix to get β value.

$$\boldsymbol{\beta} = (\mathbf{X}^T \mathbf{X})^{-1} \mathbf{X}^T \mathbf{Y} \quad (6.8)$$

The equation gives the coefficient $\boldsymbol{\beta}$ of \mathbf{Y} equation. The formulas obtained from the multiple linear regressions are listed below.

Relative displacement between adjacent girders for one truck loading

$$\Delta_{1T} = -5.87 + 1.49S - 14.56t_s - 178.05I_g + 0.47L \quad (6.9)$$

with R^2 value is 0.98

Relative displacement between adjacent girders for two trucks loading

$$\Delta_{2T} = -6.04 + 1.94S - 9.37t_s - 102.69I_g + 0.27L \quad (6.10)$$

with R^2 value is 0.98

Maximum web gap stress for one truck loading

$$\sigma_{wg1T} = 30.1 + 5.5S - 118.1t_s - 6996I_g + 5.7L \quad (6.11)$$

with R^2 value is 0.96

Maximum web gap stress for two trucks loading

$$\sigma_{wg2T} = -30.1 + 14.4S - 50t_s - 2681I_g + 2.4L \quad (6.12)$$

with R^2 value is 0.97

where Δ_{1T} = relative displacement between adjacent girders in one truck case (mm); Δ_{2T} = relative displacement between adjacent girders in two trucks case (mm); σ_{wg1T} = maximum web gap stress in one truck case (MPa); σ_{wg2T} = maximum web gap stress in two trucks case (MPa); L = span length (m); S = girder spacing (m); t_s = slab thickness (m); and I_g = girder stiffness (m^4).

The equation is only applicable for three girder bridges with two lanes. The formula is applicable for the bridge having the girder spacing between 2.1 m and 3 m, the length between 18 m and 36 m, the slab thickness between 210 mm and 300 mm, and the girder stiffness between $1.0 \times 10^{10} \text{ mm}^4$ and $1.7 \times 10^{10} \text{ mm}^4$.

CHAPTER VII

SUMMARY AND CONCLUSION

7.1 Summary and Conclusions

Dual-level finite element analyses incorporating both the global model, which encompasses the entire bridge, and submodel which encompasses a portion of bridge surrounding the studied diaphragm were performed in the present research project. In order to validate the finite element model, truck loading test composite I-girder bridge has been applied and the data was collected. A total 15 global models and 4 submodels were generated in this study. The multistep analysis was performed to validated the finite element model. A total of 108 cases for global model and sub model was validated by longitudinal stress in the bottom flange and web gap stress.

Finite element analysis was performed in the parametric study. The bridge parameters which influence lateral load distribution factor are used. The parametric study method is varying the one parameter while another parameter is fixed. The main results from the parametric study are:

- The maximum relative displacement increases as the bridge length and girder spacing increase. In contrast, it decreases with increasing slab thickness and girder stiffness.
- For one truck loading, relative displacement between adjacent girders occurred under loaded and unloaded lane is the same and for two truck case, outer-inner transverse combination shows the critical combination. In this transverse combination, the critical relative displacement occurred under truck in the inner side.
- The maximum vertical web gap stress occurred in the end of stiffener in one truck case and two truck case shows the stress in near the bottom flanges is more critical.
- Lateral load distribution factor from the parametric study shows similar trend with both the AASHTO LRFD equation and previous study from Zokaie (2000).
- For Wongsawang bridge, AASHTO and Thai trucks yielded similar lateral load distribution factor and web gap stress.

The ranking influencing bridge parameters can be summarized in Table 7.1. It shows the parameter affect based on the influenced to the relative displacement between adjacent girder, critical web gap stress, and lateral load distribution.

Table 7.1. Ranking influencing bridge parameters

Relative displacement		Critical web gap stress		LDF	
One truck	Two truck	One truck	Two truck	One truck	Two truck
Bridge length	Bridge length	Girder stiffness	Bridge length	Girder spacing	Girder spacing
Slab thickness	Girder spacing	Bridge length	Girder stiffness	Bridge length	Bridge length
Girder spacing	Slab thickness	Slab thickness	Girder spacing	Slab thickness	Slab thickness
Girder stiffness	Girder stiffness	Girder spacing	Slab thickness	Girder stiffness	Girder stiffness

The parametric study shows that the relative displacement and vertical web gap are linear function of the bridge parameter. Subsequently, the multiple linear regressions was chosen to generate the formulation of maximum relative displacement and vertical web gap stress. The empirical formula from parametric study is listed below:

Relative displacement between adjacent girders under one truck loading

$$\Delta_{1T} = -5.87 + 1.49S - 14.56t_s - 178.05I_g + 0.47L \quad (7.1)$$

Relative displacement between adjacent girders under two trucks loading

$$\Delta_{2T} = -6.04 + 1.94S - 9.37t_s - 102.69I_g + 0.27L \quad (7.2)$$

Maximum web gap stress under one truck loading

$$\sigma_{wg1T} = 30.1 + 5.5S - 118.1t_s - 6996I_g + 5.7L \quad (7.3)$$

Maximum web gap stress under two trucks loading

$$\sigma_{wg2T} = -30.1 + 14.4S - 50t_s - 2681I_g + 2.4L \quad (7.4)$$

where Δ_{1T} = relative displacement between adjacent girders in one truck case (mm); Δ_{2T} = relative displacement between adjacent girders in two truck case (mm); σ_{wg1T} = maximum web gap stress in one truck case (MPa); σ_{wg2T} = maximum web gap stress in two truck case (MPa)

in two trucks case (MPa); L = span length (m); S = girder spacing (m); t_s = slab thickness (m); and I_g = girder stiffness (m^4).

The equation is only applicable for composite I-steel girder which has similar dimension and behavior with Wongsawan bridge. The range of applicability is as follows. The girder spacing between 2.1 m and 3 m, the length between 18 m and 36 m, the slab thickness between 210 mm and 300 mm, and the girder stiffness between $1.0 \times 10^{10} \text{ mm}^4$ and $1.7 \times 10^{10} \text{ mm}^4$.

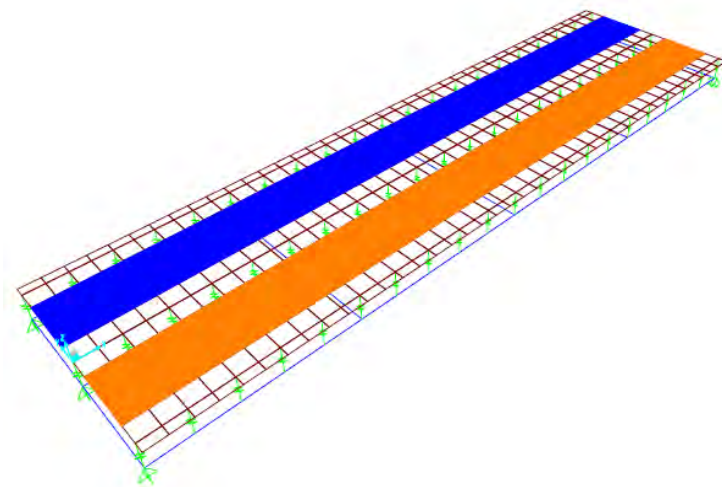
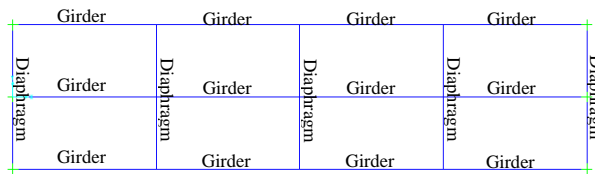
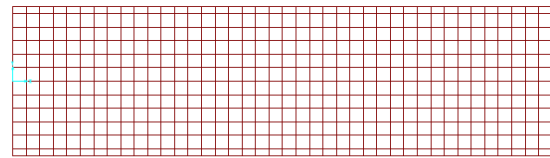
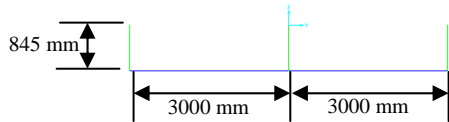
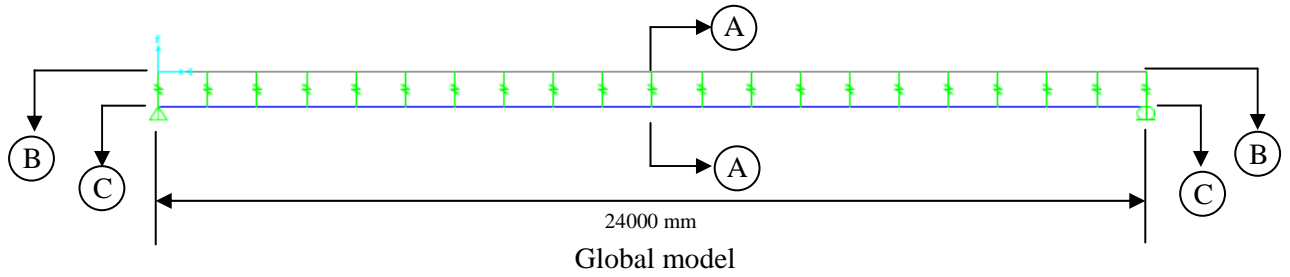
7.2 Suggestion for Future Work

The suggested future work are briefly explained as follows:

- ❖ Fatigue crack can be occurred in the stiffener-to-flange weld. This crack shows there is other critical location in the connection which is cannot be modeled in the finite element model in this research. Furthermore, the more appropriate and better model is needed to modeling the crack in this area.
- ❖ Skew of angle parameter was excluded in this research. The research in effect angle of skew influence to the distortion induced stress is needed to investigate.
- ❖ The simple equation of critical web-gap stress can be obtained from relative displacement between adjacent girders.
- ❖ Real bridge dimension can be used to obtain more accurate formula of critical web gap stress.

APPENDIX A

CONSTRUCTION of GLOBAL MODEL



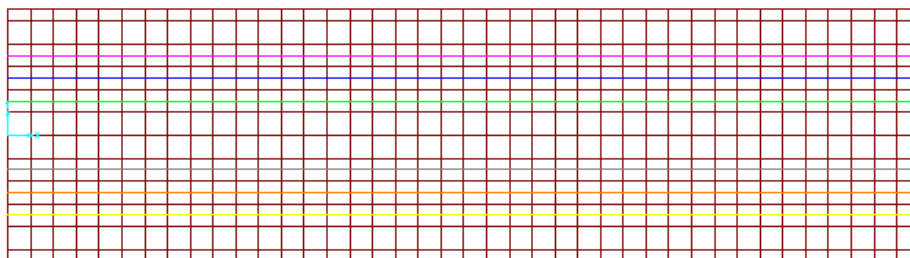
Material properties

- Concrete
 - Modulus of elasticity = 24000 MPa
 - Poisson ratio = 0.2
- Steel
 - Modulus of elasticity = 200000 MPa
 - Poisson ratio = 0.3

Member properties

- Concrete thickness = 240 mm
- Girder = I-1450×450×12×22
- Diaphragm = I-678×240×12×16

Multistep analysis



Six lane of truck moving load

HS20-44 was applied to each line simultaneously to get the transverse position and longitudinal position which is result critical relative displacement between adjacent girders. Two truck case is considered.

SAP2000 modeling

1. Click the **File menu** > **New model** command to access the *New Model* form
2. Click the drop-down list to set the unit to
3. Click on the **Blank** to access the *Blank* windows. It mean the model will not use the template from SAP2000
4. Click the **Define menu** > **Coordinate systems/Grids** command to access the *Coordinate/Grid System* form.
5. In that form click the **Modify/Show System** button to access the *Define Grid Data* form. Fill in the form as shown in figure A-1. Type values in the Grid ID and Ordinate cells;

click the **Line Type, Visibility, and Bubble Loc. Cells** until the appropriate option appears:

Define Grid Data

System Name: GLOBAL Units: N, mm, C

Grid Lines: Quick Start...

X Grid Data

	Grid ID	Ordinate	Line Type	Visibility	Bubble Loc.	Grid Color
1	x1	0.	Primary	Show	End	
2	x2	6000.	Primary	Show	End	
3	x3	12000.	Primary	Show	End	
4	x4	18000.	Primary	Show	End	
5	x5	24000.	Primary	Show	End	
6						
7						
8						

Y Grid Data

	Grid ID	Ordinate	Line Type	Visibility	Bubble Loc.	Grid Color
1	y1	-3300.	Primary	Show	End	
2	y2	-3000.	Primary	Show	End	
3	y3	0.	Primary	Show	End	
4	y4	3000.	Primary	Show	End	
5	y5	3300.	Primary	Show	End	
6						
7						
8						

Z Grid Data

	Grid ID	Ordinate	Line Type	Visibility	Bubble Loc.	Grid Color
1	z2	-845.	Primary	Show	End	
2	z1	0.	Primary	Show	End	
3						
4						
5						
6						
7						
8						

Display Grids as: Ordinates Spacing

Hide All Grid Lines

Glue to Grid Lines

Bubble Size: 2438.4


Reset to Default Color

Reorder Ordinates

OK Cancel

Figure A-1

- Click the **OK** button on the *Define Grid Data and Coordinate/Grid Systems* form to exit the forms.
6. Click the **Define menu > Frame Section** to access the *Frame Properties* form. In that form:
- Click the **Add New Property** button to display the section *Add Frame Section*

Frame Property form. After Select Property Type, click **I/Wide Flange** button  to access the *I/Wide Flange Section* form. Fill in the form based on girder and diaphragm member properties, as shown in figure A-2 and figure A-3.

The screenshot shows the 'I/Wide Flange Section' dialog box with the 'Section Name' set to 'GIRDER'. The 'Material' is set to 'STEEL'. The dimensions are: Outside height (t3) = 1450, Top flange width (t2) = 450, Top flange thickness (tf) = 22, Web thickness (tw) = 12, Bottom flange width (t2b) = 450, and Bottom flange thickness (tfb) = 22. A small diagram on the right shows the cross-section of the girder with dimensions labeled. The 'Display Color' is set to green.

Figure A-2

The screenshot shows the 'I/Wide Flange Section' dialog box with the 'Section Name' set to 'DIAPHRAGM'. The 'Material' is set to 'STEEL'. The dimensions are: Outside height (t3) = 678, Top flange width (t2) = 253, Top flange thickness (tf) = 16, Web thickness (tw) = 12, Bottom flange width (t2b) = 253, and Bottom flange thickness (tfb) = 16. A small diagram on the right shows the cross-section of the diaphragm with dimensions labeled. The 'Display Color' is set to yellow.

Figure A-3

- Click the **OK** button on the *I/Wide Flange Section* form to exit the forms.
7. Click the **Define menu > Area Section** to access the *Area Section* form. In that form:
- Click the drop down list in *Select Section Type To Add* to change to
 - Click the **Add New Section** to access the *Shell Section Data* form. Fill in the form based on the material and member properties, as shown in figure A-4.

The screenshot shows the 'Shell Section Data' dialog box. The 'Section Name' is 'slab'. The 'Material' is 'CONC'. The 'Material Angle' is 0. The 'Thickness' is set to 240 for both 'Membrane' and 'Bending'. The 'Type' is 'Shell - Thin'. The 'Display Color' is yellow. There are buttons for 'Modify/Show...', 'Modify/Show Layer Definition...', 'Modify/Show Shell Design Parameters...', 'Set Modifiers...', and 'Thermal Properties...'. The 'OK' and 'Cancel' buttons are at the bottom.

Figure A-4

8. Click the **Define menu > Link/Support Properties** to access the *Link/Support Properties* form. In that form:
 - Click the drop down list in *Link/Support Type* to change to
 - Fill in the *Property Name* edit box
 - Couple all the box in *Directional Properties* area, as shown in figure A-5

Link/Support Property Data

Link/Support Type:

Property Name:

Property Notes:

Total Mass and Weight

Mass: Rotational Inertia 1:

Weight: Rotational Inertia 2:

Rotational Inertia 3:

Factors For Line, Area and Solid Springs

Property is Defined for This Length In a Line Spring:

Property is Defined for This Area In Area and Solid Springs:

Directional Properties

Direction	Fixed	Properties
<input checked="" type="checkbox"/> U1	<input checked="" type="checkbox"/>	<input type="button" value="Modify/Show for All..."/>
<input checked="" type="checkbox"/> U2	<input checked="" type="checkbox"/>	
<input checked="" type="checkbox"/> U3	<input checked="" type="checkbox"/>	
<input checked="" type="checkbox"/> R1	<input checked="" type="checkbox"/>	
<input checked="" type="checkbox"/> R2	<input checked="" type="checkbox"/>	
<input checked="" type="checkbox"/> R3	<input checked="" type="checkbox"/>	

P-Delta Parameters:

Figure A-5

9. Click the **Set Default 3D View** to change to the default 3-d view in the right windows.
10. In the left windows click **View menu > Set 2D View** to access *Set 2D View* form. Fill in $Z = -845$ in *XY plane*
11. Click the **Quick Draw Frame/Cable/Tendon button** or click the **Draw menu > Quick Draw Frame/Cable/Tendon** command to access the *Properties of Object* form. By default, the line *Object Type* should be Straight frame. Click the *Section Box* to display the drop-down list and click on the frame section which is defined before.

Connect the intersection as shown in figure A-6. Girder section was applied to the frame member number 1 until 11 and diaphragm section for frame number 12 until 21.

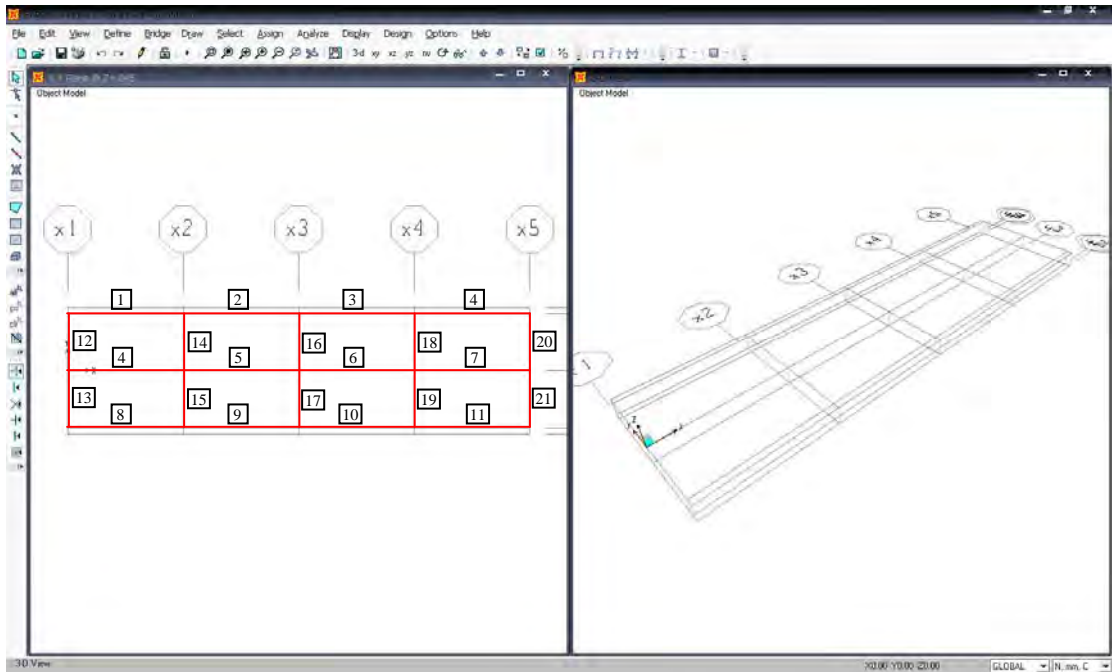
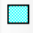


Figure A-6

12. In the left windows click **View menu > Set 2D View** to access *Set 2D View* form. Fill in $Z = 0$ in XY plane
13. Click the **Quick Draw Rectangular Area Element button**  or click the **Draw menu > Draw Rectangular Area Element** command to access the *Properties of Object* form. Click the *Section* box to display the drop-down list and click on the frame section which is defined before. Click slab section which is defined before. 16 rectangular shell elements display is shown in figure A-7.

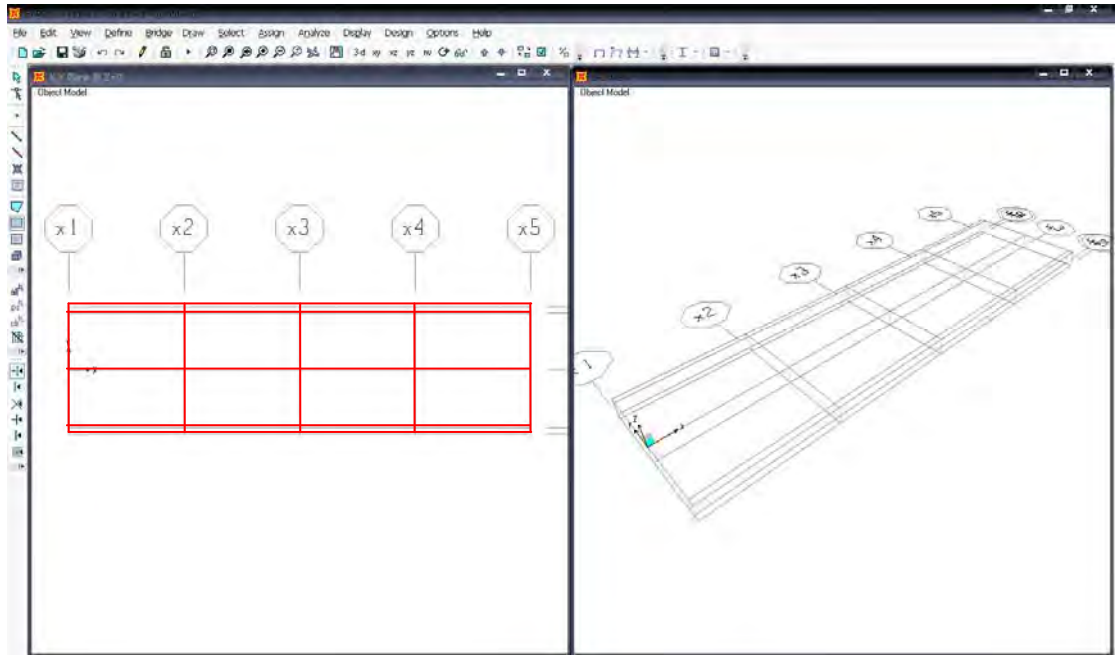



Figure A-7

14. Click the **Set Select Mode** button  to exit **Draw Mode** and enter **Select Mode**
15. Click on all Girder section frame to divide the frames. Click **Edit menu > Edit Lanes > Divide Frames** command to access the *Divide Selected Frames* form. Verify that this form is filled as shown in figure A-8.

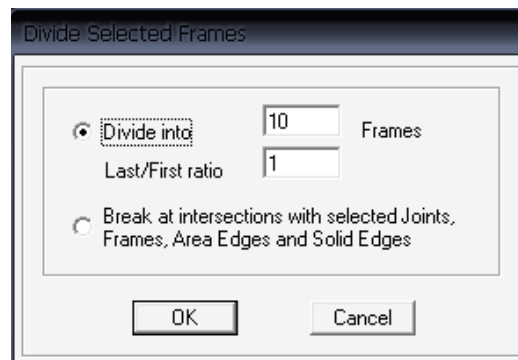


Figure A-8

16. Select all shell inside the external girder. Click **Edit menu > Edit Areas > Divide Areas** command to access the *Decide Selected Frames* form. Type 5 in the box of *Along Edge from point 1 to 3*, as shown in figure A-9.

Divide Selected Areas

Units: N, mm, C

Divide Area Into This Number of Objects (Quads and Triangles Only)

Along Edge from Point 1 to 2: 1

Along Edge from Point 1 to 3: 5

Divide Area Into Objects of This Maximum Size (Quads and Triangles Only)

Along Edge from Point 1 to 2: []

Along Edge from Point 1 to 3: []

Divide Area Based On Points On Area Edges (Quads and Triangles Only)

Points Determined From:

Intersections of Visible Straight Grid Lines With Area Edges

Intersections of Selected Straight Line Objects With Area Edges

Selected Point Objects On Area Edges

Divide Area Using Cookie Cut Based On Selected Straight Line Objects

Extend All Lines To Intersect Area Edges

Divide Area Using Cookie Cut Based On Selected Point Objects

Rotation of Cut Lines From Area Local Axes (Deg): []

Divide Area Using General Divide Tool Based On Selected Points and Lines

Maximum Size of Divided Object: []

Local Axes For Added Points

Make same on Edge if adjacent corners have same local axes definition

Make same on Face if all corners have same local axes definition

Restrains and Constraints For Added Points

Add on Edge when restrains/constraints exist at adjacent corner points
(Applies if added edge point and adjacent corner points have same local axes definition)

Add on Face when restrains/constraints exist at all corner points
(Applies if added face point and all corner points have same local axes definition)

OK Cancel

Figure A-9

17. Select all shell elements. Click **Edit menu > Edit Areas > Divide Areas** command to access the *Decide Selected Frames* form. Type 10 in the box of *Along Edge from point 1 to 2*, as shown in figure A-10.

Divide Selected Areas

Units: N, mm, C

Divide Area Into This Number of Objects (Quads and Triangles Only)

Along Edge from Point 1 to 2: 10

Along Edge from Point 1 to 3: 1

Divide Area Into Objects of This Maximum Size (Quads and Triangles Only)

Along Edge from Point 1 to 2: []

Along Edge from Point 1 to 3: []

Divide Area Based On Points On Area Edges (Quads and Triangles Only)

Points Determined From:

Intersections of Visible Straight Grid Lines With Area Edges

Intersections of Selected Straight Line Objects With Area Edges

Selected Point Objects On Area Edges

Divide Area Using Cookie Cut Based On Selected Straight Line Objects

Extend All Lines To Intersect Area Edges

Divide Area Using Cookie Cut Based On Selected Point Objects

Rotation of Cut Lines From Area Local Axes (Deg): []

Divide Area Using General Divide Tool Based On Selected Points and Lines

Maximum Size of Divided Object: []

Local Axes For Added Points

Make same on Edge if adjacent corners have same local axes definition

Make same on Face if all corners have same local axes definition

Restrains and Constraints For Added Points

Add on Edge when restrains/constraints exist at adjacent corner points
(Applies if added edge point and adjacent corner points have same local axes definition)

Add on Face when restrains/constraints exist at all corner points
(Applies if added face point and all corner points have same local axes definition)

OK Cancel

Figure A-10.

18. Click the **Draw menu > Draw 2 Joints Link** command to access the *Properties Object* form. Select link properties name in the drop-down *Properties* in the form. Connect the node of Girder section frame and Slab shell element in every 1200 mm.
19. Select three nodes in the end left of girder. Click **Assign menu > Joint > Restraint** to access *Joint Restraint* form. Coupled *Translation 1, Translation 2, and Translation 3* and press **OK**. Select three nodes in the end right of girder. Click **Assign menu > Joint > Restraint** to access *Joint Restraint* form. Coupled *Translation 3* and press **OK**. All restrain is shown in figure A-11.

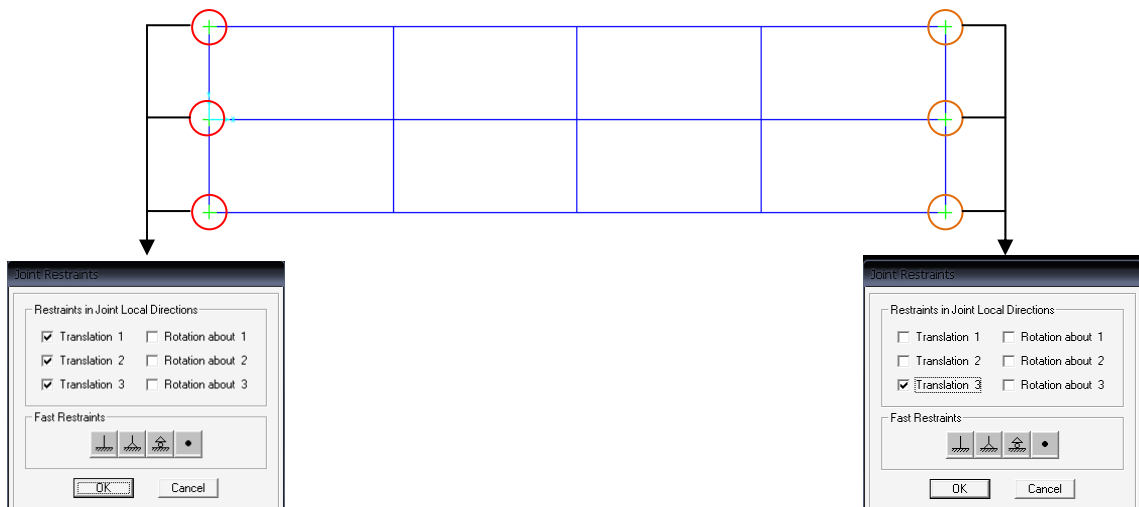


Figure A-10.

20. The finite element model is ready. Totally, it has 746 point, 130 frame element, 480 area, and 63 Links.
21. Click **Bridge menu > Layout Lines** to access *Define Bridge Layout Line* form. Click **Add New Line** to access *Bridge Layout Line Data* form, as shown in figure A-11. Type 24000 in the *End Station* edit box. Click **OK** button to return to the *Define Bridge Layout Line* form. Click **OK** button to exit all form.

Figure A-10.

22. Click **Bridge menu > Lanes** to access *Define Lanes* form. In that form:

- Click **Add New Lane Defined From Layout Line** to access *Define Lane Data* form.

In the form:

- Type OL in the *Lane Name* edit box
 - Select *Bridge Layout Lane* drop down list set to BLL1
 - Type 1 in the *Station edit* box
 - Type -2100 in the *Centerline Offset* edit box
 - Type 1800 in the *Lane Width* edit box
 - Click the **Add** button.
 - Select *Bridge Layout Lane* drop down list set to BLL1
 - Type 24000 in the *Station edit* box
 - Type -2100 in the *Centerline Offset* edit box
 - Type 1800 in the *Lane Width* edit box
 - Click the **Add** button.
 - Click **OK** button to return to the *Define Lane* form
 - Click **Add New Lane Defined From Layout Line** to access *Define Lane Data* form.
- In the form:
- Type ML in the *Lane Name* edit box
 - Select *Bridge Layout Lane* drop down list set to BLL1
 - Type 1 in the *Station edit* box

- Type -1500 in the *Centerline Offset* edit box
- Type 1800 in the *Lane Width* edit box
- Click the **Add** button.
- Select *Bridge Layout Lane* drop down list set to BLL1
- Type 24000 in the *Station* edit box
- Type -1500 in the *Centerline Offset* edit box
- Type 1800 in the *Lane Width* edit box
- Click the **Add** button.
- Click **OK** button to return to the *Define Lane* form
- Click **Add New Lane Defined From Layout Line** to access *Define Lane Data* form.
In the form:
 - Type IL in the *Lane Name* edit box
 - Select *Bridge Layout Lane* drop down list set to BLL1
 - Type 1 in the *Station* edit box
 - Type -900 in the *Centerline Offset* edit box
 - Type 1800 in the *Lane Width* edit box
 - Click the **Add** button.
 - Select *Bridge Layout Lane* drop down list set to BLL1
 - Type 24000 in the *Station* edit box
 - Type -900 in the *Centerline Offset* edit box
 - Type 1800 in the *Lane Width* edit box
 - Click the **Add** button.
 - Click **OK** button to return to the *Define Lane* form
- Click **Add New Lane Defined From Layout Line** to access *Define Lane Data* form.
In the form:
 - Type OR in the *Lane Name* edit box
 - Select *Bridge Layout Lane* drop down list set to BLL1
 - Type 1 in the *Station* edit box
 - Type 2100 in the *Centerline Offset* edit box
 - Type 1800 in the *Lane Width* edit box
 - Click the **Add** button.
 - Select *Bridge Layout Lane* drop down list set to BLL1
 - Type 24000 in the *Station* edit box
 - Type 2100 in the *Centerline Offset* edit box
 - Type 1800 in the *Lane Width* edit box
 - Click the **Add** button.

- Click **OK** button to return to the *Define Lane* form
 - Click **Add New Lane Defined From Layout Line** to access *Define Lane Data* form.
In the form:
 - Type MR in the *Lane Name* edit box
 - Select *Bridge Layout Lane* drop down list set to BLL1
 - Type 1 in the *Station* edit box
 - Type 1500 in the *Centerline Offset* edit box
 - Type 1800 in the *Lane Width* edit box
 - Click the **Add** button.
 - Select *Bridge Layout* lane drop down list set to BLL1
 - Type 24000 in the *Station* edit box
 - Type 1500 in the *Centerline Offset* edit box
 - Type 1800 in the *Lane Width* edit box
 - Click the **Add** button.
 - Click **OK** button to return to the *Define Lane* form
 - Click **Add New Lane Defined From Layout Line** to access *Define Lane Data* form.
In the form:
 - Type IR in the *Lane Name* edit box
 - Select *Bridge Layout Lane* drop down list set to BLL1
 - Type 1 in the *Station* edit box
 - Type -900 in the *Centerline Offset* edit box
 - Type 1800 in the *Lane Width* edit box
 - Click the **Add** button.
 - Select *Bridge Layout Lane* drop down list set to BLL1
 - Type 24000 in the *Station* edit box
 - Type -900 in the *Centerline Offset* edit box
 - Type 1800 in the *Lane Width* edit box
 - Click the **Add** button.
 - Click **OK** button to return to the *Define Lane* form
23. Click **Bridge menu > Vehicles** to access *Define Vehicles* form. In that form click the drop-down list in the *Choose Vehicle Type to Add* area and select *Add Standard Vehicle*. Click the **Add Vehicle** button to access the *Standard Vehicle Data* form. In that list
- In the *Data Definition* area, select HS_n-44 in the *Vehicle Type* drop down list.
 - Type 20 in the *Scale Factor* edit box if it is not already entered.
 - Click **OK** button to return to the *Define Vehicles* form


24. Click **Defined menu > Load Case** command to access the *Define Load* form. In that form:


- Type O-O in the *Load Name* edit box. In the *Type* drop-down list set to Bridge Live. Click the load list, click **Modify Bridge Live Load** button to access *Multi Step Bridge Live Load Generation* form. In this form:
 - Select Vehicle HS20-44 in the *Vehicle* drop-down list
 - Select OL in the *Lane* drop-down list
 - Accept the *Start Dist* and *Start Time* equal to zero
 - Select Forward in the *Direction* drop-down list
 - Type 1 speed in the *Speed* edit box
 - Click **Add**
 - Select Vehicle HS20-44 in the *Vehicle* drop-down list
 - Select OR in the *Lane* drop-down list
 - Accept the *Start Dist* and *Start Time* equal to zero
 - Select Forward in the *Direction* drop-down list
 - Type 1 speed in the *Speed* edit box
 - Type 24000 in the *Duration of Loading* edit box
 - Type 100 in the *Discrete Load Every* edit box
 - Click **OK** to return to de *Define Load* form
- Type O-M in the *Load Name* edit box. In the *Type* drop-down list set to Bridge Live. Click the load list, click **Modify Bridge Live Load** button to access *Multi Step Bridge Live Load Generation* form. In this form:
 - Select Vehicle HS20-44 in the *Vehicle* drop-down list
 - Select OL in the *Lane* drop-down list
 - Accept the *Start Dist* and *Start Time* equal to zero
 - Select Forward in the *Direction* drop-down list
 - Type 1 speed in the *Speed* edit box
 - Click **Add**
 - Select Vehicle HS20-44 in the *Vehicle* drop-down list
 - Select MR in the *Lane* drop-down list
 - Accept the *Start Dist* and *Start Time* equal to zero
 - Select Forward in the *Direction* drop-down list
 - Type 1 speed in the *Speed* edit box
 - Type 24000 in the *Duration of Loading* edit box
 - Type 100 in the *Discrete Load Every* edit box
 - Click **OK** to return to de *Define Load* form

- Type O-I in the *Load Name* edit box. In the *Type* drop-down list set to Bridge Live. Click the load list, click **Modify Bridge Live Load** button to access **Multi Step Bridge Live Load Generation** form. In this form:
 - Select Vehicle HS20-44 in the *Vehicle* drop-down list
 - Select OL in the *Lane* drop-down list
 - Accept the *Start Dist* and *Start Time* equal to zero
 - Select Forward in the *Direction* drop-down list
 - Type 1 speed in the *Speed* edit box
 - Click **Add**
 - Select Vehicle HS20-44 in the *Vehicle* drop-down list
 - Select IR in the *Lane* drop-down list
 - Accept the *Start Dist* and *Start Time* equal to zero
 - Select Forward in the *Direction* drop-down list
 - Type 1 speed in the *Speed* edit box
 - Type 24000 in the *Duration of Loading* edit box
 - Type 100 in the *Discrete Load Every* edit box
 - Click **OK** to return to de **Define Load** form
- Type M-M in the *Load Name* edit box. In the *Type* drop-down list set to Bridge Live. Click the load list, click **Modify Bridge Live Load** button to access **Multi Step Bridge Live Load Generation** form. In this form:
 - Select Vehicle HS20-44 in the *Vehicle* drop-down list
 - Select ML in the *Lane* drop-down list
 - Accept the *Start Dist* and *Start Time* equal to zero
 - Select Forward in the *Direction* drop-down list
 - Type 1 speed in the *Speed* edit box
 - Click **Add**
 - Select Vehicle HS20-44 in the *Vehicle* drop-down list
 - Select MR in the *Lane* drop-down list
 - Accept the *Start Dist* and *Start Time* equal to zero
 - Select Forward in the *Direction* drop-down list
 - Type 1 speed in the *Speed* edit box
 - Type 24000 in the *Duration of Loading* edit box
 - Type 100 in the *Discrete Load Every* edit box
 - Click **OK** to return to de **Define Load** form

- Type M-I in the *Load Name* edit box. In the *Type* drop-down list set to Bridge Live. Click the load list, click **Modify Bridge Live Load** button to access **Multi Step Bridge Live Load Generation** form. In this form:
 - Select Vehicle HS20-44 in the *Vehicle* drop-down list
 - Select ML in the *Lane* drop-down list
 - Accept the *Start Dist* and *Start Time* equal to zero
 - Select Forward in the *Direction* drop-down list
 - Type 1 speed in the *Speed* edit box
 - Click **Add**
 - Select Vehicle HS20-44 in the *Vehicle* drop-down list
 - Select IR in the *Lane* drop-down list
 - Accept the *Start Dist* and *Start Time* equal to zero
 - Select Forward in the *Direction* drop-down list
 - Type 1 speed in the *Speed* edit box
 - Type 24000 in the *Duration of Loading* edit box
 - Type 100 in the *Discrete Load Every* edit box
 - Click **OK** to return to de **Define Load** form
- Type I-I in the *Load Name* edit box. In the *Type* drop-down list set to Bridge Live. Click the load list, click **Modify Bridge Live Load** button to access **Multi Step Bridge Live Load Generation** form. In this form:
 - Select Vehicle HS20-44 in the *Vehicle* drop-down list
 - Select IL in the *Lane* drop-down list
 - Accept the *Start Dist* and *Start Time* equal to zero
 - Select Forward in the *Direction* drop-down list
 - Type 1 speed in the *Speed* edit box
 - Click **Add**
 - Select Vehicle HS20-44 in the *Vehicle* drop-down list
 - Select IR in the *Lane* drop-down list
 - Accept the *Start Dist* and *Start Time* equal to zero
 - Select Forward in the *Direction* drop-down list
 - Type 1 speed in the *Speed* edit box
 - Type 24000 in the *Duration of Loading* edit box
 - Type 100 in the *Discrete Load Every* edit box
 - Click **OK** to return to de **Define Load** form

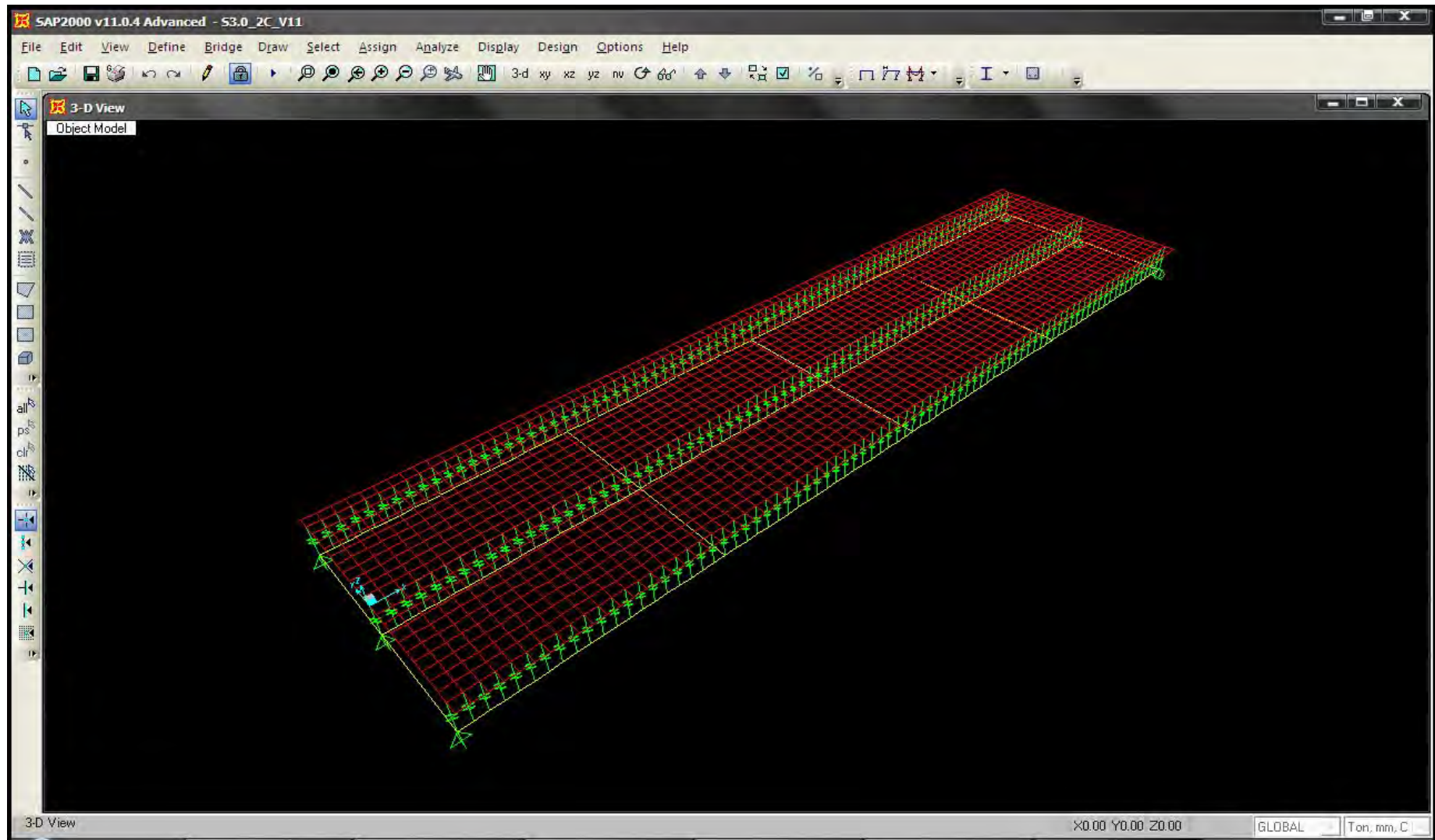
25. Click **Analyze Menu > Set Analysis Options Command** to access the *Analysis Option*

form. In that form click the **Space Frame** button  to set the available degree of freedom and click the **OK** button

26. Click the **Run Analysis** button  to display the *Set Analysis Cases to Run* form. In that form:

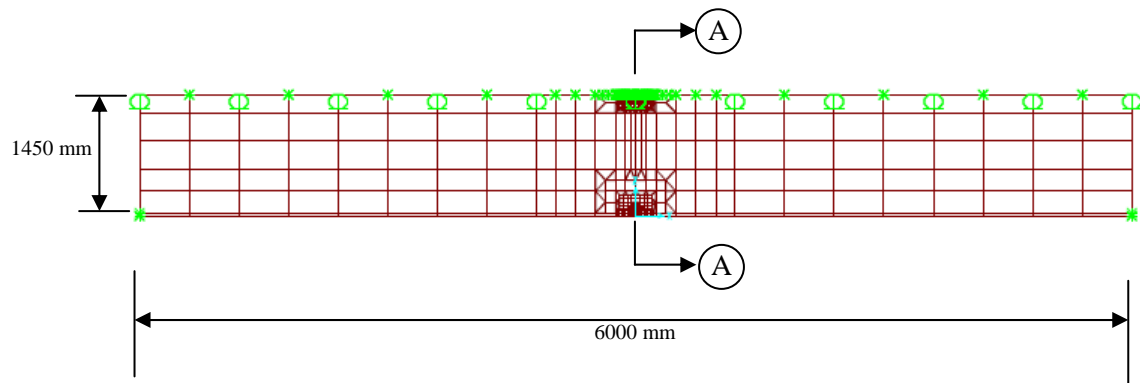
- Verify that O-O, O-M, O-I, M-M, M-I, and I-I Case Name are set to Run in the Action List.
- Click the **Run Now** button to run the analysis.

27. When the analysis is complete and if there is no warning or error, click OK to close the window.

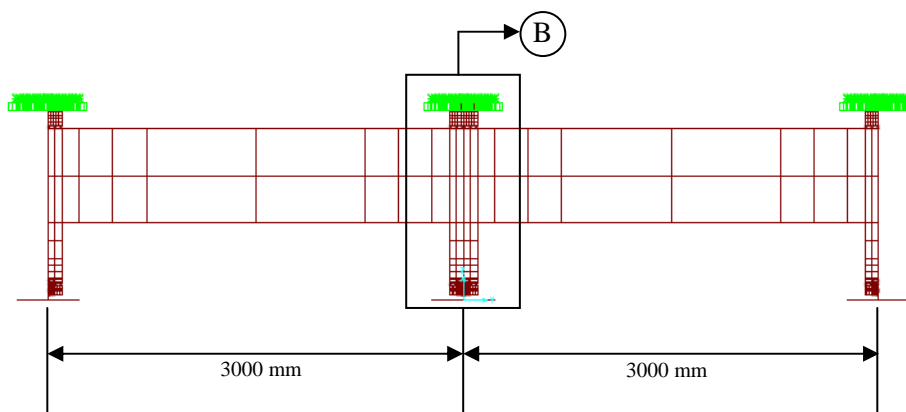


APPENDIX B

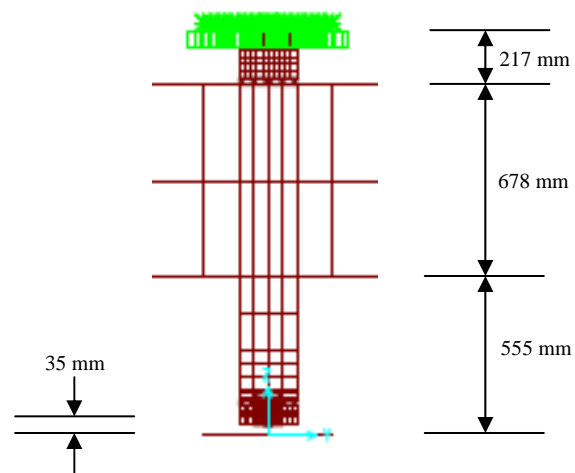
CONSTRUCTION of SUBMODEL



Longitudinal section



Section A - A



Detail B



Material properties

- Steel
 - Modulus of elasticity = 200000 MPa
 - Poisson ratio = 0.3

Member properties

- Girder = I-1450×450×12×22
- Diaphragm = I-678×240×12×16

SAP2000 modeling

1. Click the **File menu** > **New model** command to access the *New Model* form
2. Click the drop-down list to set the unit to 
3. Click on the **Blank**  to access the *Blank* windows. It mean the model will not use the template from SAP2000
4. Click the **Define menu** > **Coordinate systems/Grids** command to access the *Coordinate/Grid System* form.
5. In that form click the **Modify/Show System** button to access the *Define Grid Data* form. Fill in the form as shown in figure A-1. Type values in the Grid ID and Ordinate cells; click the **Line Type, Visibility, and Bubble Loc. Cells** until the appropriate option appears:

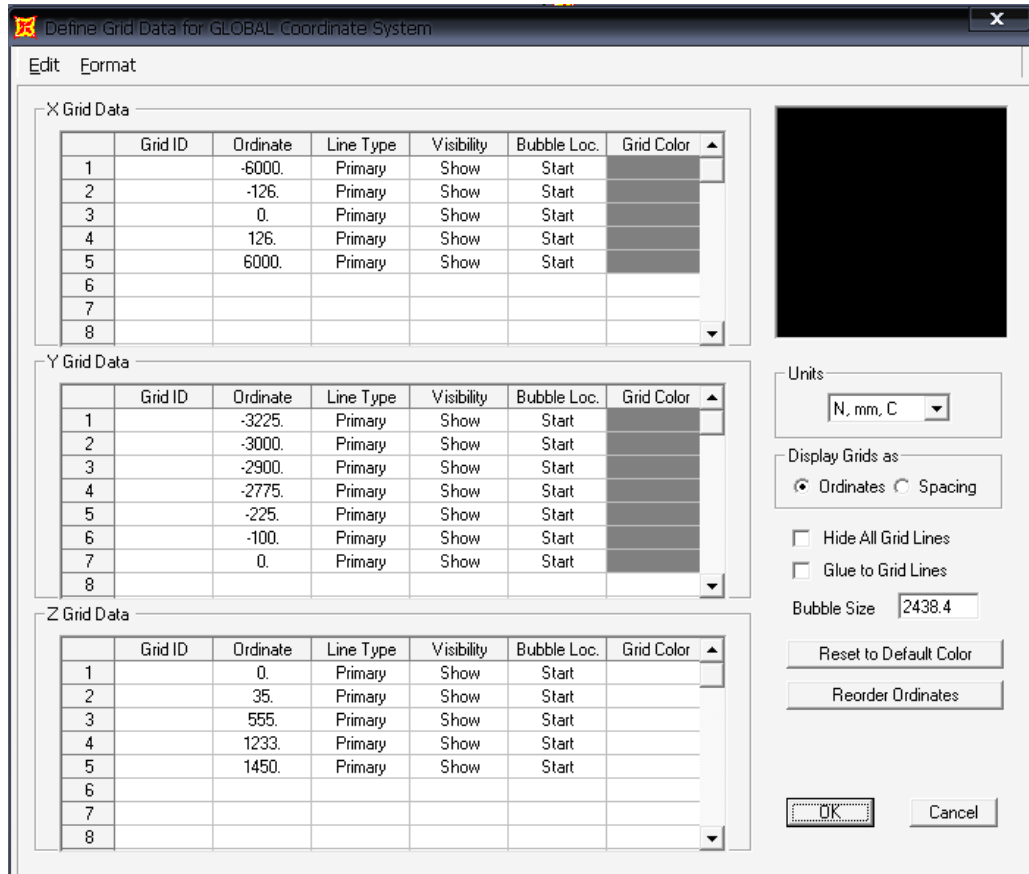
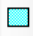


Figure B-1

6. Click the **Quick Draw Rectangular Area Element** button  or click the **Draw menu > Draw Rectangular Area Element** command to access the *Properties of Object* form. Click the *Section* box to display the drop-down list and click on the frame section which is defined before. Click slab section which is defined before. 16 rectangular shell elements display is shown in figure B-2.

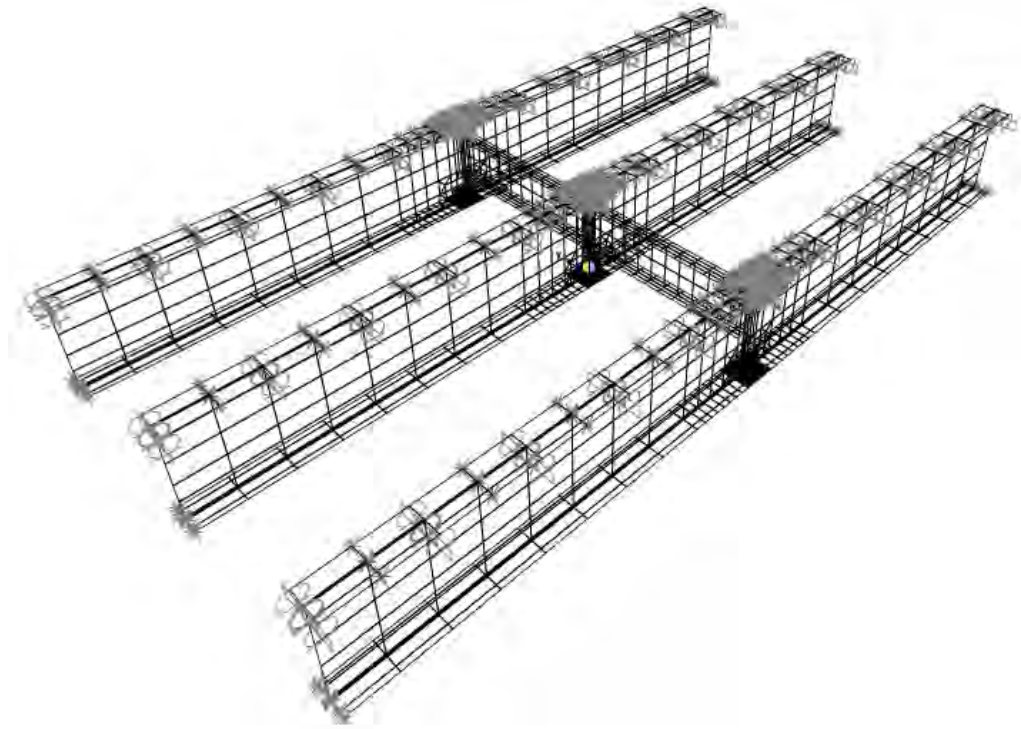


Figure B-2

7. Select all nodes in the top flange of girder. Click **Assign menu > Joint > Restraint** to access ***Joint Restraint*** form. Coupled *Translation 2, Rotation 1, and Rotation 3* and press **OK**. Select all nodes in the top flange of girder which will applied by displacement loading (called: loaded node). Click **Assign menu > Joint > Restraint** to access ***Joint Restraint*** form. Coupled *Translation 2, Translation 3, Rotation 1, and Rotation 3* and press **OK**. Select all nodes in the bottom flanges girder in the right end. Click **Assign menu > Joint > Restraint** to access ***Joint Restraint*** form. Coupled *Translation 1, Translation 2, and Rotation 1* and press **OK**. Select all nodes in the bottom flanges girder in the left end. Click **Assign menu > Joint > Restraint** to access ***Joint Restraint*** form. Coupled *Translation 2, and Rotation 1* and press **OK**.. All restrain is shown in figure B-3, figure B-4, and figure B-5.

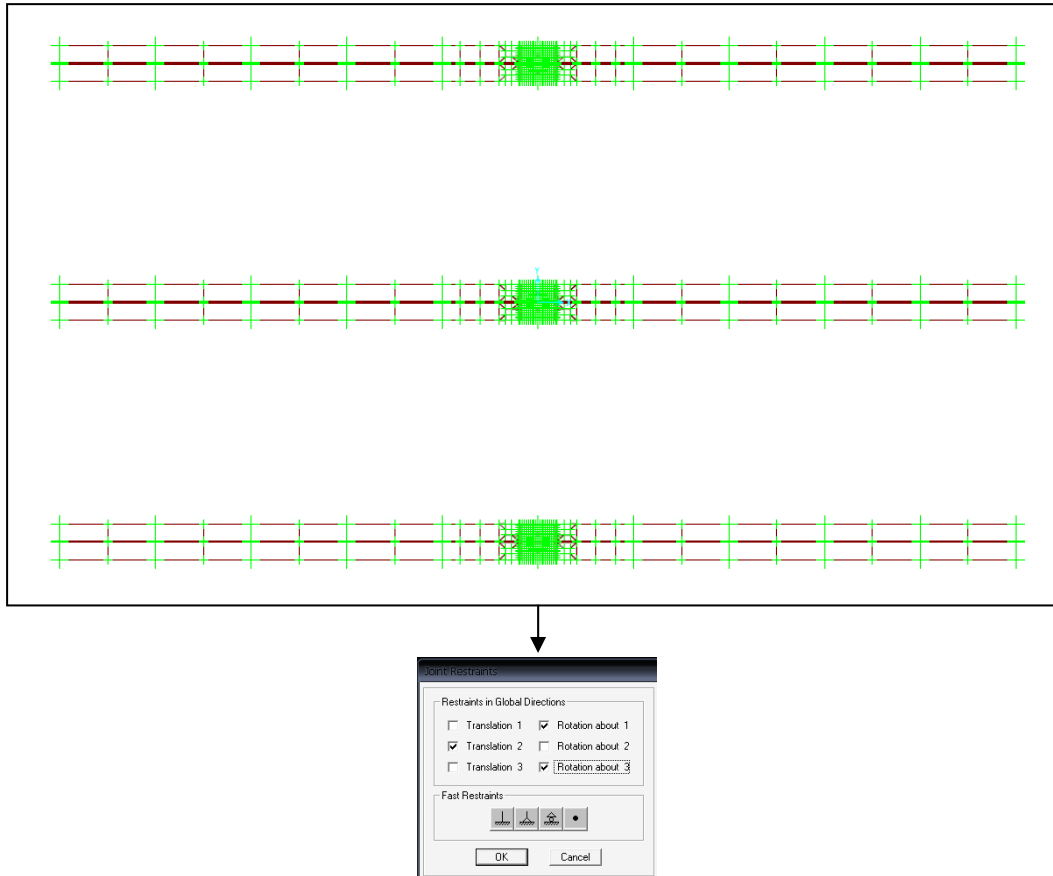


Figure B-3

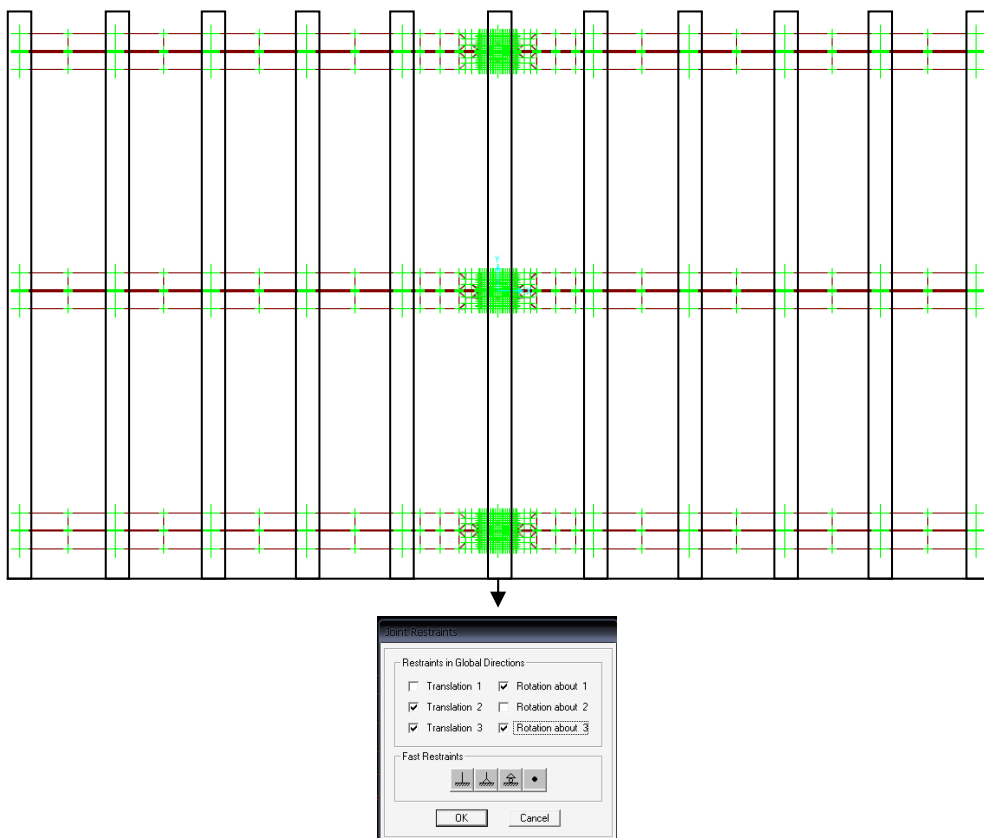


Figure B-4

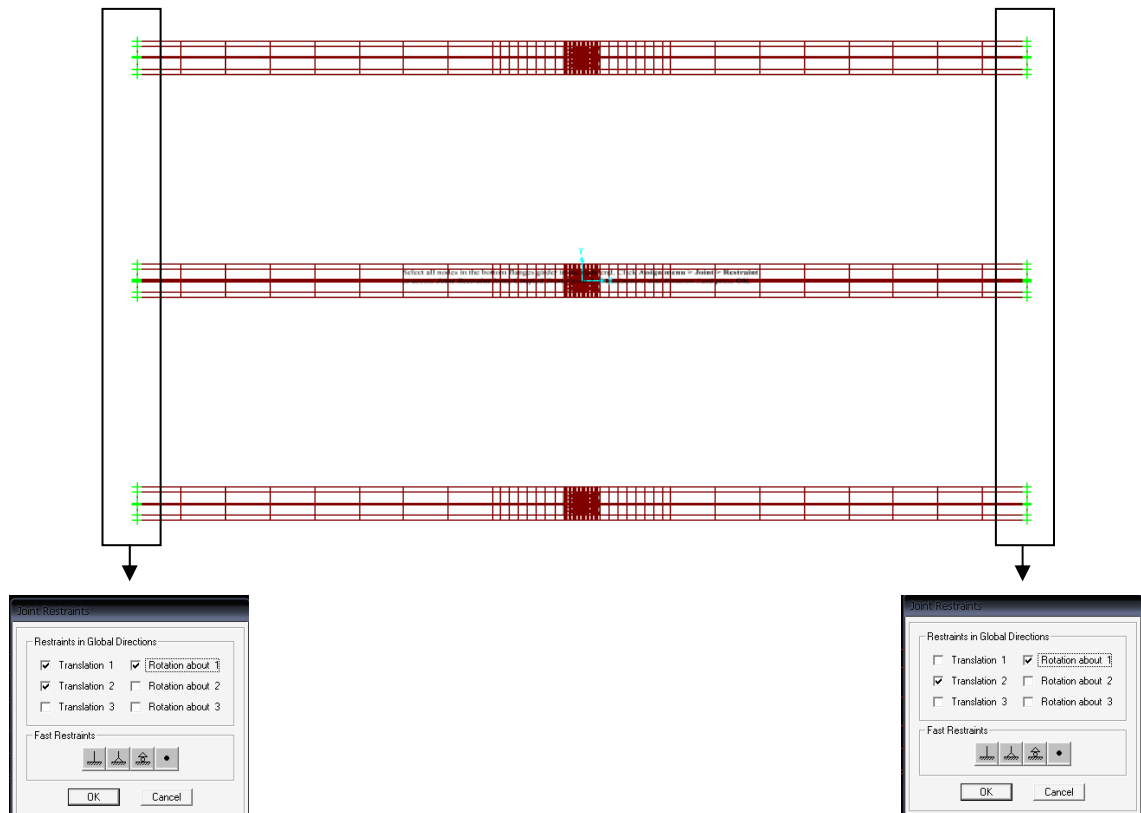


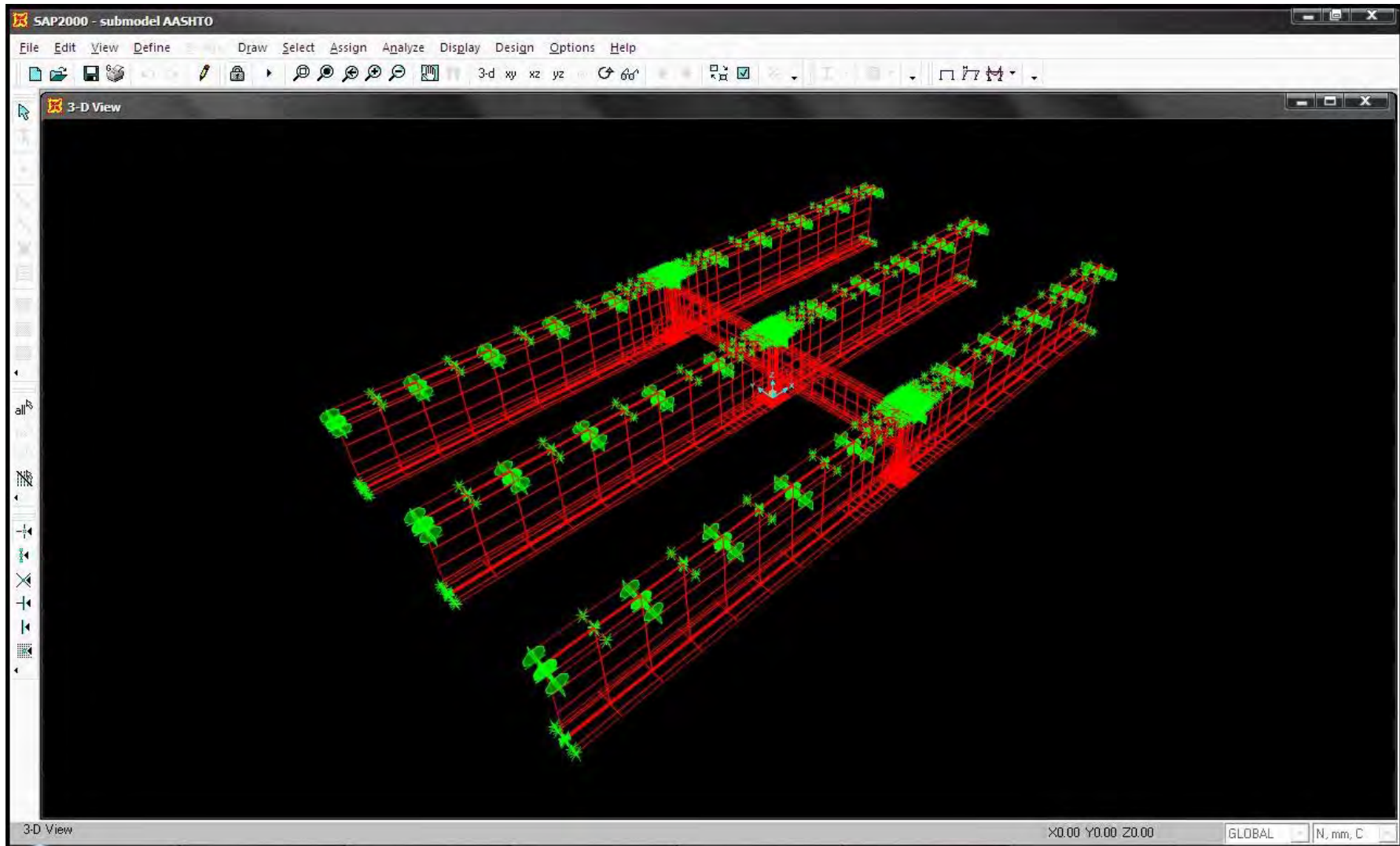


Figure B-5

8. Click **Defined menu > Load Case** command to access the *Define Load* form. In that form type T in the *Load Name* edit box. In the *Type* drop-down list set to Live.
9. Select loaded lane. Click **Assign menu > Joint Load > Displacement** to access *Ground Displacement* form. In this form type *The Translation Global Z* edit box with vertical displacement output from global model. Repeat it until all loaded node is applied by vertical displacement load.
10. Click **Analyze Menu > Set Analysis Options Command** to access the *Analysis Option*

form. In that form click the **Space Frame** button  to set the available degree of freedom and click the **OK** button

11. Click the **Run Analysis** button  to display the *Set Analysis Cases to Run* form. In that form:
 - Verify that O-O, O-M, O-I, M-M, M-I, and I-I Case Name are set to Run in the Action List.
 - Click the **Run Now** button to run the analysis.
12. When the analysis is complete and no warning or error, click OK to close the window.



REFERENCES

1. American Association of State Highway and Transportation Officials (AASHTO). **LRFD bridge specifications**. 2nd ed. Washington: AASHTO, 1998.
2. Barsom, J., M. and Rolfe, S., T. **Fracture and Fatigue control in Structures: Applications of Fracture Mechanics**. 3rd ed. Philadelphia: ASTM, 1999.
3. Becker, R. and Vexler, B. Mesh Refinement and Numerical Sensitivity Analysis for Parameter Calibration of Partial Differential Equations. **Journal of Computational Physics** (November 2004).
4. Berglund, E., M. and Schultz, A., E. Girder Differential Deflection and Distortion-Induced Fatigue in Skewed Steel Bridges. **Journal of Bridge Engineering** 11 (March/April 2006): 169 – 177.
5. Berglund, E. and Schultz, A., E. **Analysis of Tools and Rapid Screening Data for Assessing Distortional Fatigue in Steel Bridges**. Technical Report. Department of Civil Engineering. University of Minnesota, 2001.
6. Chaisomphob, T. and Lertsima, C. Effect of BMA Flyover Bridge Type on Wheel Load Distribution Factors Based on AASHTO Specification. **Thammasat International Journal Science Technology** (January-April 2000): 8 – 15.
7. Chapra, S., C. and Canale, R., P. **Numerical Methods for Engineering**. 5th ed. Singapore: McGraw-Hill Inc, 2006.
8. Chung, W., Liu, J., and Sotelino, E. D. Influence of Secondary Element and Deck Cracking on the Lateral Load Distribution of Steel Girder Bridges. **Journal of Bridge Engineering** 11 (March/April 2006): 178 – 186.
9. Chung, W. and Sotelino, E., D. Three Dimensional Finite Element Modeling of Composite girder bridges. **Journal of Engineering Structure** 28 (2006): 63-71.
10. Cook, R., D., Malkus, D., S., Plesha, M., E., and Witt, R., J. **Concepts and Applications of Finite Element Analysis**. 4th Ed. United States of America: John Wiley and Son Inc, 2002.
11. Cousin, T., E., Stalling, J., M., Lower, D., A., and Stafford, T., E. Field Evaluation of Fatigue Cracking in Diaphragm-Girder Connections. **Journal of Performance of Constructed Facilities** (February 1998): 25-32.
12. Fisher, John W., Jin, Jian, Wagner, David, and Yen, Ben. David, and Yen, Ben. Distortion Induced Fatigue Cracking in Steel Bridges, NCHRP Report 336. **Transportation Research Board, National Research Council** (Dec 1990).

13. Frasee, R., E., K., Grondin, G., Y., and Kulak, G., L. **Behavior of Distortion Induced Fatigue Cracks in Bridge Girders.** Structural Engineering Report. Department of Civil and Environmental Engineering. University of Alberta, 2000.
14. Gaylord, E., H., Jr., Gaylord, C., N., and Stallmeyer, J., E. **Steel Structures.** 3rd Ed. Singapore: McGraw-Hill International Edition, 1992.
15. Huo, X., S., Wasserman, E., P., and Zhu, P. Simplified Method of Lateral Distribution of Live Load Moment. **Journal of Bridge Engineering** 9 (July/August 2004): 382 – 390.
16. Jajich, D. and Schultz., A., E. Measurement and Analysis of Distortion-Induced Fatigue in Multigirder Steel Bridges. **Journal of Bridge Engineering** 11 (March/April 2003): 84 – 91.
17. Jajich, D., Schultz, A., E., Bergson, P., M., and Galambos, T., V. **Distortion Induced Fatigue in Multigirder Steel Bridges.** Technical Report. Department of Civil Engineering. University of Minnesota, 2000.
18. Li, H. and Schultz, A., E. **Analysis of Girder Differential Deflection and Web Gap Stress for Rapid Assessment of Distortional Fatigue in Multigirder Steel Bridges.** Technical Report. Department of Civil Engineering. University of Minnesota, 2005.
19. Liu, G. R., and Quek, S. S., **The Finite Element A practical Course.** Burlington: Butterworth-Heinemann, 2009.
20. Mabsout, M. E., Tarhini, K. M., Fredrick, G. R., and Kobrosly, M. Finite Element Analysis of Steel Girder Highway Bridges. **Journal of Bridge Engineering** 2 (August 1997): 83 – 87.
21. McGuire, William., Gallagher, R., H., and Ziemian, R., D. **Matrix Structural Analysis.** 2nd Ed, , United States of America: John Wiley and Son, Inc, 2000.
22. Nishikawa, K., Murakoshi, J., and Matsuki, T. Study on the Fatigue of Steel Highway Bridges in Japan. **Journal of Construction and Building Materials** 12 (1998): 133 – 141
23. Phuvoravan, K. Load Distribution Factor Equation for Steel Girder Bridges in LRFD Design. **in Symposium on Infrastructure Development and the Environment.** Quezon City: 2006.
24. Roddis, W., M., K. and Zhao, Y. Fatigue Crack Investigation for the Arkansas River Bridge in Hutchinson, Kansas. **Journal of Construction and Building Materials** 14 (2000): 287–295.
25. Roddis, W., M., K. and Zhao, Y. Finite Element Analysis of Steel Bridge Distortion-Induced Fatigue. **Journal of Bridge Engineering** 8 (September/October 2003): 259 – 266.
26. Roddis, W., M., K. and Zhao, Y. Out-of-Plane Fatigue Cracking in Welded Steel Bridges. **Welding Innovation** 18 (2001): 1 – 7.
27. SAP2000. **Getting started, version 7.4.** USA: Computer and Structure Inc, 2000

28. Severtson, B. Beukema, F. and Schultz, A., E. **Rapid Assessment of Distortional Stress in Multi-Girder Steel Bridges**. Technical Report. Department of Civil Engineering. University of Minnesota, 2004.
29. Sotelino, E., Chung, W., Liu, J., and Phuvoravan, K. **Simplified Load Distribution Factor for Use in LRFD Design**. Technical Report. School of Civil Engineering. Purdue University, 2004.
30. Vinnakota, Sriramulu. **Steel Structures: Behavior and LRFD**. Singapore: McGraw-Hill International Edition, 2006.
31. Yousif, Z. and Hindi, R. AASHTO-LRFD Live Load Distribution for Beam-and-Slab Bridges: Limitation and Applicability. **Journal of Bridge Engineering** 12 (November/December 2007): 765-773.
32. Zhang, H., Huang, D., and Wang, T. Lateral Load Distribution in Curved Steel I-Girder Bridges. **Journal of Bridge Engineering** 10 (May/June 2005): 281-289.
33. Zhou, Y., E. Assesment of Bridge Remaining Fatigue Life Through Field Strain Measurement. **Journal of Bridge Engineering** 11(November/December 2006): 737-744.
34. Zokaie, T. (1991). **Distribution of Wheel Load on Highway Bridges: National Cooperative Highway Research Program Report 12-26/1**, Washington, D.C: Transportation Research Board, 1991.
35. Zokaie, T. AASHTO-LRFD Live Load Distribution Specifications. **Journal of Bridge Engineering** 2 (May 2000): 83 – 87.